TÉCNICO LISBOA

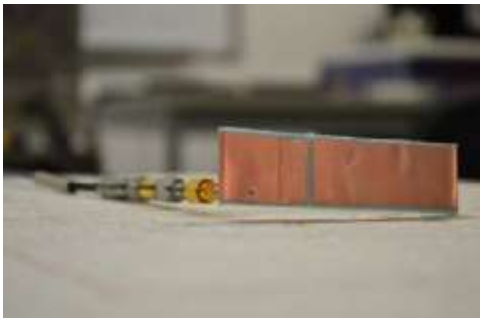

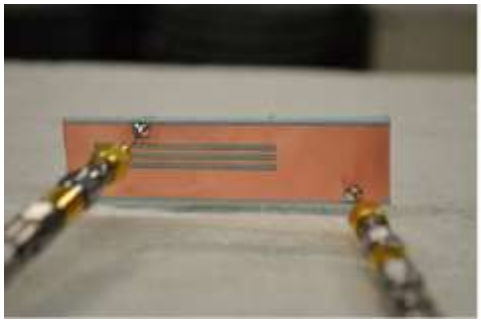

Wearable Antenna for an Ankle Bracelet Device

David Miguel Louro Gonçalves

Thesis to obtain the Master of Science Degree in

Electrical and Computer Engineering

Supervisors: Prof. António Manuel Restani Graça Alves Moreira

Dr. Nuno Miguel Faria Pires

Examination Committee

Chairperson: Prof. José Eduardo Charters Ribeiro Cunha Sanguino

Supervisor: Prof. António Manuel Restani Graça Alves Moreira

Members of the Committee: Prof. Luís Manuel de Jesus Sousa Correia

June 2019

Declaration

I declare that this document is an original work of my own authorship and that it fulfills all the requirements of the Code of Conduct and Good Practices of the Universidade de Lisboa.

Acknowledgements

Firstly, I would like to thank my parents and grandparents for their continuous support, patience and encouragement over all these years, for always being there for me through thick and thin. Without them, this work would have been much harder. In relation to my engineering course, since I can remember, my father helped me never to lose focus of the important things needed to understand the world around me and to solve some problems I came across from a simple but also discerning perspective. An engineer should always try to bear this in mind (especially when the problems seem to be too complex at first sight!). Furthermore, all my life through, my father has been a reference in relation to moral and ethical teachings. In other words, my father is an example to follow or, why ever not, a kind of hero for me.

I am thankful to my dissertation supervisors Prof. António Alves Moreira and Dr. Nuno Miguel Faria Pires for their support and knowledge sharing that has made the achievement of this dissertation possible. Their long experience with antennas design was essential in this project.

Special thanks are also due to Instituto de Telecomunicações (IT) for all the support providing the laboratory facilities that made possible the measurement campaign needed for the accomplishment of this work, and to Geosatis SA, Le Noirmont, Switzerland, for the collaboration with their expertise in the field of wearable antennas for ankle bracelet devices.

I also thank Prof. Mário Silveirinha for fruitful discussions on the possibility of placing split-ring resonators on the ground plane of the antenna under investigation. In addition, thanks are also due to Dr. João Felício, MSc. António Almeida, and Mr. Carlos Brito, for all the help in the fabrication and test of the antenna prototype.

Last but not least, very special thanks to all my university pals and close friends that contributed to my personal growth process and were usually there for me.

Abstract

Wearable devices, as well as their related applications and services, are more and more important in the steady increase of the global Internet Protocol (IP) traffic. They are now an important part of the Internet of Things (IoT)/Internet of Everything (IoE).

The proposed structure is a dual-band antenna with two metal layers for use in security, health/medical care, and personnel tracking applications. This dissertation proposes an antenna of 82.6 x 20 x 3.5 mm^3 with three parallel rectangular slots of 46.5 x 1.5 mm^2, equispaced of 1 mm, placed in ground plane and near the lowest band port. Its prototype was built and tested. The antenna operates in the Wireless-Fidelity (Wi-Fi) and Bluetooth (BT) bands, in the 2.45 GHz Industrial, Scientific and Medical (ISM) band, and in Global Positioning System (GPS)/GLONASS/Galileo L1 bands.

In two distinct stages, Scattering Parameters (S-Parameters), bandwidths, feeding, radiating patterns and radiating efficiency were analysed. First in free-space, due to isolation issues, it became necessary to approach decoupling techniques. In a second stage, the antenna was studied when folded and integrated in an ankle bracelet, inspired by a commercial application, and then when placed close to an ankle and foot model. The Specific Absorption Rate (SAR) was also evaluated.

Regarding the results of the first stage, there was a satisfactory agreement between the simulation and the experimental S-Parameters results in the bands of interest, which validates the procedure used. The second stage led to promising simulation results for a proof of concept.

Keywords

Ankle bracelet antenna; Dual-band antenna; GPS; BT; Wi-Fi

Resumo

Os dispositivos para utilização junto ao corpo humano, e aplicações e serviços associados, têm tido cada vez mais importância no aumento do tráfego IP global de informação. Constituem hoje uma parte importante da IoE/IoT.

Propõe-se uma antena dupla-banda com dois níveis de metalização, para utilização em aplicações de segurança, assistência médica e localização de pessoas. Esta dissertação propõe uma antena de $82.6 \times 20 \times 3.5$ mm^3 com três ranhuras retangulares paralelas de 46.5×1.5 mm^2, equiespaçadas de 1 mm, colocadas no plano de terra e junto do porto de banda mais baixa. O seu protótipo foi construído e testado. A antena opera nas bandas Wi-Fi e BT, na banda ISM de 2.45 GHz, e nas bandas L1 dos serviços de GPS/GLONASS/Galileo.

Em duas fases, analisaram-se parâmetros S, larguras de banda, alimentação, diagramas de radiação e eficiências de radiação. Primeiramente em espaço livre, devido a problemas de isolamento, tornou-se necessário abordar técnicas de desacoplamento. Seguidamente, estudou-se a antena quando dobrada e integrada num modelo inspirado numa tornozeleira comercial, e quando depois colocada junto a um modelo de pé e tornozelo. A avaliação SAR foi também estudada.

Com os resultados da primeira fase, verificou-se uma concordância satisfatória entre os resultados de simulação e experimentais dos parâmetros S nas bandas pretendidas, o que valida o procedimento usado. A segunda fase conduziu a resultados de simulação promissores para prova de conceito, embora requeira ainda mais estudos para validação experimental e possibilidade de utilizar esta antena nas aplicações de interesse.

Palavras Chave

Pulseira eletrónica; Antena dupla-banda; GPS; BT; Wi-Fi

Table of Contents

Table of Figures

List of Tables

List of Acronyms

ABS	Acrylonitrile Butadiene Styrene
AM	Additive Manufacturing
ATE	Artificial Tissue Emulating
BCWCS	Body Centric Wireless Communication Systems
BT	Bluetooth
CSRR	Complementary Split Ring Resonator
CST	Computer Simulation Technology
CT	Computed Tomography
EBG	Electromagnetic Band Gap
ECG	Electrocardiogram
EEG	Electroencephalogram
EM	Electromagnetic
EMC	Electromagnetic Compatibility
FFF	Fuse Filament Fabrication
FSS	Frequency Selective Structures
GA	Genetic Algorithm
GPS	Global Positioning System
HF	High Frequency
ICNIRP	International Commission on Non-Ionising Radiation Protection
ICT	Information and Communications Technologies
IMD	Implantable Medical Devices
IoE	Internet of Everything
IoT	Internet of Things
IP	Internet Protocol
ISM	Industrial, Scientific and Medical
IT	Instituto de Telecomunicações
LCP	Liquid Crystal Polymer
MBAN	Medical Body Area Network
MIC	Microwave Integrated Circuit

MICS	Medical Implant Communication Service
MIMO	Multiple Input Multiple Output
MLA	Meander Line Antenna
mm-Wave	millimetre-Wave
MRI	Magnetic Resonance Imaging
PCB	Printed Circuit Board
PDMS	PolyDiMethylSiloxane
PEC	Perfect Electrical Conductor
PET	Polyethylene TerePhta-late
PFMD	Printed Folded Meandered Dipole
PI	Polyimide
PLA	Polylactic Acid
RF	Radio-Frequency
RFID	Radio-Frequency Identification
SAR	Specific Absorption Rate
SMA	Sub-Miniature Version A
S-Parameters	Scattering Parameters
SRR	Split Ring Resonator
UHF	Ultra-High Frequency
UV	Ultraviolet
UWB	Ultra-Wide Band
VNA	Vector Network Analyser
WBAN	Wireless Body Area Network
WCS	Working Coordinate System
Wi-Fi	Wireless-Fidelity
WLAN	Wireless Local Area Network

Chapter 1

Introduction

1.1 Motivation

Over the years, Information and Communications Technologies (ICT) systems have been the core of knowledge-based world. Depending on the type of application to be deployed, these systems should guarantee adequate specification levels, including mobility, connectivity, bandwidth and flexibility. In that regard, many new ICT trends have been emerging in different ways [1].

In communications networks, Next-Generation Networks (whether wired, wireless, mobile or Optical) are emerging as result of the market and societal needs. In communications systems, there are many challenges in smart antennas, wearable antennas, Massive millimetre-Wave (mm-Wave) Multiple Input Multiple Output (MIMO) systems, and smarter Smartphones/Tablets [1] [2]. Within the communication systems, wearable antennas and devices, as well as certain applications and services pose together significant issues and challenges that enable research opportunities. Mobility or portability is frequently equated with wearability, where a set of components integrated into wearable devices or attached to the human body provides freedom and utility for people in their day-to-day tasks. Wearable devices include smartwatches, wristbands, anklets, glasses, shirts, earrings, shoes, cameras, belts, buttons, among many others [3]. However, wearable antennas design faces off unique difficulties in respect of miniaturisation and operation near the human body. Therefore, antennas specifically designed to work while being worn have been demonstrating an extraordinary potential, and becoming increasingly common in the current consumer electronics, thus they are a technology trend of utmost interest.

Bracelet-Wearable devices are already available in the market today. The keen interest and market in smart devices have increased significantly over the past few years. Thus far, most bracelet-wearables are not completely standalone devices, because they lack an internet connection. Hence, many of the bracelet wearable devices have been designed to connect, mostly via BT, with other devices that do have Internet connectivity, namely smart phones, tablets or computers [4].

Bracelet-wearables present big challenges. One of them is the power management, due to the trade-off between the size of the batteries, constrained by the total size of the device, and their power capacity. One issue that follows from this is the miniaturisation of wearable devices [4]. Nonetheless, the antenna design and inclusion of certain frequency bands such as Wi-Fi, GPS and BT are the matter of investigation, in this project. Specific needs cause distinct requisites, leading to different applications and services, varying from market information, financial, education and medical services to music, sports, cinema, or even fashion services. To sum up, bracelet-wearable devices are extremely versatile and easily extended to many different purposes.

1.2 Objectives

The main scope of this project is the design and development of a dual-band antenna with two metal layers for possible use in security, health/medical care, or personnel tracking applications, and for integration into an ankle bracelet-wearable device. This antenna has been conceived to operate in the 2.4 GHz Industrial, Scientific and Medical (ISM) Band, and in the upper Navigation Services L1 bands, in the context of off-body communication systems.

Within the 2.4 GHz ISM Band, it is intended to cover the BT band (2400 - 2483.5MHz, including guard bands 2 MHz wide at the bottom end, and 3.5 MHz wide at the top), and Wi-Fi 802.11 (2401 - 2495 MHz). The upper L1 bands include Global Positioning System (GPS) L1 (1563 - 1587 MHz), Galileo E1 (1559 - 1591 MHz) and GLONASS G1 (1593 - 1610 MHz).

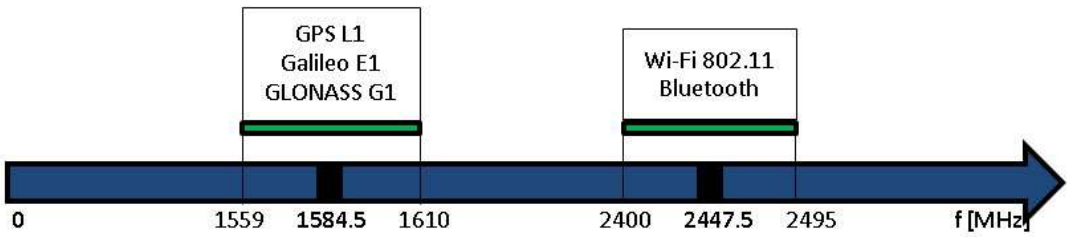

Figure 1.1: Frequency bands of interest

The proposed antenna should have good performance in different scenarios, taking into account the S-Parameters, radiation patterns and radiation efficiency around the operating frequencies of interest. Considering the most common criterion in antenna design, the S-Parameters should be below - 10 dB for both the reflection and transmission losses. Regarding the radiation efficiencies, there are not recommended values, even though GPS antenna efficiencies are typically on the order of -9 dB to -3 dB (12.5 - 50 %) [5], and Wi-Fi antenna efficiencies for handheld mobile devices are typically on the order of -6 dB to -2 dB (25 - 63 %) [6]. The antenna should work near the human ankle and, therefore, its radiation patterns should be directed off-body and above the ankle.

The miniaturisation of the global antenna structure should be of concern, as well as the study of bending and casing scenarios in order to fit into a commercial ankle bracelet. Moreover, according to International Commission on Non-Ionising Radiation Protection (ICNIRP), the levels of SAR for extremities such as hands, wrists, feet, and ankles must be higher up to 4 W/kg for any 10 g.

The final objective of this project is to fabricate and test a prototype of the proposed antenna, at least in free-space conditions, in consideration of the agreement with the simulation results and fulfilment of the requirements specified above.

1.3 Dissertation Outline

This dissertation is structured in five chapters, including this introductory one. As seen before, this first chapter described the motivation, objectives and dissertation outline.

Chapter 2 is related to the state-of-the-art of wearable antennas used for bracelet devices and their applications. Firstly, this chapter provides a very brief overview of conductive materials, dielectric materials, fabrication methods and techniques suitable for the development of bracelet-wearable antennas. the more common human body models for numerical simulations are also described. Thereafter, some relevant antennas used in the context of wearable applications are presented. Lastly, in this chapter, the human body proximity effects on the antennas are featured and Body Centric Wireless Communication Systems (BCWCS) are briefly investigated through the introduction of the most important bracelet antennas applications.

In Chapter 3, the design procedure of the proposed antenna is described, by including the choice of the antenna structure and geometry, substrate material, conductive material, feeding structure, and the fabrication method/ technique. A set of simulations and measurements were performed through the evaluation of free-space results for return loss, gain, operation bands, radiation pattern and radiation efficiency. The measurement setup is detailed, by including the measurement steps needed.

Chapter 4 describes the procedure that was carried out, in order to study the bending and casing effects on the antenna performance (already optimised in Chapter 3), already optimised in the previous chapter. It is presented the chosen human body model, and the simulation results of the study related to the effects of human body on the antenna near-field region.

Finally, Chapter 5 summarises the work performed throughout this dissertation, important conclusions, and further considerations. Outlook for future work is suggested here, based on the key topics identified in previous chapters.

Chapter 2

State-of-the-Art of Wearable Antennas

In section 2.1, the most commonly used materials in wearable antennas are shown, by focusing more on the context of bracelet devices. This section comprises two subsections: one dedicated to conductive materials and the other dedicated to dielectric ones. Here, not only the traditional materials but also the more and more trendy and forward-looking ones are discussed.

Section 2.2 shows the most popular techniques used for fabrication of wearable antennas. From the most conventional technique, line patterning, to the most recent recent Additive Manufacturing (AM) processes, many others are briefly described, taking into account their main advantages and disadvantages.

Section 2.3presents some examples of wearable antennas, each one accompanied by a general overview of the most significant results, in terms of radiation performance in the context of certain applications/services with the citation of pertinent graphics and tables presented in literature, whenever possible.

In section 2.4, it can be seen how to evaluate the interactions between the human body and the electromagnetic waves radiated from antennas, by using numerical models or tissue-equivalent experimental phantoms, instead of using a real human body. Here, theoretical and voxel phantoms are also approached.

Finally, in section 2.5, some examples of applications/services within the contexts of medical/health care, security and rescue, and sport applications/services are introduced, considering the different types of communication covered by the Wireless Body Area Network (WBAN).

2.1 Materials

The design procedure of wearable antennas comprises different steps, varying from choice of materials to antenna measurements. Firstly, materials are chosen, properties of the selected materials must be collected, and then radiating patch, feed positioning and feed line are properly designed, simulated and optimised [7].

2.1.1 Conductors

For conductive materials, certain requirements must be accomplished, including high conductivity, cost-effectiveness, waterproof, resistance to tensile strength, and oxidation/corrosion resistance. In case of integration with textiles, flexibility (bending, stretching and crumpling) and capability to be sewed and embroidered must be considered. However, this last scenario is not the main issue of interest, in this dissertation.

Pure Metal

These materials are used in respect to wearable textile-based antennas, namely silver paste [8], copper gauze [9], as well as copper and aluminium foils (other metal foils may also be utilised as stated in [10]).

The main advantages of using such materials should be highlighted: high conductivity, cost-effectiveness and fabrication simplicity (using soft Printed Circuit Board (PCB) fabrication process [10]). Additionally, when the above-referred metallic materials are integrated with clothing textiles, adhesive laminates or supporting foams, sewing and embroidering can be avoided.

Conductive Ink

Conductive ink consists of printed objects which conducts electricity, by infusing graphite or other conductive materials into ink. This metal may be regarded itself as a new solution for flexible antennas design.

Their main advantages are the following ones: fabrication simplicity, low manufacturing cost, suitability for industrial scale-up, and compatibility with standard screen-printing and inject-printing fabrication methods. The effective conductivity is achieved by doping the intrinsic material with solvent impurities, through the thermal annealing process [11]. However, this process can deform or even degrade the under-lying substrate, limiting applications on textiles.

A different approach using metallic nanoparticles inks is frequently used, but their high surface area can interact with atmospheric water or oxygen. This property leads to faster oxidation and degradation than using bulk metals [12].

Conductive Graphene Layers

The need of higher efficiency and reduced CO_2 emission is moving forward to the use of carbon-based materials in attempt to reduce the number of metal parts, as far as possible. Disposable and environmentally friendly materials are thus required for today technology [12].

Metal parts of the antennas have a high specific weight, which represent a high cost in terms of thermal energy, and can suffer from oxidation and corrosion. In general, the production of wearable antennas involves chemical etching, which requires various pollutant chemical agents, could also damage the substrate [12].

A graphene layer consists of combination of carbon atoms, arranged in a honeycomb lattice. Ideally, a single monolayer of graphene could even show better conductivity than the most conductive metals, such as copper or silver. Ideally, its high mobility of charges and high charge density combined together allows a high conductivity, low sheet resistance, and a high optical transparency. In order to get a better view, its conductivity can reach approximately $5\ 10^8$ S m $^{-1}$ (it is known that the electrical conductivity of pure silver and copper are $6.3\ 10^7 \mathrm{S} \cdot \mathrm{m}^{-1}$ and $5.98\ 10^7\ \mathrm{S} \cdot \mathrm{m}^{-1}$, respectively[1]) [12].

[1] The electrical conductivity depends on the temperature of the metal material. These ones are the reference values at 20 ºC

Conductive Spray

More recently, spray-printing antennas on surface is a promising solution that has been creating new opportunities in terms of size, weight, flexibility, and possibly even transparency.

The basic component of these conductive materials is called MXenes. MXenes consist of a combination of carbon or nitrogen atoms that creates a material, with a few atoms thick. Besides, these promising materials can be made by using different metals such as titanium, molybdenum, vanadium and niobium.

Moreover, they are transparent to light, electronically conductive, chemically stable, very strong and a stable water-based ink, when mixed with water. MXene antennas are made through a nano-materials fabrication process, in two steps: (1) by mixing the MXenes with water, and (2) by spraying it on with an airbrush.

These conductive materials could outperform antennas made of other high-tech nanomaterial-based materials, such as carbon nanotubes, graphene and nano-silver ink [13].

2.1.2 Dielectrics

Dielectrics of substrate materials are mainly used to support the above-referred conductive elements of the antenna, in the previous subsection 2.1.1. According to the properties of the conductive materials utilised in the design, different types of flexible substrates are adopted. In this respect, the permittivity, flexibility and loss tangent, amongst others, are the properties that matter the most. In this subsection, both cutting edge and conventional substrates films are approached.

Soft PCB Substrate

In respect to soft PCB processes, flexible films are the principal materials for supporting overlays, namely Polyimide (PI) films [14] [15], polyester films (commonly referred to as Polyethylene TerePhta-late (PET) films) [16] [17], and Liquid Crystal Polymer (LCP) films [18] [19] [20]. All of these ones have common advantages, such as high flexibility, low loss tangent, and availability of low thicknesses. Kapton®, for example, being a high-performance PI film, has a good soldering tolerance to flexible antenna fabrication, and is able to resist high temperatures, which is required in thermal annealing of ink-jet-printed antennas [21]. Furthermore, it is easier to electrodeposit pure metal materials [14] [18] [19] [22] and conductive inks [15] [17] [10] onto these soft films of base substrate.

Paper

Paper substrates can be utilised in screen-printing and inkjet-printing fabrication methods based on conductive inks. Paper is a light weight, low cost, biodegradable material that comes from a renewable source [23]. Furthermore, paper can be modified to have hydrophobic and re-retardant properties [24]. However, it is also lossy and frequency-dependent. A dispersion model is required for accurate Radio-Frequency (RF) simulation and analysis [25].

PolyDiMethylSiloxane (PDMS)

Polymers, such as PDMS, are a good solution when it comes to rheological properties, water-resistance, stability under high temperatures, and capability of being modified to achieve higher permittivity values. However, high cost and manufacturing complexity (described in [26] [27] [28] constitute their main disadvantages).

Foams

Foam substrates are mainly used for the purpose of mechanical support, because their dielectric constant is very close to that of air. Foam substrates can be embroidered within clothing, with no precise patterning of conductors required, and are low-cost. According to [29] [30], the wearable antennas concerned are fabricated using foam substrate.

2.2 Fabrication Techniques

Following on from what was previously written, in respect to the choice of materials (as explained in section 2.1), depending on antenna topology and type of materials used in design process, a fabrication technique is selected. Lastly, the antenna must undergo a series of measurement tests that could be more or less stringent (in accordance with project requirements), regarding its S-Parameters, radiation patterns, gain, operating band and efficiency. Besides these conventional tests, other ones must be realised in order to fulfil all requirements such as SAR, bending, crumpling, durability, involves taking out the printed mask, applying an ultra-sonic energy on the substrate, in a toluene solution for robustness, humidity, thermal, and Electromagnetic Compatibility (EMC) [7].

Line Patterning

Line patterning is one of the simplest and cheapest solutions when it comes to fabrication of Radio-Frequency Identification (RFID)s and flexible electronics. First, it is developed a design of a negative figure of the intended pattern, with the aid of a computer design program. Secondly, a conductive polymer is deposited on the substrate. The last step involves taking out the printed mask, applying an ultra-sonic energy on the substrate, in a toluene solution for about 10 seconds [3]

Screen-printing

Screen-printing is another cost-effective technique used by flexible electronics manufacturers, particularly in respect to flexible transparent antennas and RFIDs [31]. This technique is fast, simple and, at the same time, environment-friendly.

Firstly, it is developed a mask with the desired pattern, developed and then applied directly on a flexible substrate, where the conductive ink must have to be thermally treated to evaporate the solvent excess.

However, there are some drawbacks related to this technique, which include the temperature dependence of its inks needed, as well as the limited thickness of the deposited ink layers and resolution of the deposited patterns [7] [32].

Flexography

This technique, similar to a letterpress, consists of a print-making process of a figure, which is obtained by applying ink on a protuberating surface of the printing, plate while predetermined areas are left ink-free. The thickness of the printed image depends on print speed and pressure [7] [32].

Flexography is mainly used for packaging applications and significantly used for fabrication of RFID, because of its cost-effectiveness, relatively high resolution of figures (but limited as shown in [33] [34]), and compatibility with web processing [35].

Comparing to screen-printing technique, it is required a lower viscosity ink but, even though it is necessary to have higher conductivity, in order to decrease the sheet resistance, due to the fact that the efficiency of the antennas depends on the electrical conductivity of the radiating element.

Photolithography

Photolithography initially emerged to target the PCB industry. Nowadays, this technique is the most common for fabrication of printed Ultra-Wide Band (UWB) antennas [32]. Firstly, photo-resist and chemical agents must be used, in order to corrosively remove the undesired area. Hence, it is then possible to produce the desired metallic patterns. In fact, this technique can produce accurate patterns with fine details [7].

Currently, the fabrication of antennas and RF circuits based on photolithography is preferable to be led, by using corrosively positive photo-resists, because those negative photo-resists often result in a swell-edging, which compromises the consistency and resolution of the resulting pattern. When photolithography is carried out to produce flexible electronics, single or double-sided substrates are used, where the intended pattern is achieved by etching regions of either or both sides. Furthermore, this technique offers the possibility of stacking multi- flexible patterned layers [7].

The main disadvantages of photolithography are the following ones: low throughput, high time consumption, high labour intensity, high-cost, as well as the involvement of environmentally detrimental waste and hazardous chemicals (the etching solvent is corrosive, for example). Thus, it is not very suitable for commercial production [7] [36].

Thermal Evaporation

Thermal evaporation consists of a vapour deposition process, which is one of the most widely deposition techniques used of thin films. This method involves a vacuum process, where a pure material coating is administered over the film surface.

This process is conducted by heating a solid material inside a vacuum chamber, where a vapour pressure is created. Consequently, the evaporated material is deposited on the substrate. In antennas and RFIDs, the coating material is usually a pure metal. It should be noted that this process is usually accompanied by a photolithography process [7] [37].

Ink-jet Printing

Ink-jet printing of antennas and RF circuits, using highly conductive inks based on nano-structural materials, are extremely popular nowadays. Ink-jet material printers operate by releasing pico-litre sized ink droplets, which give rise to high-resolution patterns and compact designs [7].

Electromagnetic Band Gap (EBG) arrays can be fabricated using ink-jet printing in [38]. Furthermore, inkjet printing can also be combined with AM processes such as stereo-lithography in [39].

3D Printing/Additive Manufacturing (AM)

Now, it is presented the trendiest technique that allows the fabrication of complex structures from a digital model, by printing layer after layer. AM has becoming more and more an alternative to traditional manufacture methods for customised objects [39] [40]. Within the area of electronics [41], antennas and microwave systems engineering can bene t with lighter weight waveguides fabricated by copper plating plastics forms [42]; substrates with new properties [43]; development of innovative Frequency Selective Structures (FSS) with fully [44], and partially [45] metalising 3D printed elements; fabrication of non-uniform EBG structures on printed substrates [40] [44]; antennas testing in 3D printed phantoms [46], as well as the development of nanoparticle silver inks that can be used for inkjet printing technique.

One of the most common and low-cost 3D printing fabrication techniques is Fuse Filament Fabrication (FFF), in which 3D objects are created by melting plastic and then deposited in layers. The dominant plastics are Polylactic Acid (PLA) and Acrylonitrile Butadiene Styrene and Acrylonitrile Butadiene Styrene (ABS), being standard PLA suitable for wearable antennas (as in [47]), where a Wireless Local Area Network (WLAN) antenna was integrated into a 3D printed bracelet [39] [40] [46].

Within AM, it is worth to note that there is a laser-based layer-by-layer additive process, stereo-lithography, used to fabricate RF microwave components. This process is a rapid tool-less fabrication technique that is well described, systematically in [48].

2.3 Wearable Antennas in the Literature

In the general context of microwave systems, according to [49], there are four distinct standard categories of antennas that can be developed for different applications and services (see Table B.**1**).

In fact, from that table of Appendix B, in respect to wearable antennas, the category of interest is the printed antenna. This subgroup of microwave antennas enables easy integration with fabrics of Microwave Integrated Circuit (MIC) and active wearable devices. According to the different types of communication in WBANs, the possibilities that these antennas can provide are referred through the next main examples found in the literature.

On-Body Communication

In [50], a low-profile antenna composed of eight planar dipole antenna elements, symmetrically around the z-axis and with monopole-like radiation for WBAN on-body communications, was proposed. This antenna can cover the ISM 2.45 GHz band (2.4-2.485 GHz) and, being designed considering the human body effect, has overall dimensions of 0.44 λ_0 x 0.44λ_0 x 0.013 λ_0 at 2.45 GHz, in the ISM 2.45 GHz band, as well as a -10 dB return loss bandwidth of 4.9% ranging from 2.4 to 2.52 GHz.

The antenna was fabricated on a FR-4 (ε = 4:4, tan δ = 0:0245) with a substrate of 1.6 mm thick. The antenna is excited by a centred coaxial cable. The dipole element is 1.4 mm wide and 11.8 mm long.

In order to experimentally analyse the antenna performance, a two-thirds muscle-equivalent semi-solid phantom (ε = 35:5, σ = 1.2 S $\cdot$ m^{-1}) with dimensions of 200 mm 200 mm 70 mm was used.

In [52], a planar Medical Implant Communication Service (MICS) band spiral microstrip antenna of dimensions 2.5 $\times$ 1.8 cm^2 and 2 mm thickness is combined with an electrode for Body Communication Channel (BCC). The radiating element and ground plane of this antenna are placed side-by-side, and can be attached to human body. The proposed design enables a body sensor network controller to communicate with health-care devices located on and inside a patient's body.

The body channel with propagation losses is measured when the proposed antenna is used as the skin interface for BCC, in the 10-70 MHz band and for 20-150 cm distances. The equivalent-circuit model of the antenna as the electrode is also derived from the measured impedance characteristics, leading to an LC circuit.

The operating frequency of this on-body antenna is 400 MHz and its bandwidth is 36 MHz. The path-loss measurement, inside the human phantom, shows that the signal radiated from the proposed antenna attenuates with a 28 dBm^{-1} rate, and the minimum power received by the implanted antenna is 75 dBm, at 1.2 m distance. Due to the protective layer on the radiating element of the antenna, the 6 dB channel loss is added. The electrical circuit modelling of the on-body antenna in the 25-100 MHz frequency indicates that the capacitance of the antenna increases three times due to skin contact. To drive the large capacitive load of the antenna with low power consumption, the LC series resonance is used in the BCC transmit buffer. As a result, the power saving of 50% - 70% is achieved.

Off-Body Communication

In [51], the first time that were applied 3D printing techniques related to development of conformal antennas, for diversity wrist-worn wireless communications, is proposed.

In relation to the antenna fabrication, three processes concerning the deposition of metallic layers on a bracelet by using FFF are described (see [51] to understand each process).

The fabricated antennas cover 2.4 GHz and 5.5 GHz used for WLAN communication with the reflection coefficients less than -10 dB, and are nearly omnidirectional in free-space and directional in the close proximity of human wrist. When the three WLAN antennas are combined, the radiation patterns improve, in all directions, for the transmitting or receiving signals (particularly for off-body applications), due to antenna system diversity.

These antennas were fabricated at different positions and shape angles within the bracelet.

As it is known, dipole antennas are one of the simplest radiating structures that can be used for testing and fabrication processes, as well as for evaluation of the human body effects on antenna performance.

Here, each dipole arm has two sections, the longer (L) for the 2.4 GHz and the shorter (S) for the 5.5 GHz WLAN bands. The final dimensions of the dipole antenna, with such two resonant arms at each end, are as followed: A = 42.4 mm, B = 9 mm, S = 9 mm, L = 24 mm, G = 0.4 mm, T= 2 mm.

The inner radiuses of the elliptical bracelet substrate are 35 and 30 mm, and the thickness is 3 mm. Low-cost PLA material with dielectric constant of ε = 2:4 and loss tangent of tan δ = 0:01 is used as substrate.

For the study of the human body effect on wrist-worn antenna, a three-tissue body model was used. The antenna and bracelet are mounted on an elliptical non-homogeneous human tissue layer-based model with the following dimensions: skin (1 mm), fat (2 mm) and muscle (29 mm). The length of the wrist model used for the simulation was 24 mm. The human body produced a shift in the operating frequency, and significantly reduced the back-radiating power.

In order to achieve diversity, two more antennas were added symmetrically at a distance of 50.3 mm from the antenna at the centre. In this way, each antenna may be connected to its own RF circuit, being able to send information such as location of the wearer.

In-Body Communication

In [53], a compact printed meandered folded dipole antenna, with a volume of 114 mm^3, which is suitable for implantation in a range of different body tissue types with different electrical properties, was proposed. This antenna operates in the 2.36 - 2.4 GHz Medical Body Area Network (MBAN) band, and 2.4 GHz ISM bands.

Its performance was compared with that of a wire dipole and slot loaded monopole antenna in an implant phantom testbed, containing tissue equivalent liquids which emulate body tissues with high and low water content. The proposed antenna can achieve an equivalent or better return loss, radiation efficiency and total radiation efficiency performance in the bands of interest, having approximately half the physical length in comparison with a fundamental wire dipole antenna. It must be noted that this Printed Folded Meandered Dipole (PFMD) can be integrated with a battery and transmitter circuit.

2.4 Human Body Models

Interaction with the human body requires validation of the antenna performance. A numerical model can be designed and simulated, but that could not be enough in order to have a realistic idea about the environment, which is subject to various interferences. Thus, there is a need for validation of any wearable devices to have measured in a special non-free-space condition (see [54])

Testing a newly designed device that is expected to have significant interaction with the human body may harm a living body. As an example, Implantable Medical Devices (IMD) are used for imaging of the human body from inside. Hence, for security purposes, it becomes important to

have physical body phantoms or Artificial Tissue Emulating (ATE) phantoms. A phantom can be a simulated biological body, numerical phantoms, and/or a physical model that is capable of simulating properties of biological tissues or even whole organs. A phantom must be anatomically realistic, as well as have a long lifetime and dielectric precision across a certain frequency range [54].

Phantoms can be classified in terms of frequency range, as well as tissue type intended to emulate. For the majority of human tissues, the water content of the tissue cells is a good distinguishing criterion. Low-water content tissue, such as bones and fats, relates to low permittivity and low loss tangent. High-water content tissues, such as brain, muscle, and skin, relate to higher permittivity and loss According to these criterions, a phantom can also be classified based on the manufacturing material, which can be liquid, gel, semisolid (jelly/gel), or solid (dry) [54]. That being said, considering well-known properties of the human tissues, phantoms can be Physical (real physical structures) or Numerical (simulated biological tissues).

Theoretical Phantoms

Firstly, it is worth to be noted that these numerical phantoms have a simple shape, taking into account the reduction of simulation time [55]. The human phantoms could be modelled as homogeneous (single-layer) or as heterogeneous (multi-layer). Single-layer or layered at phantoms are the simplest ones to evaluate Electromagnetic (EM) dosimetry. In these phantoms, energy is radiated from simple sources such as a plane wave, half-wave dipole or a small dipole antenna. Spherical models are mainly used for evaluation of EM dosimetry inside the human head and eyes. Cylindrical shaped phantoms are used for arms and legs, or even as whole-body model.

Voxel Phantoms

Voxel phantoms are more realistic and complex than those theoretical above-mentioned. Recent progress in medical imaging technologies, such as Magnetic Resonance Imaging (MRI) and Computed Tomography (CT) and huge advancement in computational capability regarding time and complexity have been allowing the development of more and more precision body voxel models [54].

Voxel models are composed of several elements, voxels, which are more detailed, by many different containing parameters of the simulated human tissue. In addition, SAR results inside a certain voxel model can vary for different age, weight and gender, for example, which justifies the development of voxel phantoms with higher spatial resolution and many different types of tissues, according to the underlying application [54].

2.5 Applications

Before presenting the different types of applications and scenarios focused in the context of bracelet-wearable devices, it is crucial to present all the today's different types of communication that can exist in the vicinity of the human body. According to the type of communication, WBAN can be separated in four distinct categories: On-Body, Off-Body and In-Body (see Figure 2.1 adapted from [56]).

The first category of WBAN is On-Body communication. In this case, communication occurs between different wearable devices that are mounted on the same body, by exploiting the relatively high conductivity of certain parts of the human body, in order to transform it into a transmission channel for wireless signals. In short, this communication uses the human body itself as a transmission medium or channel. Thus, it is more commonly used in the context of medical7health care applications to ensure ongoing monitoring of biological signals and thereby assist in the prevention, diagnosis, and rehabilitation.

The communication between any of the body-worn devices and an external unit characterise an Off-Body communication. Smart phones, tablets, home appliances, computers, base stations or even other wearable devices mounted on a different wearer. The last one could lead to a sub-group of Off-body communication the so-called Body-to-Body communication.

In-Body communication provides a communication between implanted devices and devices mounted on the human body surface. This type of WBAN category raises an important issue related to the lossy nature of the human tissue that absorbs electromagnetic energy, causing a strong attenuation. Hence, in-body communication is mainly used for medical purposes.

Any WBAN must guarantee certain important specifications, such as the following ones [57]:

- **Higher Security:** confidential user data;
- **Sensor Integration:** guaranteed usability;
- **Cost Structure:** miniaturisation and human compatibility;
- **Topology Changes:** human body movements (translation, rotation, etc);
- **Heterogeneous Nodes:** several sensor functions in each node;
- **Early Event Detection:** taking into account emergency states;
- **Channel Models:** modelling human body;
- **Context Awareness:** system response based on current situation.

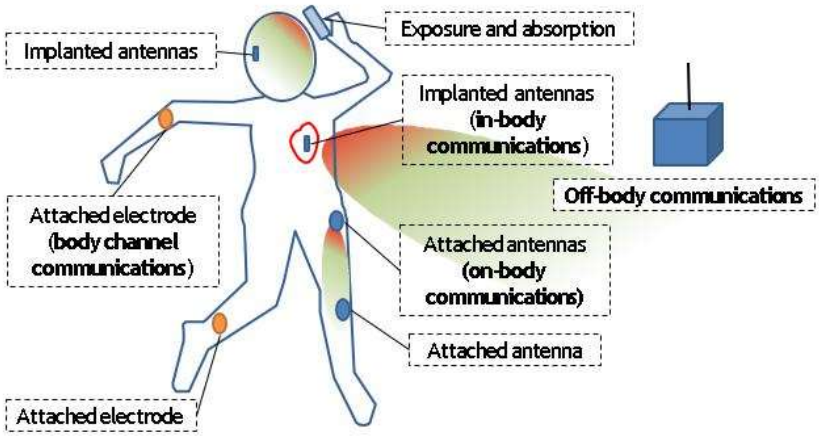

Figure 2.1: Types of communication in a Near-Body Radio-wave Propagation

Medical/Health Care

In fact, medical applications and IMD exploit, on a large-scale, the concepts of WBAN [58] and MBAN [53], by reducing medical costs and, at the same time, improving people's health and quality of life. It is obtained through the monitoring of user's biological signals, movement patterns and/or body posture with the aid of implantable and wearable wireless sensors. These real-time systems sense, sample, and forward underlying information to a centre device, coordinator, which processes the data for diagnostics, prescription, wellness, entertainment, or security purposes.

Recent examples of IMDs include wireless implantable heart failure monitoring systems [59], brain-computer interface [60] and artificial bladder sphincter control devices [61].

According to [58], the existing applications in the context of medical/health care are the following ones:

- **Telemedicine:** Monitor patient's health and treatment outcomes. Apps: Remote Health monitoring; emergency rescue; chronic diseases monitoring; prevention and detection of diseases; daily-life activity monitoring; post-surgery in-home recovery monitoring user data. As representative technologies, there are accelerometers Electroencephalogram (EEG), Electrocardiogram (ECG), blood pressure, temperature and respiration sensors;

- **Rehabilitation:** Assist with rehabilitation of patients with mobility problems. Apps: Daily lifeand rehabilitation. As representative technologies, there are accelerometers, EEG, ECG, posture, gyroscopes, magnetometers and respiration sensors;

- **Assisted Living:** Improve quality of life for people with disabilities. Apps: Assisted living for elders; treatments of people at home. As representative technologies, there are accelerometers, EEG, ECG, blood pressure, temperature and location sensors;

- **Biofeedback:** Assist with controlling emotional states. Apps: User biofeedback activity. As representative technologies, there are EEG, ECG, blood pressure and posture sensor.

Security and Rescue Service

In these applications, wearable antennas are mostly used for security and defence applications, within different rescue services, such as firefighters, mountain and water rescue workers. Wearable devices in today's operations of modern security and rescue services are important as shown in [62]. Different parameters can be monitored with units integrated in their garments like psychological parameters, actual position or the environment and weather conditions on the field where they operate [63].

Frequency bands intended for security and rescue applications are regulated by special government regulatory offices. Besides, there are two key requirements for most of the wearable antennas used in security and rescue applications: the size miniaturisation and the resilience of the antenna to the environment and weather conditions [63].

Sports

Nowadays, people enjoy tracking their performances, while practising sports activity. Wearable ap-plications can track positions and record speed, elevation, distance, amongst other parameters.

Although most of the tracking can be performed with the current smartphones, some wearable devices also exist. Several wristwatches with built-in GPS antennas, that allows the wearer to collect certain parameters, even including the heart rate, can be found on the market. Here, wearable GPS antennas play an important role in terms of performance [63]. Furthermore, for the purposes of professional athletes, wearable devices are used in a more extensive manner, because all the collected data from different wearable sensors are analysed, and used for further improvement, in respect to sports-people performances [64].

Interesting examples of wearable antennas intended for integration into the shoes [65] [66], as well as wrist devices [66] are presented. Two different UWB wearable antenna prototypes (a monopole and a Vivaldi antenna) are proposed, in order to provide a link between the footwear sensors, and the rest of the body-centric network [65]. In respect to overall communication, the channel properties and the influence of certain foot movements are studied [66].

Chapter 3

Ankle Bracelet Antenna Design in Free-Space

The purpose of this work is to develop and test an ankle bracelet antenna for off-body communications, in the vicinity of the human body. Wi-Fi, BT and GPS bands were chosen because the communication systems, based on the technology required to the applications previously referred, demand at least these three operating bands.

Amongst the wide variety of existing dual-band antennas, it was favoured a configuration with low cost, lightweight, simple fabrication technique, and adequate low thickness, compactness and flexible materials in order to fit into the reference bracelet model. In more technical terms, the chosen antenna must have a minimum impedance bandwidth around the central frequencies under consideration and appropriate radiation patterns and efficiency. This chapter provides an overall analysis of the suggested antenna behaviour in the free-space context. Primarily, a flat antenna structure is simulated based on a parametric study of the respective parameters and then, after a suitable optimisation, the final prototype design is presented.

Firstly, subsection 3.1 presents the structure of the suggested antenna, making reference to the work that served as a starting point for the study of the proposed antenna behaviour in free-space. The structure and geometry of the reference antenna is then described in subsection 3.1.1, inspired in [4]. In subsection 3.1.2, the initial choice of the substrate material, as well as the initial dimensions of radiating elements and ground plane, are presented and explained. In subsection 3.1.3, the chosen way to approach the study of the feed line and position is discussed.

In section 3.2, from an initial antenna design with certain values for its own parameters as well as from a fixed feed position with discrete ports, a parametric study varying the design parameters is carried out in order to understand their effects on the antenna behaviour. Finally, an overview of the main conclusions according to this parametric study in terms of S-Parameters is carried out.

In 3.3, feeding is simulated in different positions. Once optimised these positions (after time and effort spent), coaxial cables are included instead of discrete points and simulation results compared. In view of decoupling problems issues encountered between the two feed points, section 3.4 analyses the use of defected ground structures in order to mitigate them. Once the most favourable solution has been chosen, in terms of S-Parameters, the radiation patterns and efficiency issues are raised and analysed.

In 3.5, subsection 3.5.1 presents a flat antenna prototype and the fabrication process is briefly explained. The measured results for both return losses and operating bands are presented in 3.5.2.

Lastly, in Section 3.6, the main conclusions of this chapter are reported. Additionally, some considerations are done before moving to the next chapter.

3.1 Flat Structure Design

In [4], an existing bracelet antenna is studied. In that work, it is shown that the design concept of the antenna has good performance, when applied to smartwatches.

In this dissertation, the developed antenna structure has two metal layers, and its prototype can also be fabricated with simple techniques. The proposed antenna fits into a commercial ankle bracelet, which motivated the use of this antenna concept in this study. Considering the requirements presented in Chapter 1, the antenna is then designed and optimised for the operating bands of interest: BT, Wi-Fi and the upper L band (1559 - 1610 MHz), having the GPS L1, Galileo E1 and GLONASS G1.

3.1.1 Structure and Geometry

According to [4], the structure consists of two rectangular metal layers placed closed together being connected by two shorting walls and having a common ground plane (see Figure 3.1). The initial values of different parameters are shown in Table 3.1.

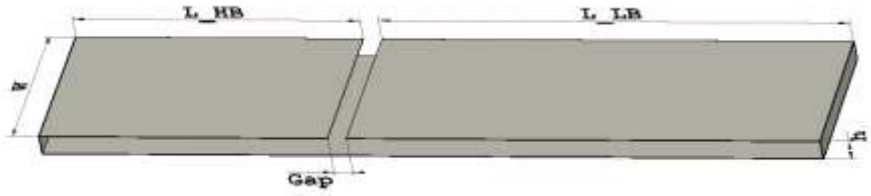

Figure 3.1: Reference Structure of the Antenna

Table 3.1: Initial values for the parameters of the proposed antenna

Parameter	Value [mm]
h	2.5
Gap	2
W	20
L_HB	30.6
L_LB	47.3

As a first approximation based on [30], the initial values with respect to high band and low band radiating element lengths (L_HB and L_LB) were chosen taking as reference the quarter wavelength corresponding to the intended centre frequencies (see expressions (3.2) and (3.3)). These centre frequencies for the lowest and highest bands are respectively $f_{LB} = 1.5845$ GHz and $f_{HB} = 2.45$ GHz. According to the expression (3.1) that relates the speed of light and these centre frequencies, it is not difficult to determine those lengths.

$$\lambda = \frac{c}{f} \tag{3.1}$$

Taking then as reference the above quarter wavelength relation,

$$L\_LB = \frac{c}{4 \times f_{LB}} = 47.3\ mm \tag{3.2}$$

$$L\_HB = \frac{c}{4 \times f_{HB}} = 30.6\ mm \tag{3.3}$$

The values for h and W were chosen considering the approach in [4], the maximum dimensions of the reference bracelet, and margin enough for parametric study in 3.2.

3.1.2 Radiating Elements, Substrate Material and Ground Plane

It is known that the performance of a printed antenna depends on the choice of the substrate, feeding lines, and in this case on the bracelet device's shape and radiating elements materials.

At a first stage, in 3.1.3 and 3.2, the radiating elements, ground plane and the shorting walls of the antenna structure are 3D modelled with Perfect Electrical Conductor (PEC) with a thickness of 0.1 mm. In 3.3.4, and from then on for the purposes of simulation, the metal parts of the antenna are modelled with pure copper, with similar electrical properties to the *Kapton*™ material, anticipating that the antenna must be bent (Chapter 4).

The substrate material used between the radiating elements and ground plane was air. This approach was followed for reasons of simplicity. Further on, there was a need to insert a different substrate material due to the fabrication process. The change of substrate material can make the global structure of the antenna more compact, and it can as well shift the centre frequencies to lower resonant ones (see a section related to the effect of a high permittivity material on overall antenna performance in [4]). To summarise, in this project, the only constraints considered for the substrate material were then the following: very low permittivity, and flexibility and robustness in order to withstand the bending process and fit into the bracelet (described in Chapter 4).

3.1.3 Feed Line and Feed Point

Antenna feeding arrangements impact the simulating of S-Parameters. Even the coaxial cables length counts, as can be seen later in 3.3.4, due to the relatively small dimension of the ground plane on the antenna structure.

In the next figure, the initial approach for the feeding position, by using discrete ports, is shown. This approach is used through the parametric study of the flat antenna.

Figure 3.2: Initial approach for feed line and feed point

3.2 Parametric Study of the Flat Antenna

In this section, a parametric study of the flat antenna is carried out. The parameters include height h, width W, high band radiating element length L _HB, low band radiating element length L _LB and gap. Their values were swept around their optimal values to find out the influence on the antenna behaviour.

In addition to the mentioned parameters, as stated before, throughout these parametric studies, the parameter range and some design constraints are also defined. Then, the results of each parameter sweep are analysed, considering the goals related to return loss, operating bands, bandwidth, as well as isolation between ports.

First, it is important to specify what are the reference values for return loss and isolation between ports to be accomplished. S-Parameters should be at least - 10 dB for both the reflection and transmission coefficients over the bandwidth around the centre frequencies of interest.

For all the simulations presented from now on, it was always used a *Setup Solver* with the following properties:

- ***Module:*** *Time Domain Solver* (more efficient for most high frequency applications);
- ***Mesh Type:*** *Hexahedral;*
- ***Accuracy:*** - 30 dB.
- ***Optimizer:*** *Trust Region Framework*

3.2.1 Height

The simulated reflection and transmission coefficients are shown in Figure 3.3 and Figure 3.4, respectively. Values of 1, of 2.5 and 4 mm have been considered. The upper value of this parameter range was chosen so that the reference ankle bracelet model has an available space of roughly 5 mm to case the antenna (as seen later in section 4.1 of Chapter 4. For that reason, it was decided to guarantee a margin of 1 mm, at least.

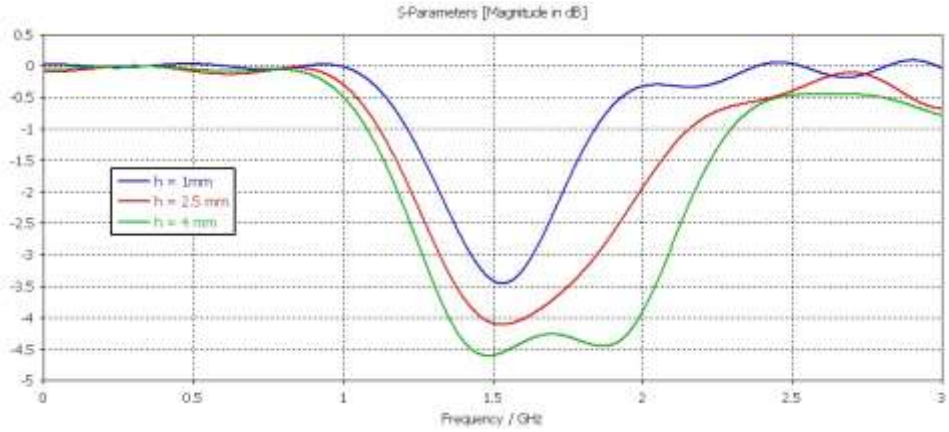

Return loss of the low band port (S_{22})

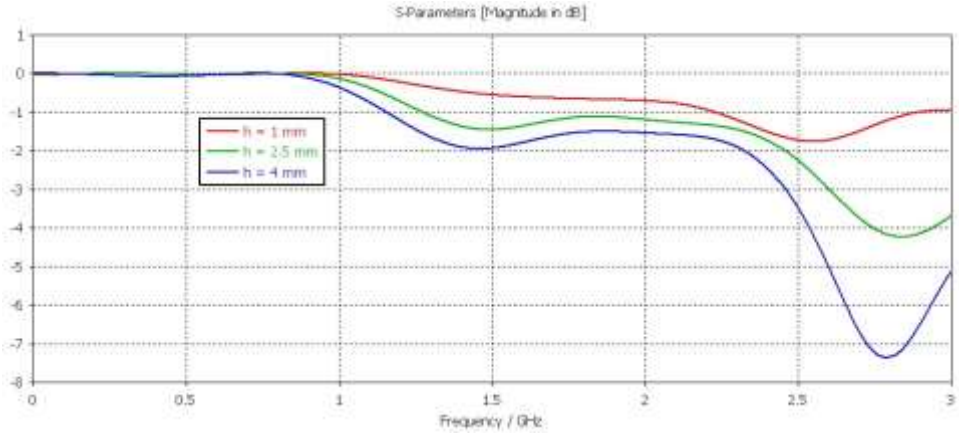

(a) Return loss of the high band port (S_{11})

Figure 3.3: Return loss by changing the height h

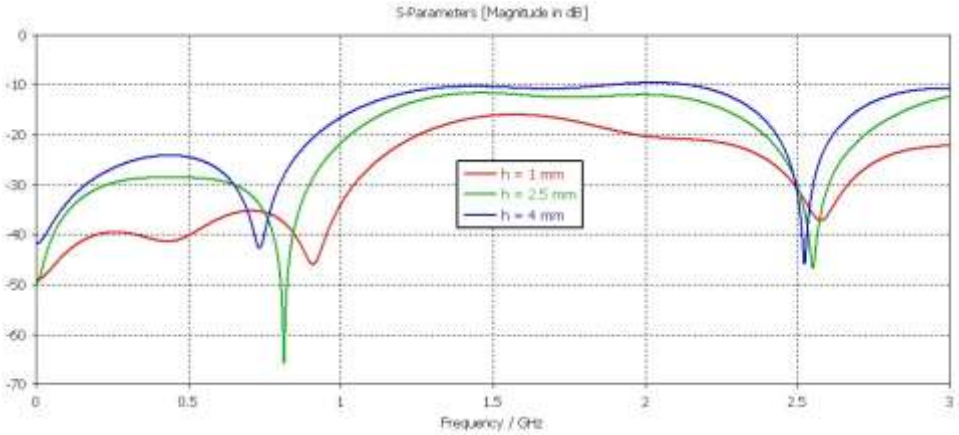

(a) Decoupling between the high band port and the low band port (S_{21})

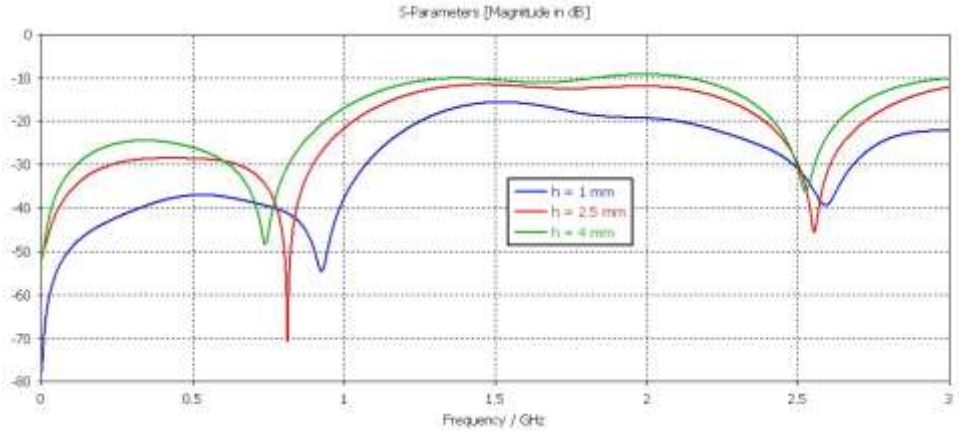

(b) Decoupling between the high band port and the low band port (S_{12})

Figure 3.4: Decoupling between ports by changing the height h

From Figure 3.3, it can be concluded that the return losses (S_{22} and S_{11}) and respective bandwidths, around the centre frequencies of interest (1.5 GHz and 2.45 GHz), are better and wider for higher values of h, respectively (see curve of h = 4 mm). S_{22} values do not match the minimum of -10 dB. Even though S_{11} values are still above the target required, they are much closer than S_{22} ones (~ - 7.3 dB as its most favourable value).

From Figure 3.4, the isolation between ports is bigger for smaller values of h, around the two operating frequencies of interest (S_{21} of ~ - 15 dB, and S_{12} of ~ - 28 dB, at 1.5 GHz and 2.45 GHz, respectively). Moreover, both S_{12} and S_{21} plots show a similar behaviour, where a first big lump starts emerging around 800 MHz, barely widening the bandwidth in the upper part of the frequency spectrum, starting there a smaller lump around 2.5 GHz.

From this point forward, this noticeable trade-off between resonance and isolation shall be especially considered thinking about the final optimisation presented at the end of this chapter.

3.2.2 Width

Figure 3.5 and Figure 3.6 show the reflection and transmission coefficients, respectively. Values of 14, 20 and 27 mm have been considered. The reference ankle bracelet with an available space of roughly 35 mm can accommodate an antenna with these dimensions with some margin.

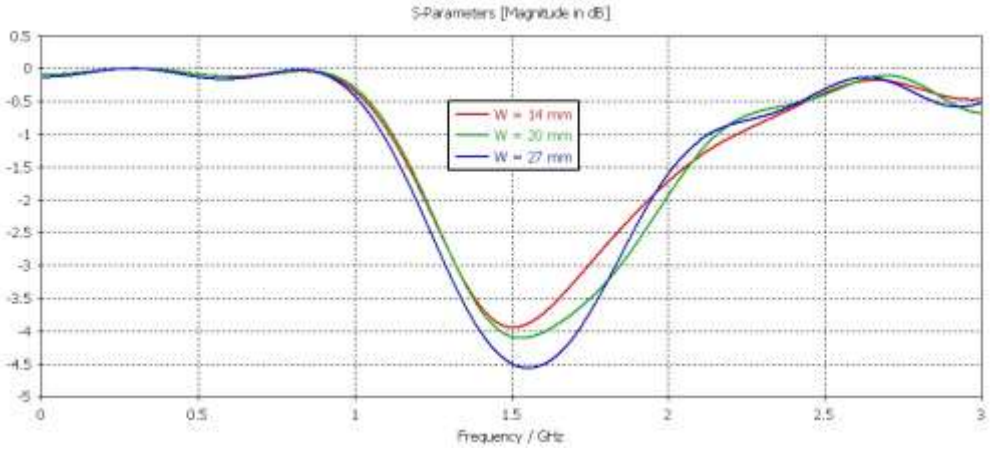

(a) Return loss of the low band port (S_{22})

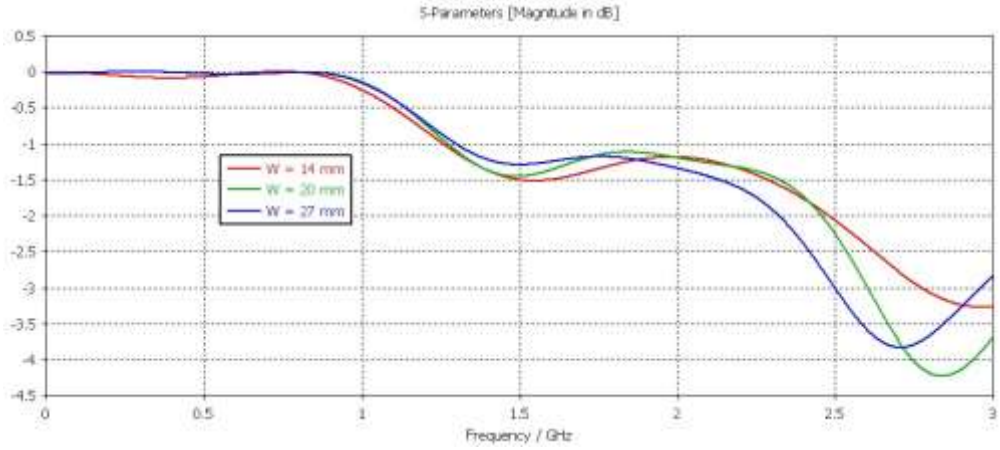

(b) Return loss of the high band port (S_{11})

Figure 3.5: Return loss by changing the width W

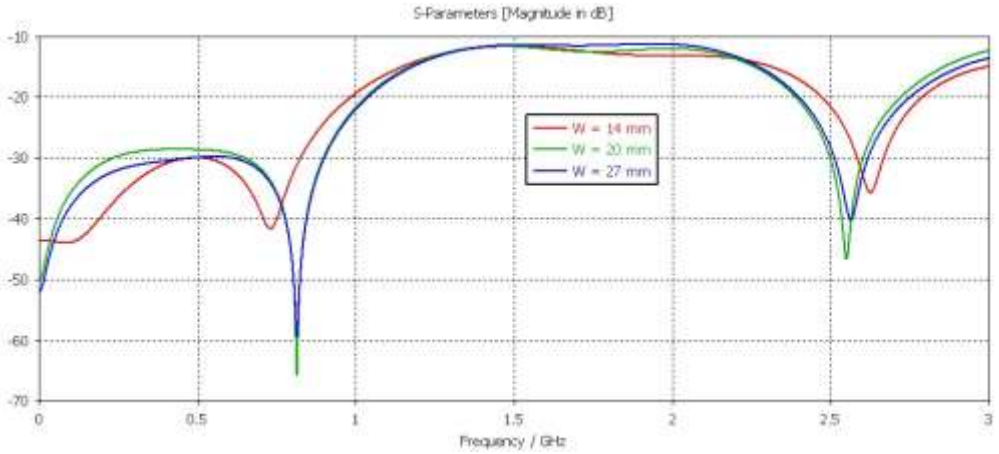

(a) Decoupling between the high band port and the low band port (S_{21})

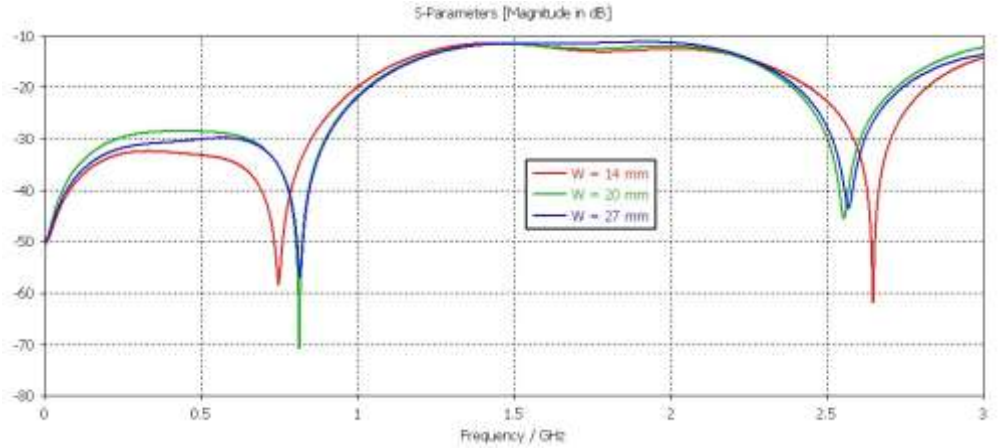

(b) Decoupling between the high band port and the low band port (S_{12})

Figure 3.6: Decoupling between ports by changing the width W

In relation to the high band port, it can be noticed that the resonance frequencies are shifted down, as the width W of the antenna increases, while the same curve behaviour does not happen in the low band port. In this port, it can be observed an improvement in the respective return loss (S_{22}) and no frequency shifts, as the width W increases. Both S_{11} and S_{22} plots never reach a minimum below ~ -4.5 dB. Moreover, the width W does not influence the bandwidth around the centre frequencies of interest.

In the case of the isolation between ports, for both S_{21} and S_{12}, there is not a linear behaviour as width W varies, but for higher values of width W, the decoupling between the two ports tends to be better. Moreover, their plots show a similar sequence of minimums, when compared with the respective sweep results in 3.2.1. Also, the width W does not affect the bandwidth.

3.2.3 High Band Patch Length

In Figure 3.7, it is shown how the return losses vary with the lengths L_HB, by fixing the initial values of length L_LB and gap, and, therefore, by varying the ground plane length. It was chosen values of 20.6, 30.6 and 40.6 mm. Figure 3.8 shows the transmission coefficients for the same values.

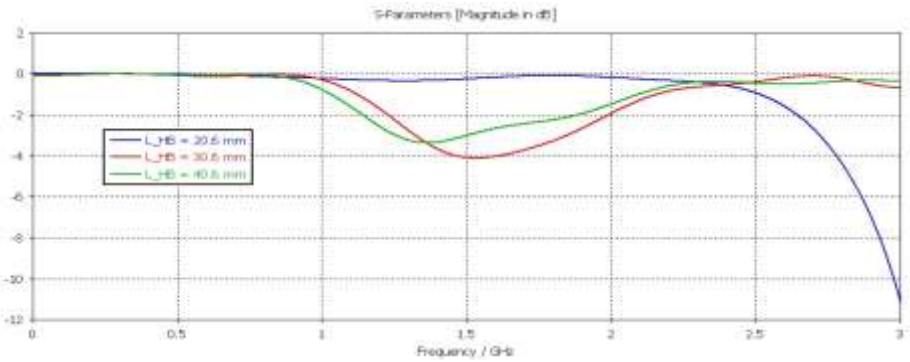

(a) Return loss of the low band port (S_{22})

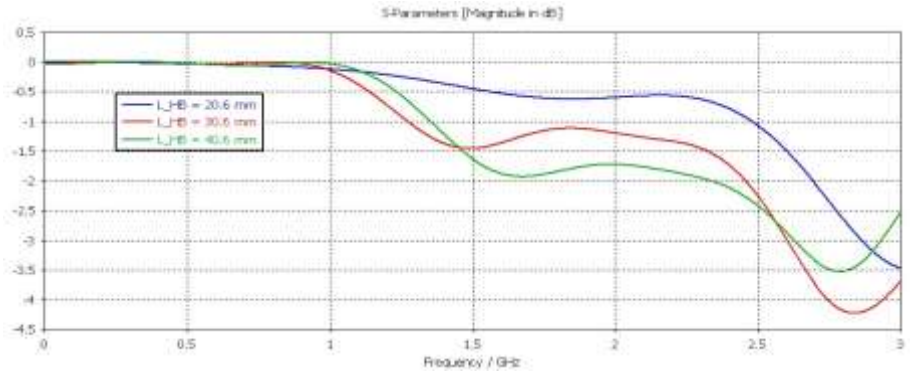

(b) Return loss of the high band port (S_{11})

Figure 3.7: Return loss by changing the length L_HB

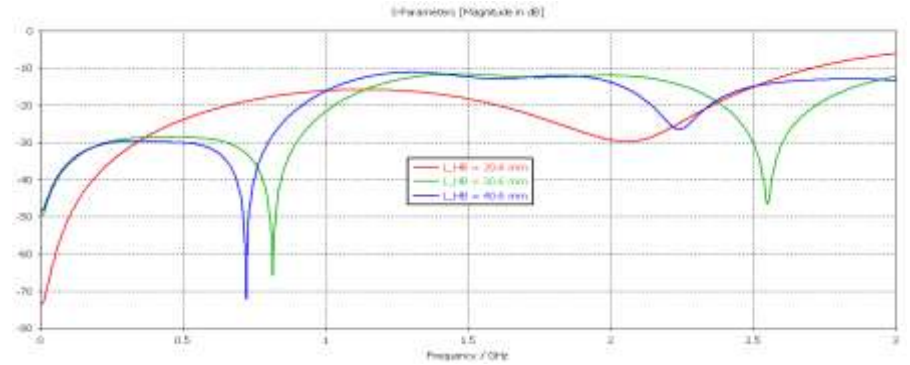

(a) Decoupling between the high band port and the low band port (S_{21})

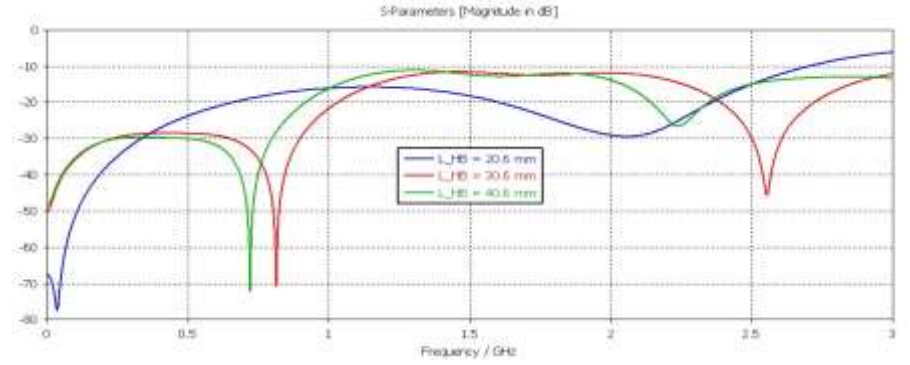

(b) Decoupling between the high band port and the low band port (S_{12})

Figure 3.8: Decoupling between ports by changing the length L_HB

As expected, the operating frequencies are shifted down as length L_HB increases for both ports, because of the inevitable coupling between the two radiating elements. S_{11} and S_{22} plots have a minimum of ~ - 4 dB around their respective operating frequencies (1.5 GHz and 2.7 GHz, respectively). Moreover, the bandwidth is the widest for the lowest value of L_HB.

For S_{21} and S_{12}, when comparing with the previous parameters, the antenna bandwidth tends to be much wider for lower values of length L_HB. However, the most favourable resonance of S_{21} curve occurs in the intermediate value of 30.6 mm, near 2.45 GHz, while the S_{12} curve shows higher magnitudes for lower values of L_HB, near 1.5 GHz.

3.2.4 Low Band Patch Length

The effects of the variation of the length L_LB with respect to reflection and transmission coefficients are shown in Figures 3.9 and 3.10, respectively. The variations in the values of the other parameters were the same as in the study carried out for length L_HB. It was considered values of 40, 50 and 60 mm for L_LB.

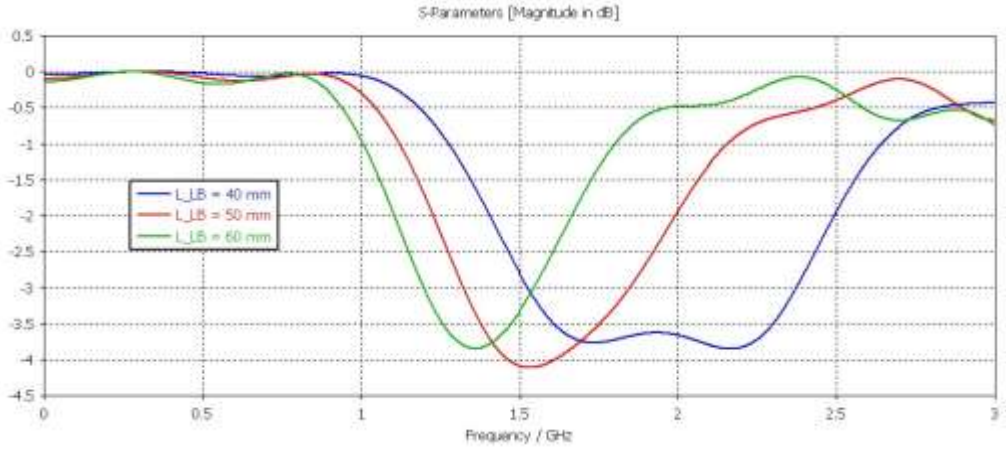

(a) Return loss of the low band port (S_{22})

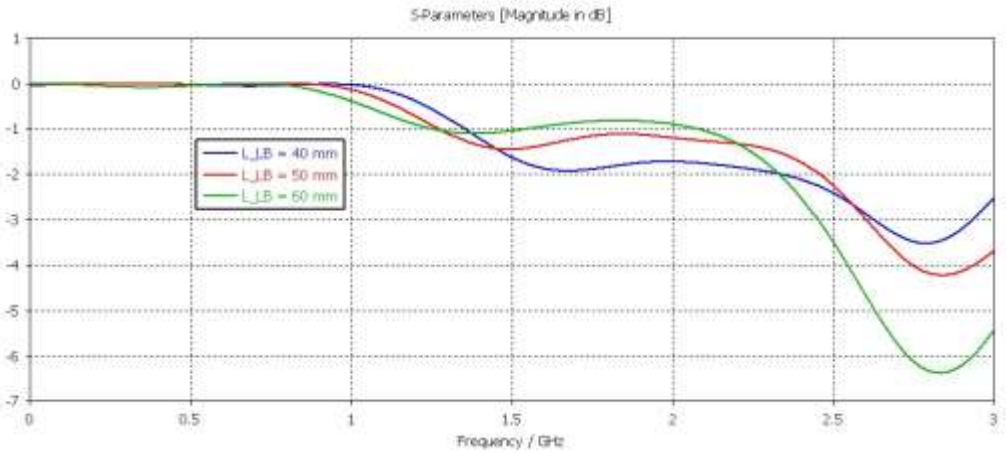

(b) Return loss of the high band port (S_{11})

Figure 3.9: Return loss by changing the length L_LB

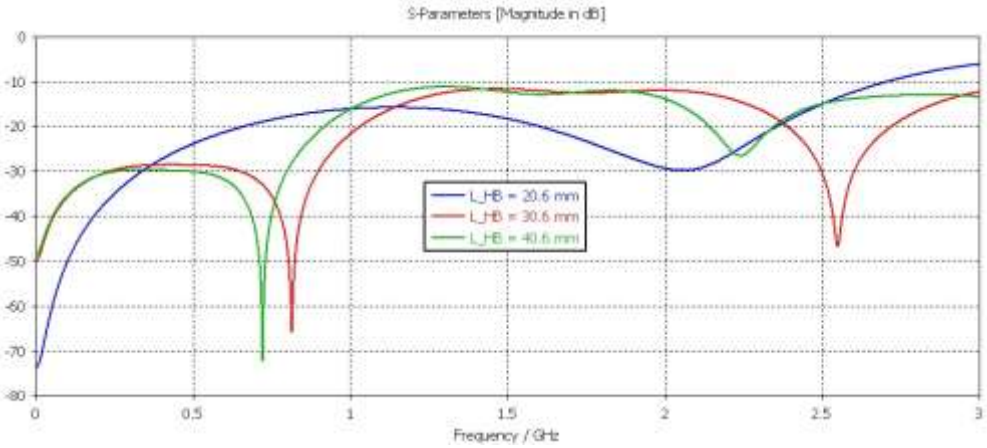

(a) Decoupling between the high band port and the low band port (S_{21})

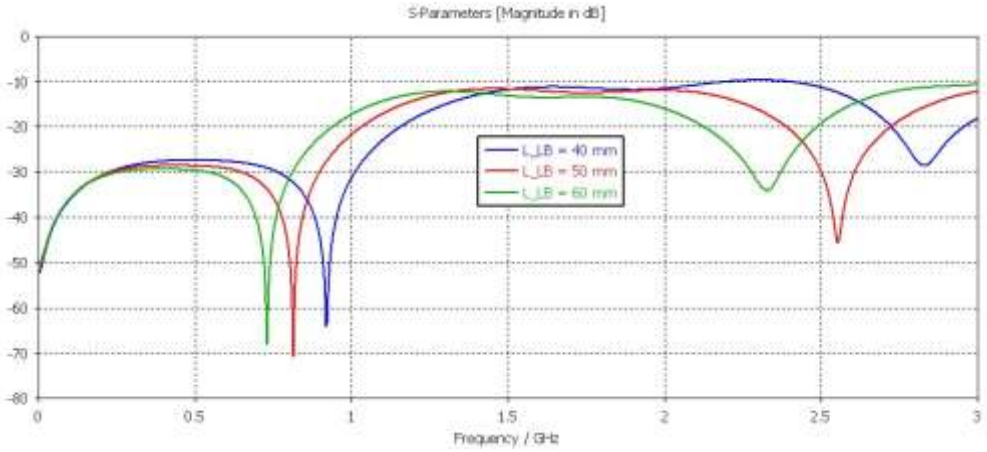

(b) Decoupling between the high band port and the low band port (S_{12})

Figure 3.10: Decoupling between ports by changing the length L_LB

The return loss in the low band port is shifted down and the bandwidth is decreased as the length L_LB increases. The same, however, cannot be said in respect to the high band port, in which there is a better return loss for higher values of the length L_LB. S_{11} and S_{22} plots have a minimum of ~ - 6 dB and, such as in subsection 3.2.3, ~ - 4 dB, respectively.

The transmission coefficients are shifted down as the L_LB increases, where the transmission coefficient is more convenient for L_LB of 50 mm.

3.2.5 Gap

Finally, the influence of the variation of the gap on the reflection and transmission coefficients are shown in Figures 3.11 and 3.12, respectively. Values of 1, 2 and 3 mm have been considered for the gap.

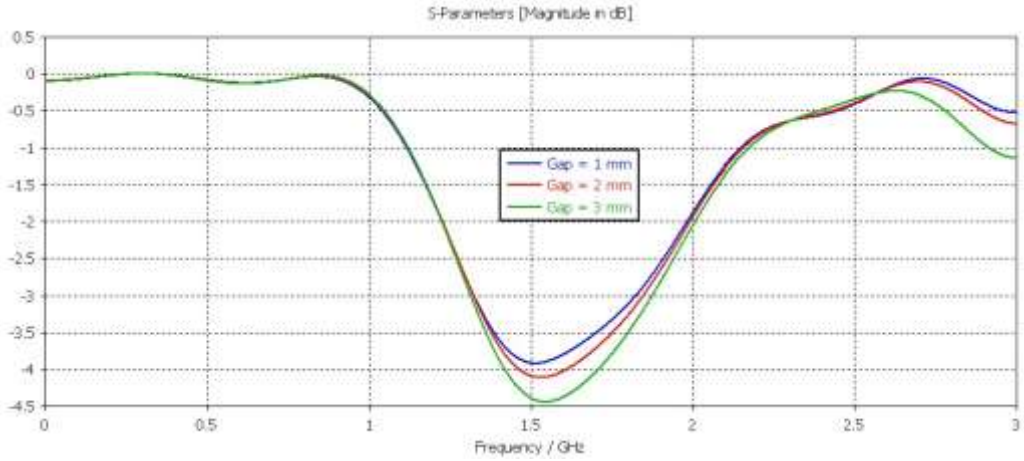

(a) Return loss of the low band port (S_{22})

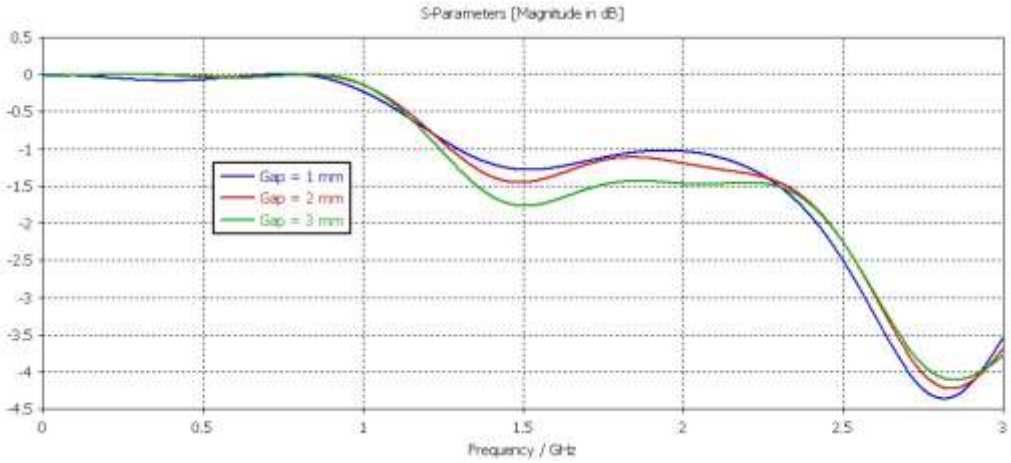

(b) Return loss of the high band port (S_{11})

Figure 3.11: Return loss by changing the gap

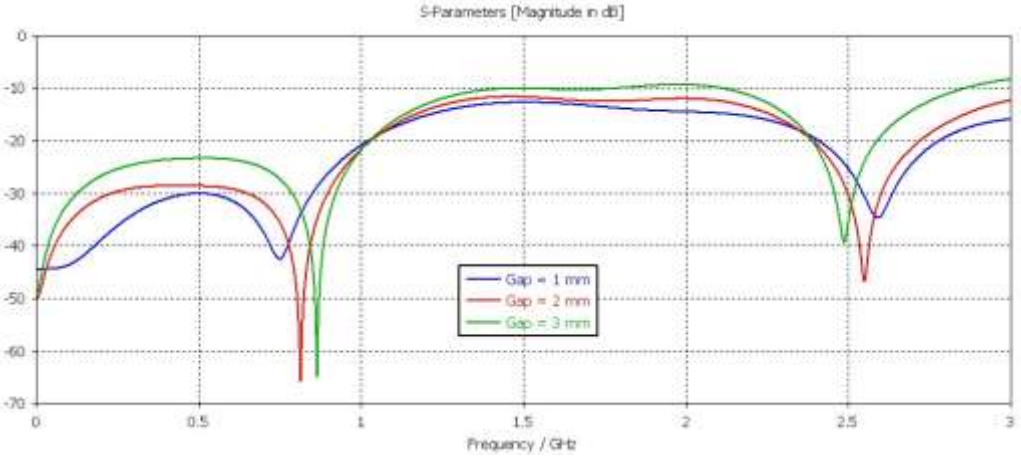

(a) Decoupling between the high band port and the low band port (S_{21})

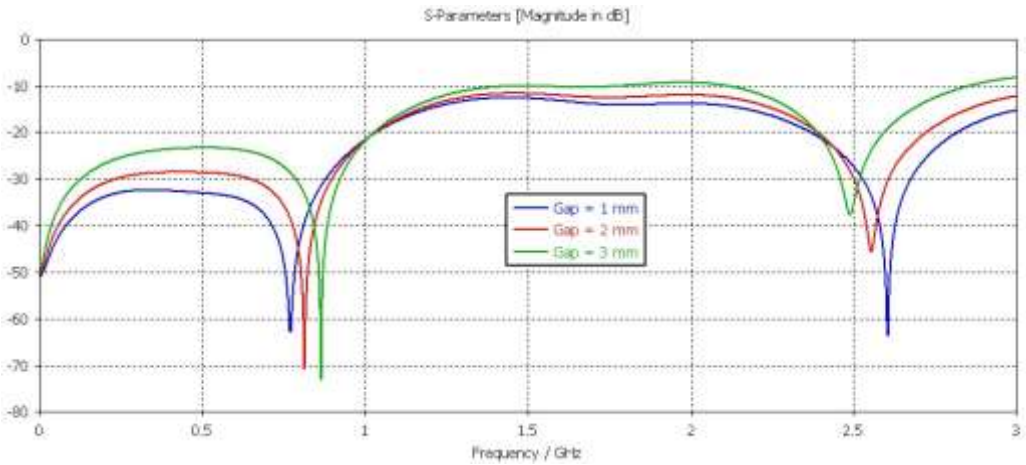

(b) Decoupling between the high band port and the low band port (S_{12})

Figure 3.12: Decoupling between ports by changing the gap

The gap essentially affects the coupling between the two radiating elements. As the gap gets smaller, the operating frequency of S_{21} shifts up, while the operating frequency of S_{12} shifts down. In respect to reflection coefficients, S_{11} plot shows better results for lower values of the gap, while S_{22} shows better antenna performance for higher values of the gap with minimums of ~ - 4.5 dB. The bandwidth remains the same for each value of gap

3.3 Study of Feed Line and Feed Positioning

After realising how the different parameters of the antenna structure affect its S-Parameters and bandwidth, the main effects of the feed line and positioning on the antenna performance were studied.

In a first stage, being always used discrete ports for feeding, a parametric study of feed positioning was carried out. Primarily, different positions were considered with the feed points on the same side (Figure 3.13 and Figure 3.16); secondly, the feed points on opposite sides were placed at different positions (Figure 3.19); thirdly, the feed points were placed at other alternative positions (Figure 3.23). Note that the same initial values for the antenna parameters (as shown in Table 3.1) had been assumed.

In a second stage, after reaching the most favourable positions for feed points, a 3D model of a semi-rigid coaxial cable that is described in section 3.3.4 was created, in order to understand if there were significant differences between discrete ports and coaxial cables. Moreover, it is studied the sensitivity of S-Parameters to changing the length of coaxial cables.

3.3.1 Parametric Study of the Feed Points on the Same Side

In this subsection, the parametric study was done with the two feed points on the same side, by changing the position of a discrete port and fixing the position of the other one.

Changing High Band Feed Point

Firstly, it was assumed to fix the position of the low band port, and then the position of the high band one was changed, in order to study the effects on the antenna performance, by placing the feed points on the same side of the antenna.

For this purpose, a parameter sweep for the high band feed point position was carried out with $v \in [0,29]$ mm, according to Working Coordinate System (WCS) in Figure 3.13. In this figure, a side view of the antenna with the high band feed point placed at the upper simulated value of v ($v = 29$ mm) is shown. In Figure 3.14 and Figure 3.15 the reflection and transmission coefficients, respectively, are shown.

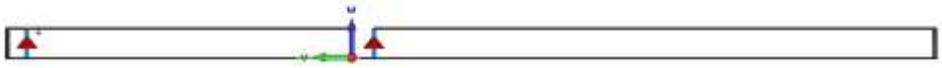

Figure 3.13: Example of position of the high band discrete port, fixing the low band one on the same side

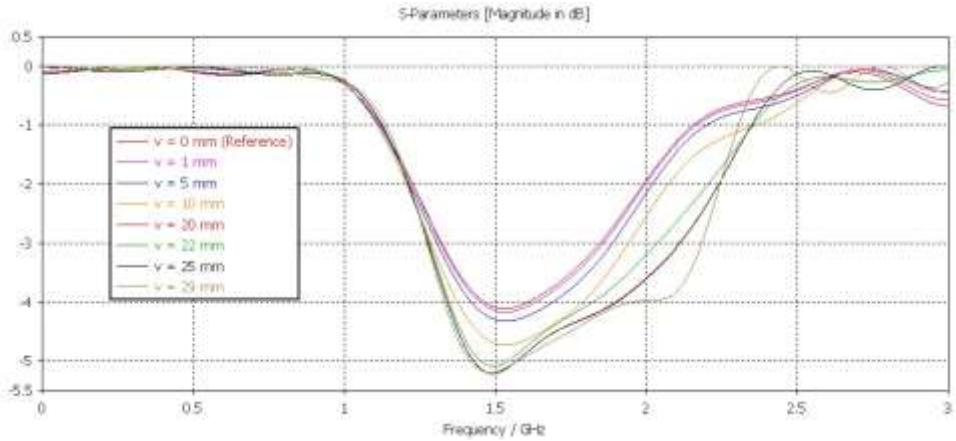

(a) Return loss of the low band port (S_{22})

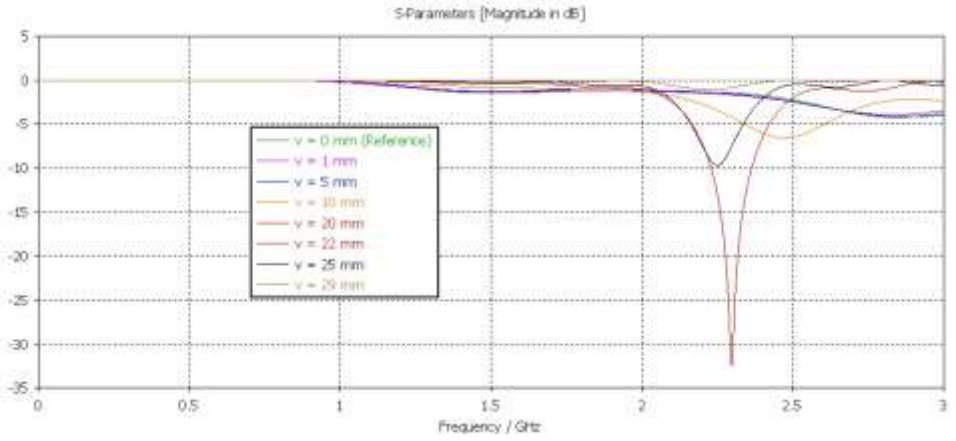

(b) Return loss of the high band port (S_{11})

Figure 3.14: Return loss by changing the position of the high band port

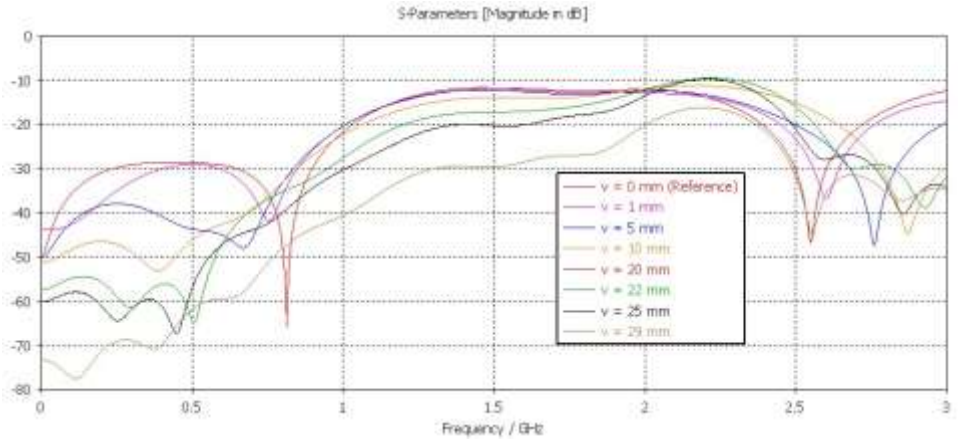

(a) Decoupling between the high band port and the low band port (S_{21})

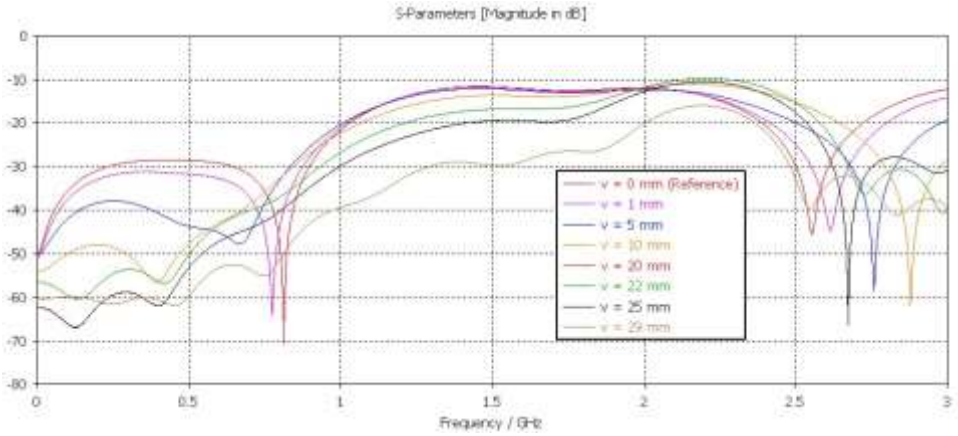

(b) Decoupling between the high band port and the low band port (S_{12})

Figure 3.15: Decoupling between ports by changing the position of the high band port

From this parametric study, it can be concluded that in the high band for reflection coefficient (S_{11}) there is not a regular behaviour over the frequency. However, it can be observed that for intermediate values ($v \in [10,22]$ mm) the return loss values are closer to target, being the minimum located at $v = 22$ mm with roughly -30 dB. In the low band port for S_{22}, there is a regular variation for the respective curves along the v axis. As expected, a bigger v yields a more favourable S_{22}.

In terms of transmission coefficients, in the high band port S_{12} is shifted up in frequency as v increases, while in the low band port S_{21} is shifted down in frequency and, at the same time, loses its resonance as v increases.

Changing Low Band Feed Point

Here, it is assumed to fix the position of the high band port, and then the position of the low band one is changed, in order to study the effects on antenna performance, by placing the feed points on the same side of the antenna.

A parameter sweep for low band feed point position was carried out with $v \in [0,49]$ mm, according to WCS in Figure 3.16. In this figure, it can be observed a side view of the antenna with the low band feed point placed at the upper simulated value of v ($v = 49$ mm). In Figure 3.17 and Figure 3.18 are shown the reflection and transmission coefficients, respectively.

Figure 3.16: Example of position of the low band discrete port, fixing the high band one on the same side

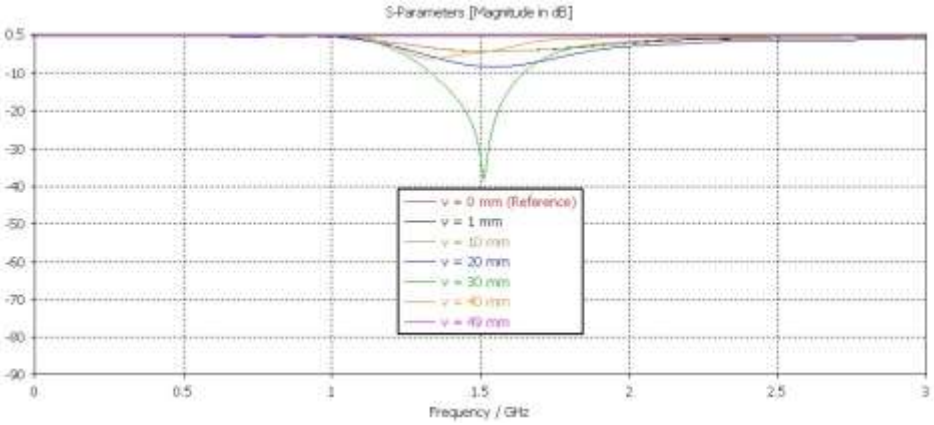

(a) Return loss of the low band port (S_{22})

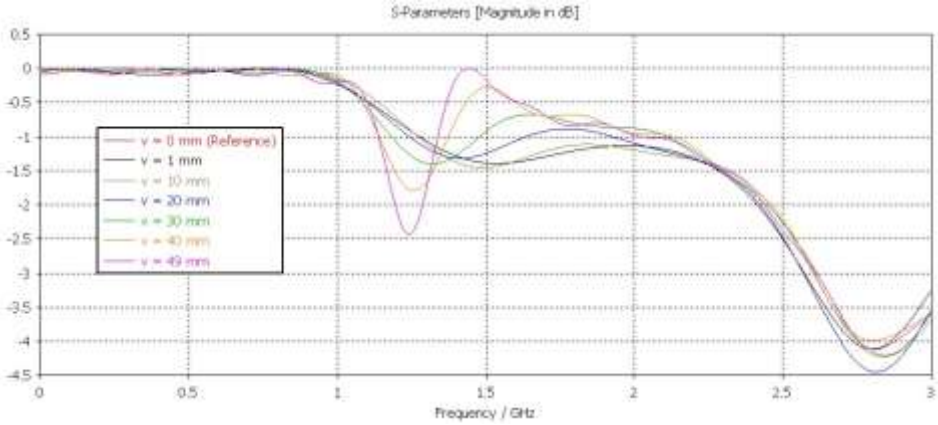

(b) Return loss of the high band port (S_{11})

Figure 3.17: Return loss by changing the position of the low band port

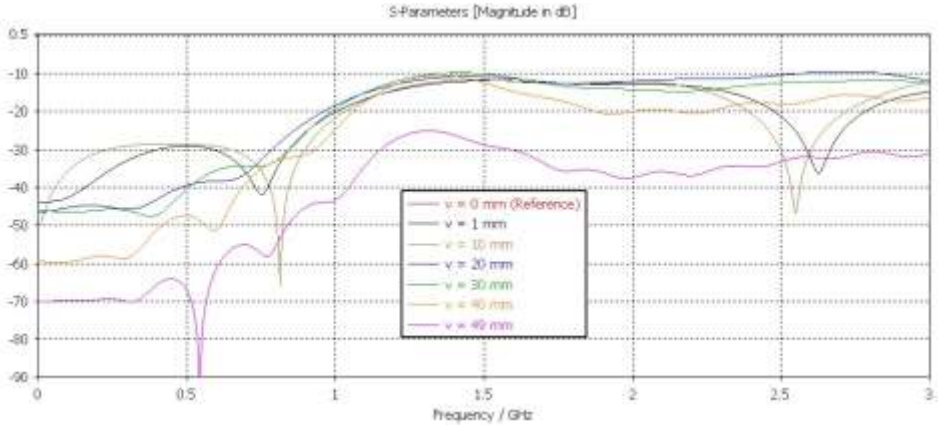

(a) Decoupling between the high band port and the low band port (S_{21})

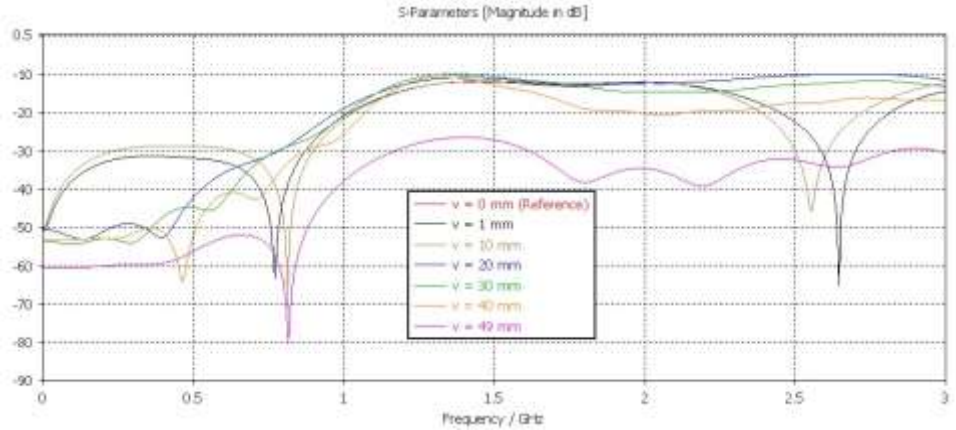

(b) Decoupling between the high band port and the low band port (S_{12})

Figure 3.18: Decoupling between ports by changing the position of the low band port

From this parametric study, it was concluded that, in the high band for reflection coefficient (S_{11}) there is not a regular behaviour over the frequency. It can be observed, once again, that for intermediate values ($v \in [20,30]$ mm) there are return loss values closer to target, but always above - 4.5 dB. In the low band port for S_{22}, there is not a regular variation for the respective curves along the v-axis. Only for $v = 30$ mm, S_{22} is below the goal of - 10 dB (approximately - 40 dB).

In terms of transmission coefficients, in the high band port S_{12} is shifted down in frequency and, at the same time, loses its resonance as v increases. Thus, the most favourable resonances occurred at the lower values of v ($S_{12} \in [-40, -60]$ mm for $v \in [1, 10]$ mm, near 2.45 GHz). In the low band port S_{21} has its operating frequency far from 1.5 GHz, being closer to this frequency of interest for lower values of v.

After these two parametric studies of the feed points position on the same side, it can be concluded that the most favourable positions along the v-axis, taking into account essentially the return losses and the operating bands of interest, are the following ones presented in the next table.

Table 3.2: Most favourable positions for feed points placed on the same edge of the antenna.

Port	Position of Feed Point along v-axis [mm]
High Band (1)	22
Low Band (2)	30

3.3.2 Parametric Study of the Feed Points on Opposite Sides

For simplicity, at this stage, there are only three distinct cases to consider, since the most favourable position for feeding was achieved with some approximation in the previous subsection.

The three cases are shown in Figure 3.19. Noting that in case 1, the feed points are placed at opposite sides at a point mid-way the length of the respective radiating elements. Therefore, the high band feed point is placed at $v = 15.3$ mm, and the low band one is placed at $v = 25$ mm. In case 2, the feed points are placed at the positions illustrated by Table 3.2.

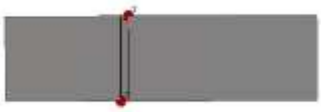

(a) Reference case for position of the high and low band ports placed at opposite sides

(b) Case 1 of the position of the high and low band ports placed at opposite sides

(c) Case 2 of the position of the high and low band ports placed at opposite sides

Figure 3.19: Feeding points placed at opposite sides

In Figure 3.20 and Figure 3.21 is shown a comparison between the three cases that were referred above in terms of reflection and transmission coefficients, respectively.

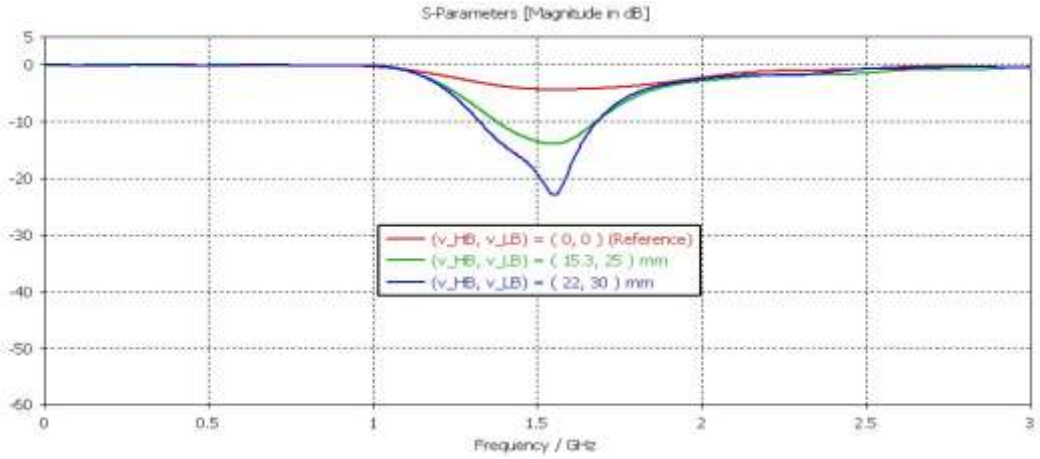

(a) Return loss of the low band port (S_{22})

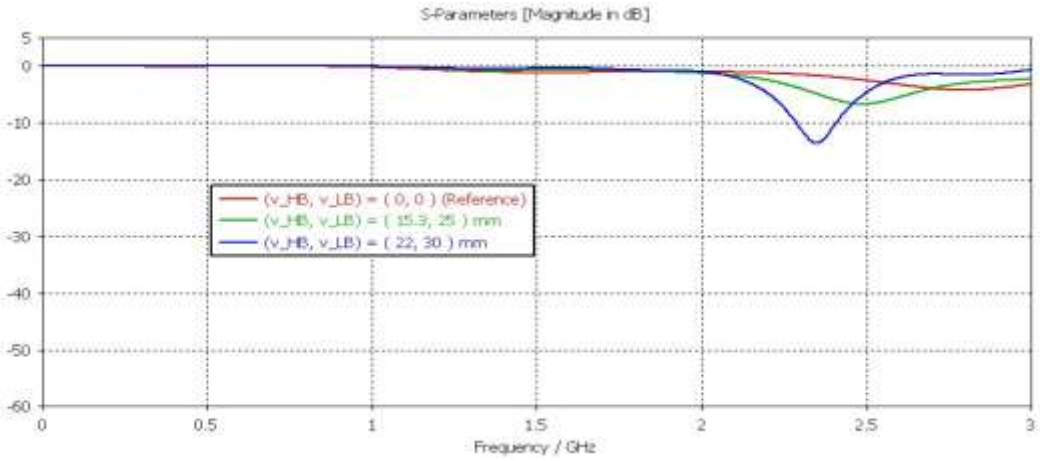

(b) Return loss of the high band port (S_{11})

Figure 3.20: Return loss by changing the position of ports placed at opposite sides.

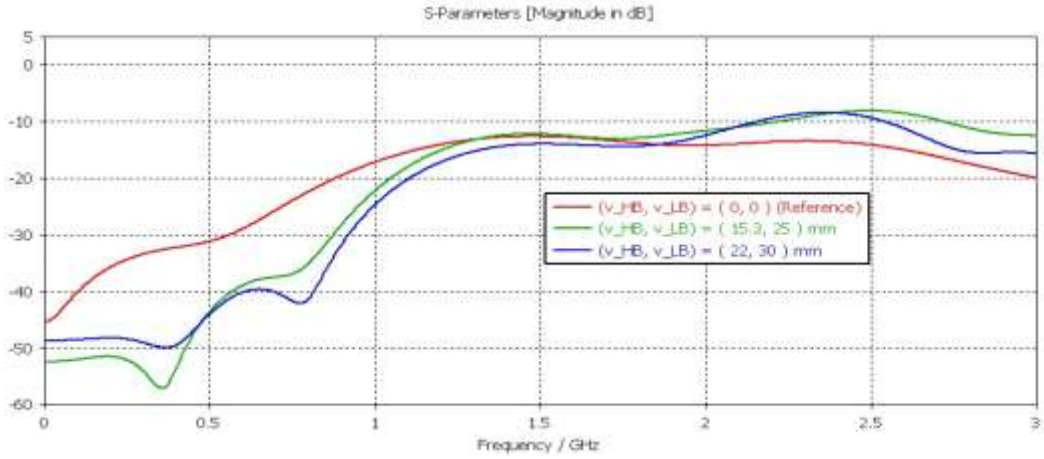

(a) Decoupling between the high band port and the low band port (S_{21})

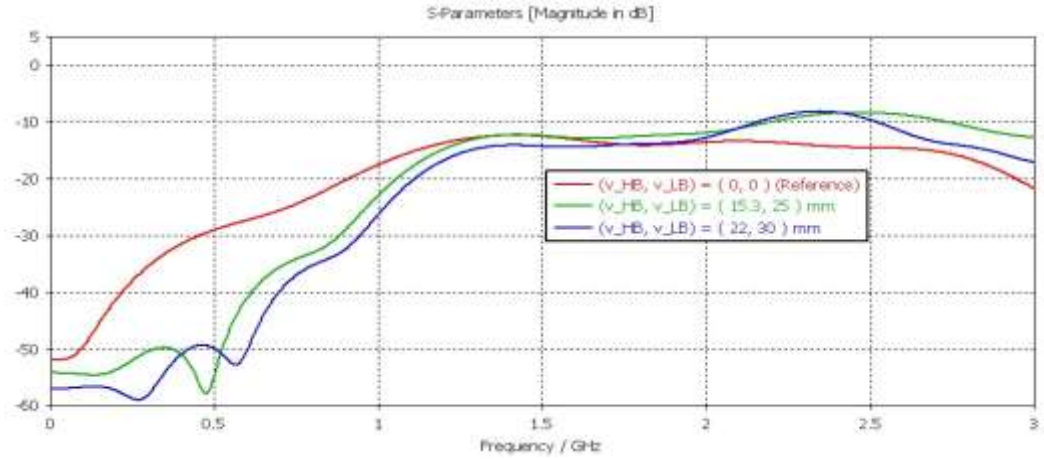

(b) Decoupling between the high band port and the low band port (S_{12})

Figure 3.21: Decoupling between ports by changing the position of ports placed at opposite sides

From Figure 3.20, it can be concluded that the return loss results closer to minimum goal occur in case 2 with $S_{22} \approx -20$ dB near 1.5 GHz and $S_{11} \approx -12.5$ dB near 2.45 GHz.

From Figure 3.22, it can be noticed that S_{21} is a little bit better in case 2 ($S_{21} \approx -14$ dB), but S_{12} is better in the reference case ($S_{12} \approx -15$ dB).

3.3.3 Other Positions

Lastly, the two feed points are still placed at other two different positions. The two cases are shown in Figure 3.22. Noting that in case 1 the feed points are centred along the width W axis and radiating elements axis. Therefore, the high band feed point is placed at u = 10 mm and v = 15.3 mm, and the low band one is placed at u = 10 mm and v = 25 mm. In case 2 the feed points are placed at the positions illustrated in Table 3.2 along the v-axis and at u = 10 mm. Next, the reflection and transmission coefficients, for both cases 1 and 2, are shown in Figure 3.23 and Figure 3.24, respectively.

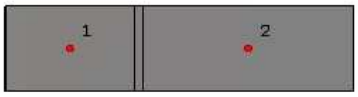

(a) Case 1 of the position of the high and low band ports placed at other positions

(a) Case 2 of the position of the high and low band ports placed at other positions

Figure 3.22: Feeding points placed at other positions

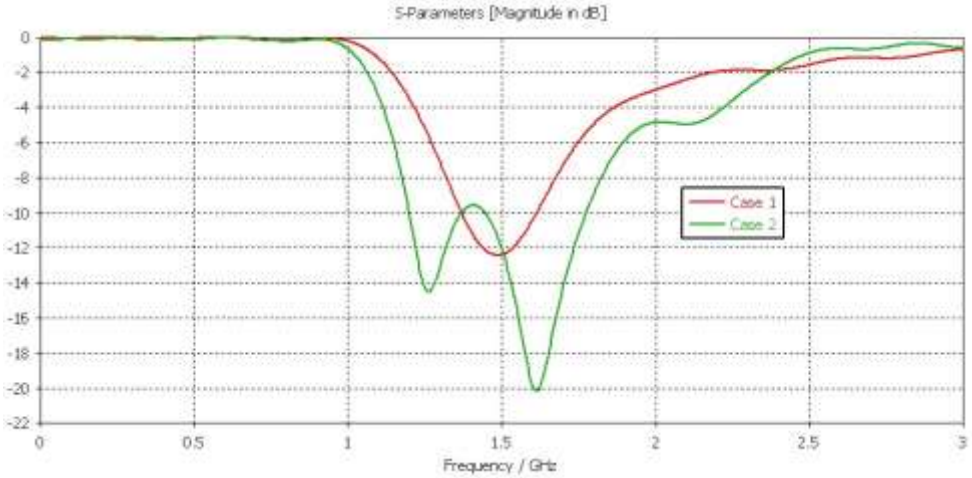

(a) Return loss of the low band port (S_{22})

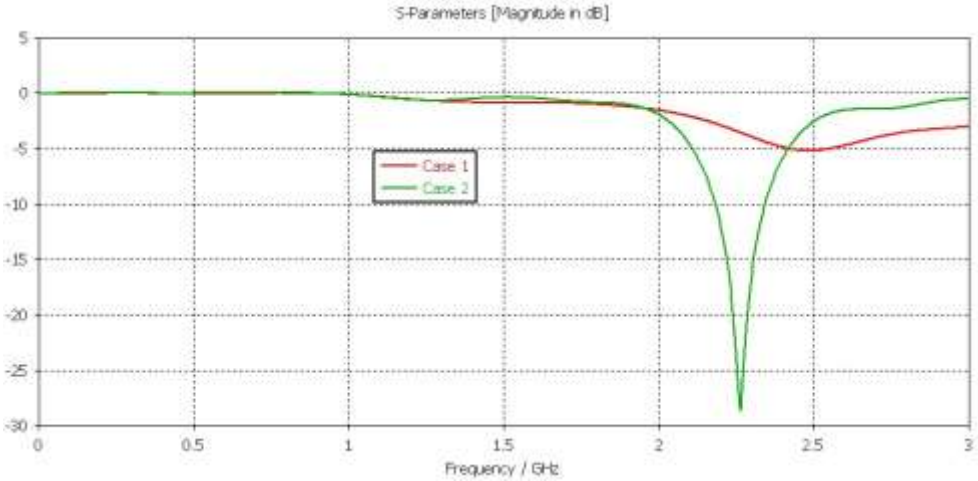

(b) Return loss of the high band port (S_{11})

Figure 3.23: Return loss by changing the position of ports placed at opposite sides

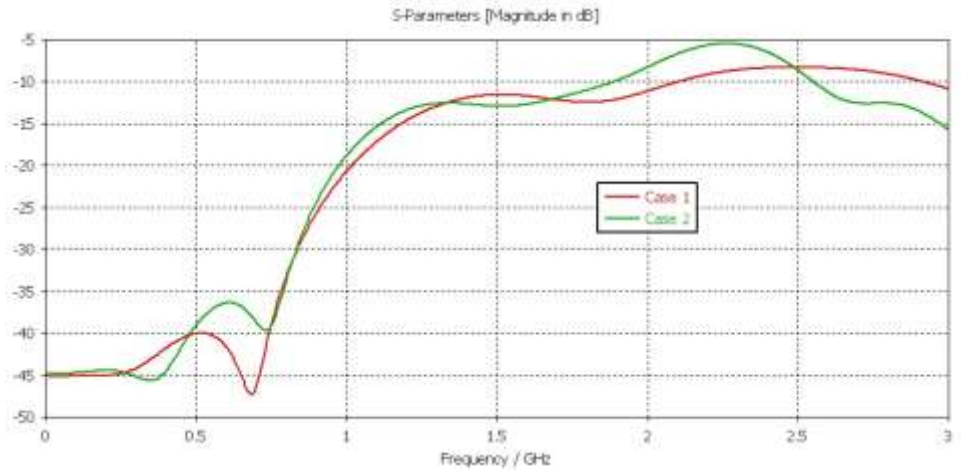

(a) Decoupling between the high band port and the low band port (S_{21})

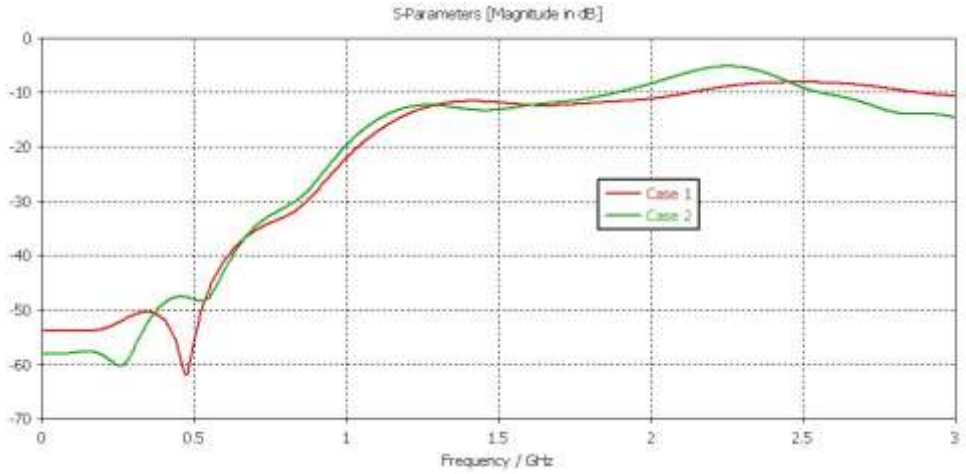

(b) Decoupling between the high band port and the low band port (S_{12})

Figure 3.24: Decoupling between ports by changing the position of ports placed at opposite sides

Up to this point, there is no solution that satisfies all the goals related to S-Parameters and operating bands. However, it is the case 2 of the feed points placed at opposite sides that shows the most favourable results, in which S_{21} is still a little above -10 dB

3.3.4 Effect of Coaxial Cables

A pure copper available in the the Computer Simulation Technology (CST) *Material Library* instead of the previous PEC material, holding constant the thickness of 0.1 mm for metal parts, is then used. In respect to feeding structure, as reference a semi-rigid coaxial cable with a copper outer conductor (RG405/U-086 [67]) is utilised. In section 3.4, this coaxial cable is replaced by another one, due to a reason that will be explained there.

In Figure 3.25, it can be seen the above-referred model for the antenna where, in addition to the change of material and placement of the semi-rigid coaxial cables centred, that results in the optimal positions (according to 3.3), it was needed to extend the inner conductor of each coaxial cables from the ground plane to the respective radiating element.

Figure 3.25: Optimal solution for position of the high band and low band ports placed at opposite positions with coaxial cables

As a result of these changes, it can be seen in Figure 3.26 the results for S-Parameters with the most crucial frequencies marked around the operating frequencies of interest. To get these S-Parameters, the CST macro called *Optimiser* was used in order to tune the antenna parameters (h, W, L_HB, L_LB and gap) and coaxial cables position, by setting as target the before-mentioned magnitude (dB) of -10 dB for S-Parameters in the operating bands.

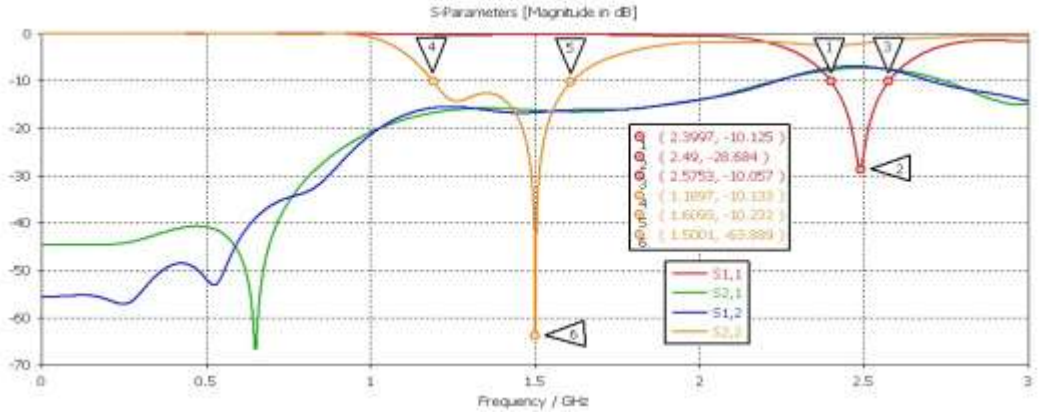

Figure 3.26: S-Parameters for the optimal solution of the high and low band ports placed at opposite positions with 20 mm long coaxial cables

Coaxial cables were then chosen so that simulations would be closer to the conditions of the prototype. In conclusion, coaxial cables strongly influence some of the results observed. From what can be noted in Figure 3.27 and Figure 3.28, even their length has to be accounted for. In this respect, for lower coaxial cable lengths are obtained the most favourable magnitude results for both return loss and decoupling values, being the improvements much more significant in terms of return loss. However, the bandwidth for the return losses is a bit narrower for lower coaxial cables lengths.

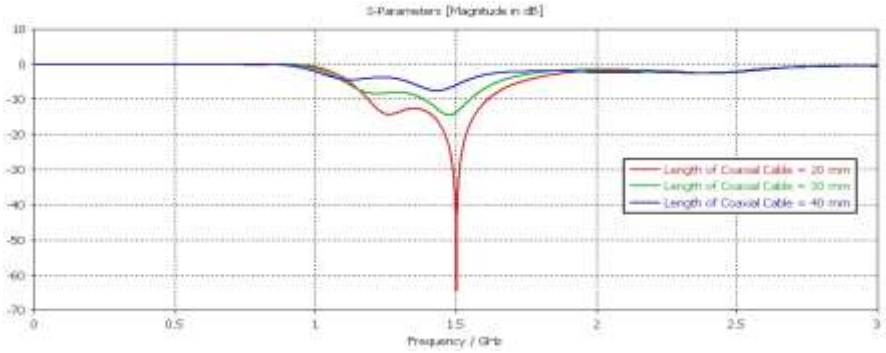

(a) Return loss of the low band port (S_{22})

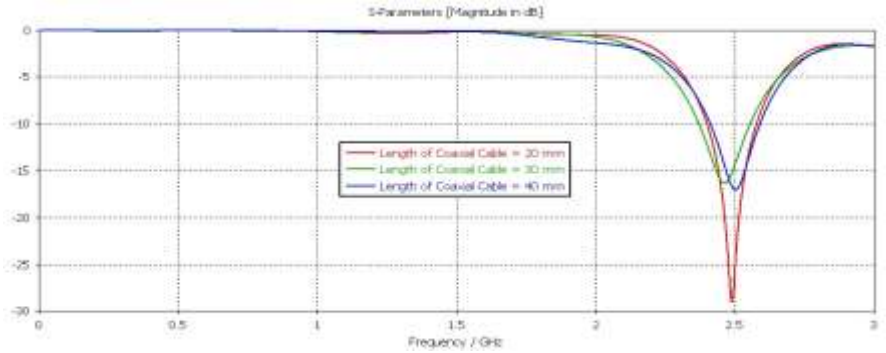

(b) Return loss of the high band port (S_{11})

Figure 3.27: Return loss sensitivity to changing the length of the coaxial cables

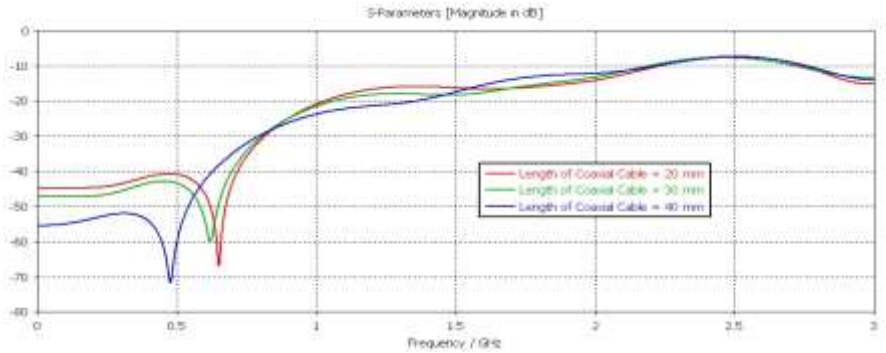

(a) Decoupling between the high band port and the low band port (S_{21})

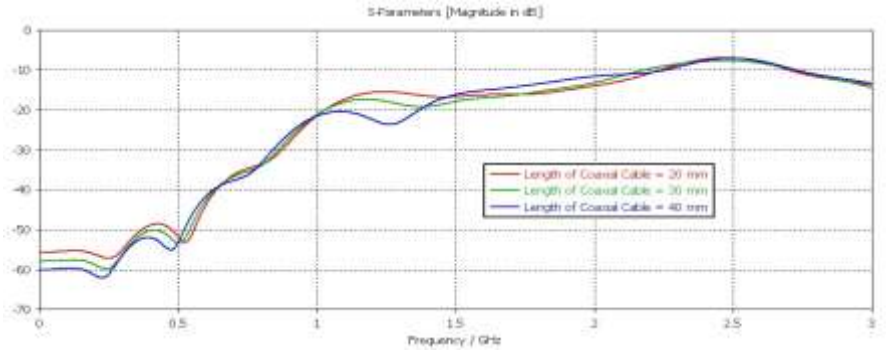

(b) Decoupling between the high band port and the low band port (S_{12})

Figure 3.28: Decoupling between ports sensitivity to changing the length of the coaxial cables.

3.4 Effect of Defected Ground Structures

3.4.1 Introduction

The parametric studies that were shown previously until now did not lead to acceptable results in terms of decoupling, it was crucial to find a way to overcome this problem. From [68], there are two distinct ways of enhancing the isolation/decoupling for dual or multi-port antennas:

- Changing or redesigning the antennas structure;
- Adding an external microwave feed network to the antenna without making any changes to the already designed antenna structure.

The first approach is more common in literature. The second approach is more general as it could be applied to any similar antenna with changes in certain parameters and would require more physical space [68].

In the second approach, it is needed to impose a pure reactance from the mutual impedances between antennas at the operating frequency, in order to realise a decoupling network, by connecting a lossless network between the input ports and the antenna ports. In other words, it is intended to use transmission lines as antenna decouplers. However, these decouplers are inherently narrowband and limited by the antenna bandwidth. Therefore, the first approach was the concern of this project. Within this context, there are two distinct cases:

- Operating frequency bands are sufficiently widely separated;
- Operating frequency bands have to be closely spaced or even have to occupy the same band such as MIMO.

In this project, given the fact that the two operating frequency bands of interest are approximately separated by 1 GHz, the first case is the matter of interest. Thus, the solution with an embedded or external microwave filtering structure can be taken in order to achieve the required decoupling.

Decoupling enhancement can be achieved by separating the feeding ports and/or the radiating elements by multiples of half a wavelength. However, there are physical space limitations. Thus, it is needed to find a cancellation technique. To summarise, there are three distinct techniques that were found in the literature:

- Sharing a loaded ground plane with resonant defects such as slots, slits and/or stubs [68] [69];
- Introducing Split Ring Resonator (SRR)s between closely-separated antennas [68] [70] [71];
- Augmenting the common area of the ground plane, between the antennas, with EBG structures.

In this project, it is considered the use of slots (3.4.2 and 3.4.3), for purposes of simulation and test. As an option, it is discarded the use of EBG structures, because these structures consist of a

periodic arrangement of metal patches on a dielectric substrate. As stated above, there are some limitations of physical space, and therefore such structures cannot be a solution.

3.4.2 Horizontal Slots

This subsection shows the simulation results by using horizontal slots placed at the ground plane, near the low band feeding port. Given the fact that only the S_{21} parameter is above - 10 dB, the physical length of the slots was dimensioned with a quarter-wavelength long at approximately the centre frequency of 1584.5 MHz. The idea behind it is that the transmission, at 1584.5 MHz, must be ideally zero without significantly disturbing the overall antenna performance, at the same time. After doing some slight changes in respect to the dimensions, placement and number of slots, the effect of the horizontal quarter-wavelength slots it was then observed, by showing figures with the surface current density distribution in the antenna, when necessary.

Figure 3.29 shows the three different configurations of interest with horizontal slots placed near the low band feeding port.

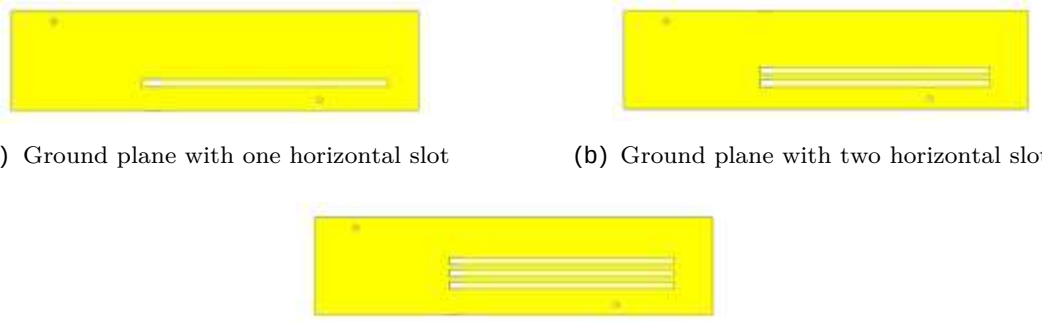

(a) Ground plane with one horizontal slot

(b) Ground plane with two horizontal slots

(c) Ground plane with three horizontal slots

Figure 3.29: Defected ground plane with horizontal slots

In Figure 3.30 and Figure 3.31, it can be seen the simulation results are closer to target return loss and decoupling of the ground plane with only one slot, respectively. It is now important to explain why there are simulations for two different coaxial cables in the next six figures (Figure 3.30 to Figure 3.35), being the above-referred semi-rigid one with copper outer conductor (RG405/U-086 [67]) named as coaxial cable 1, and the new here coaxial cable named as coaxial cable 2 (EZ 47-TP/M17 [72]). This change was done because it would be necessary to have thinner coaxial cables in order to fit the reference bracelet. To that end, both the antenna and the coaxial cables must be bent. Here, 20 mm long coaxial cables are used.

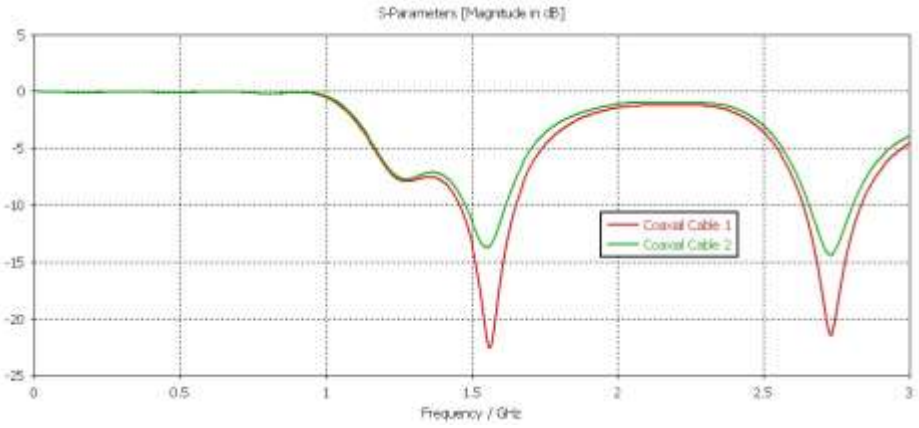

(a) Return loss of the low band port (S_{22}).

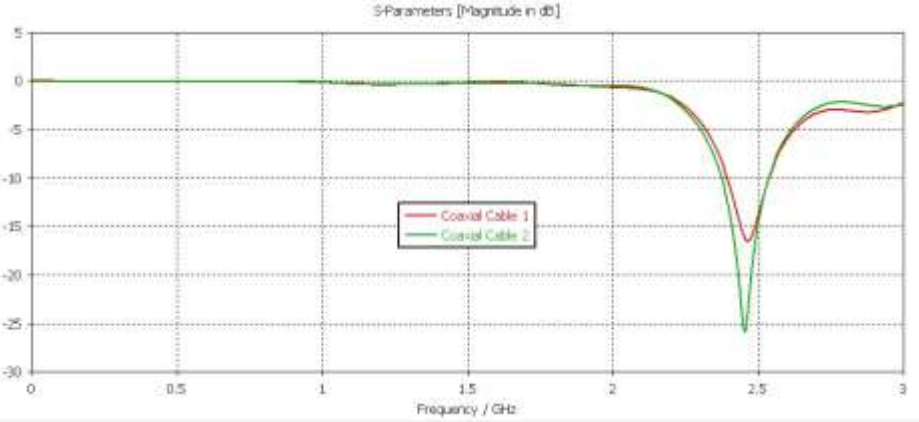

(b) Return loss of the high band port (S_{11}).

Figure 3.30: Return loss for ground plane with one horizontal slot, being fed by two different coaxial cables.

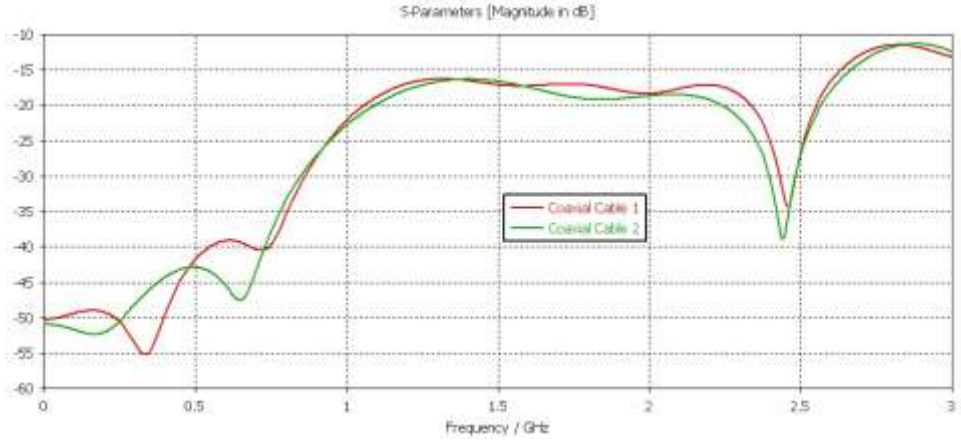

(a) Decoupling between the high band port and the low band port (S21).

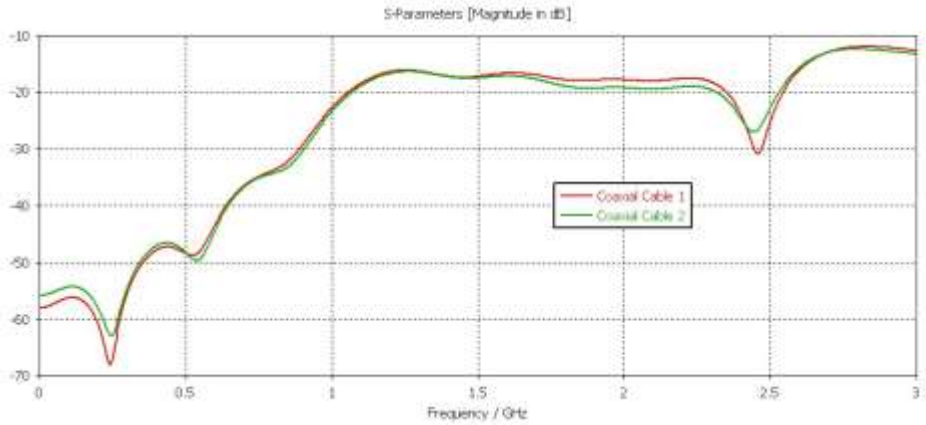

(b) Decoupling between the high band port and the low band port (S_{12}).

Figure 3.31: Decoupling between ports for ground plane with one horizontal slot, being fed by two different coaxial cables.

As can be seen, compared with the solution found in subsection 3.3.4 (see Figure 3.26), this design, characterised by a defected ground plane with only one slot, improved the low band port isolation (S_{12}) by about 23 dB.

In Figure 3.32 and Figure 3.33, it can be seen the simulation results are closer to target return loss and decoupling for the ground plane with two slots, respectively.

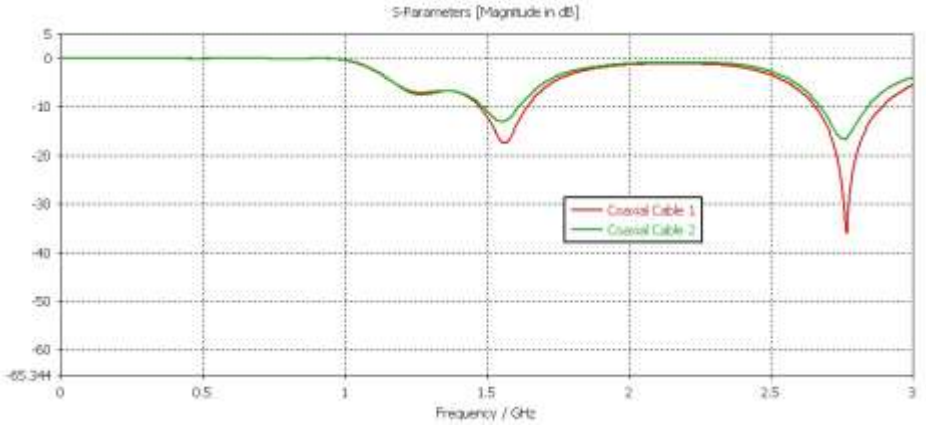

(a) Return loss of the low band port (S_{22})

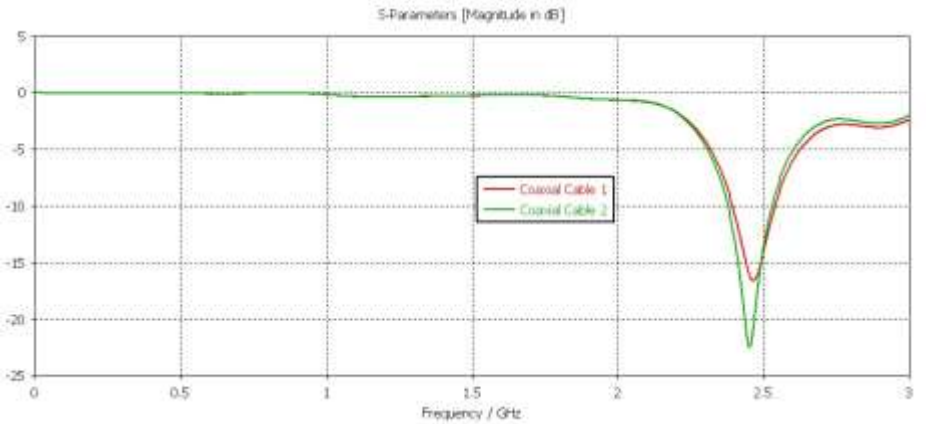

(b) Return loss of the high band port (S_{11})

Figure 3.32: Return loss for ground plane with two horizontal slots, being fed by two different coaxial cables

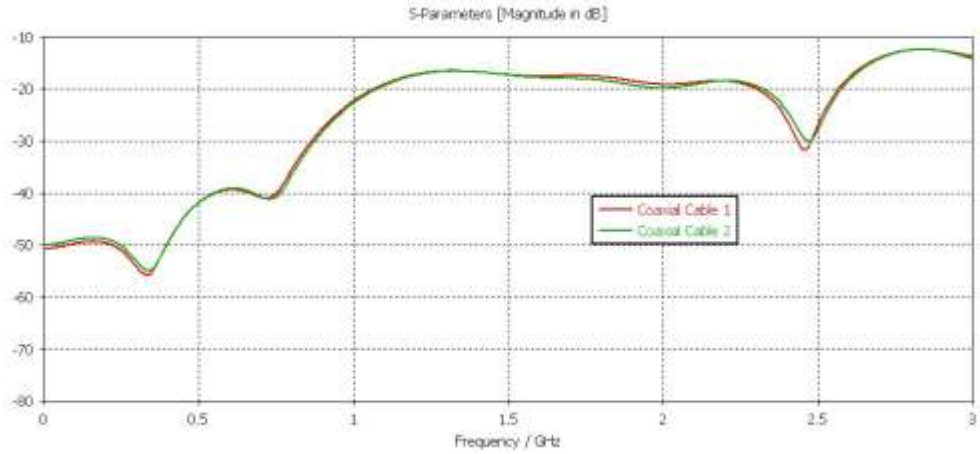

(a) Decoupling between the high band port and the low band port (S_{21})

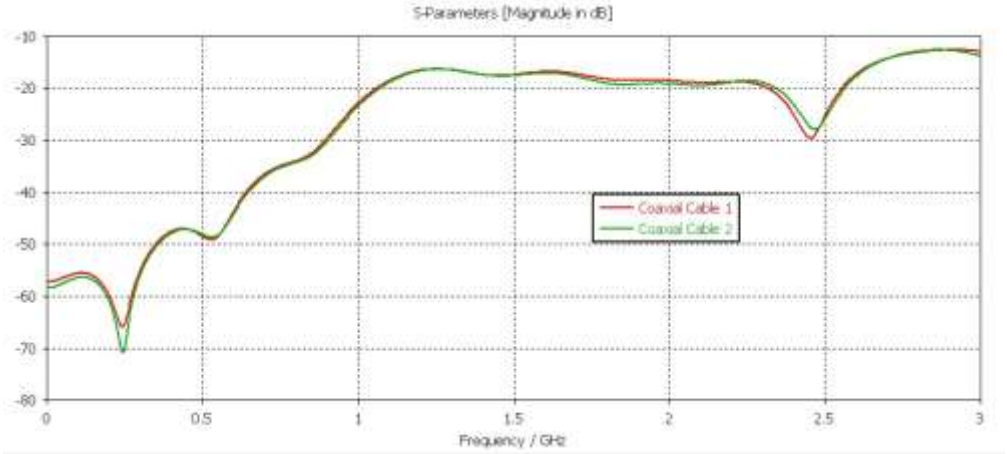

(b) Decoupling between the high band port and the low band port (S_{12})

Figure 3.33: Decoupling between ports for ground plane with two horizontal slots, being fed by two different coaxial cables

Finally, in the Figure 3.34 and Figure 3.35, the closer to target results are shown for both the return loss and decoupling of the ground plane with three slots against the most favourable case with no slots, respectively.

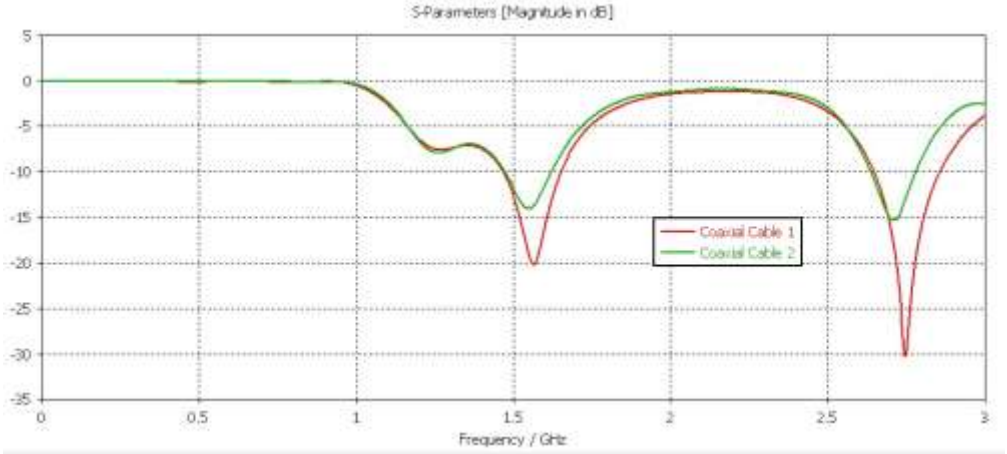

(a) Return loss of the low band port (S_{22})

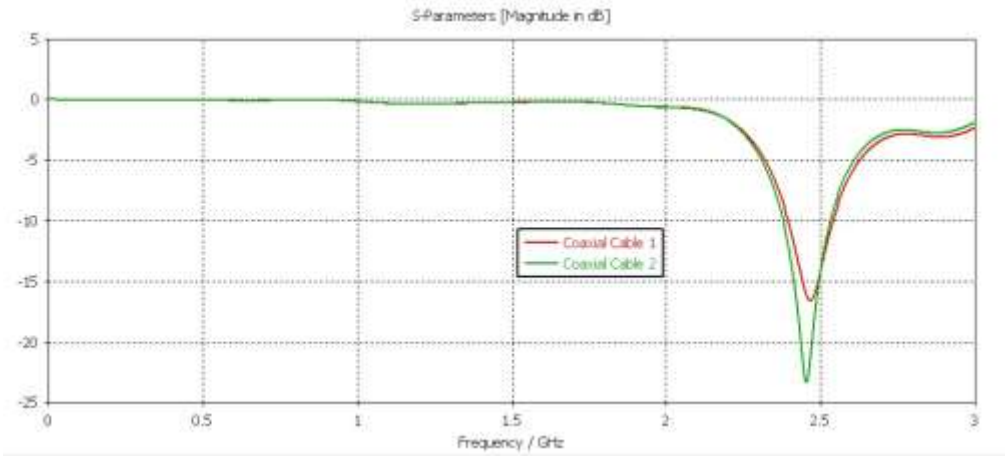

(b) Return loss of the high band port (S_{11})

Figure 3.34: Return loss for ground plane with three horizontal slots, being fed by two different coaxial cables

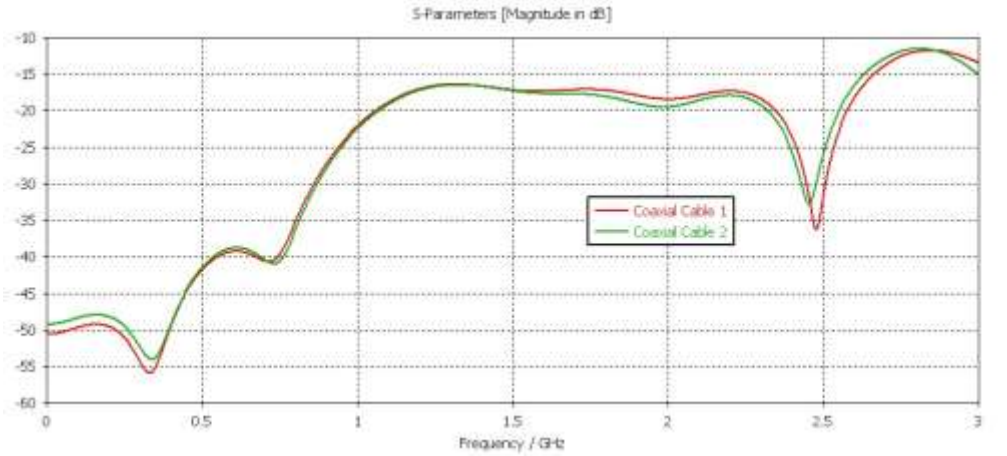

(a) Decoupling between the high band port and the low band port (S_{21}).

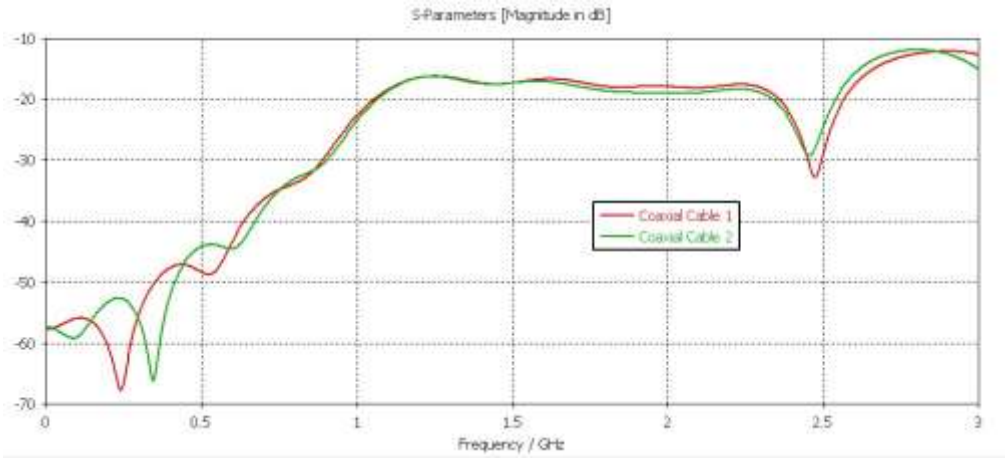

(b) Decoupling between the high band port and the low band port (S_{12})

Figure 3.35: Decoupling between ports for ground plane with three horizontal slots, being fed by two different coaxial cables

After these simulations, it is important to note that, apart from the decoupling enhancement of the low band port, a new operating frequency is created, at approximately 2.75 GHz, by introducing the slots on the ground plane. In addition, by comparing Figure 3.31(b), Figure 3.33(b) and Figure 3.35(b), there is no significant difference in terms of enhancement of S_{12}, around 2.45 GHz. Furthermore, the replacement of coaxial cables affects more significantly the reflection coefficients. There are sharper resonance peaks in S_{11} curves with the coaxial cable 2, the use of the coaxial cable 1 causes sharper resonance peaks in S_{22} curves. This may be because the thickest coaxial cable (1) is closer in size to that of the longest radiating element (closest to the port 2), whereas the thinnest coaxial cable (2) is more comparable in size to that of the shortest radiating element (closest to the port 1).

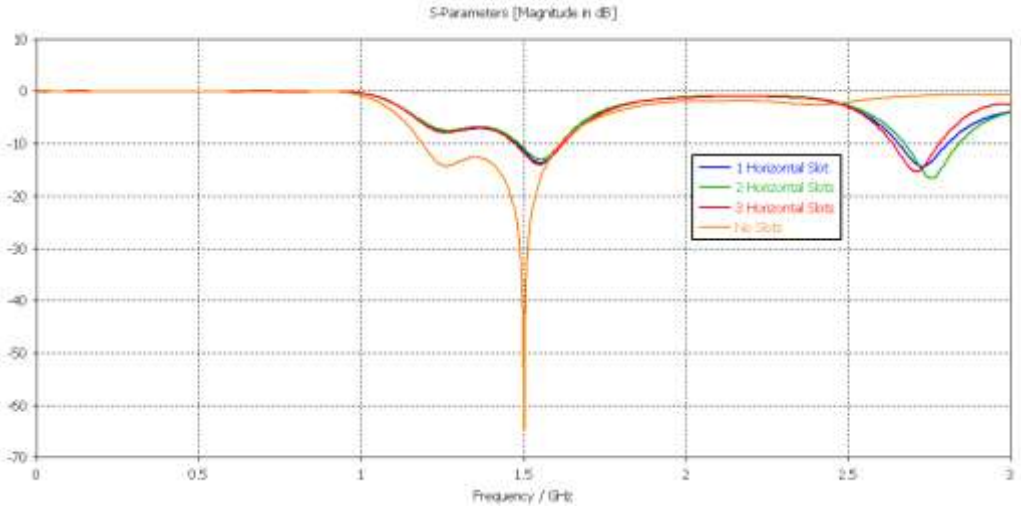

(a) Return loss of the low band port (S_{22})

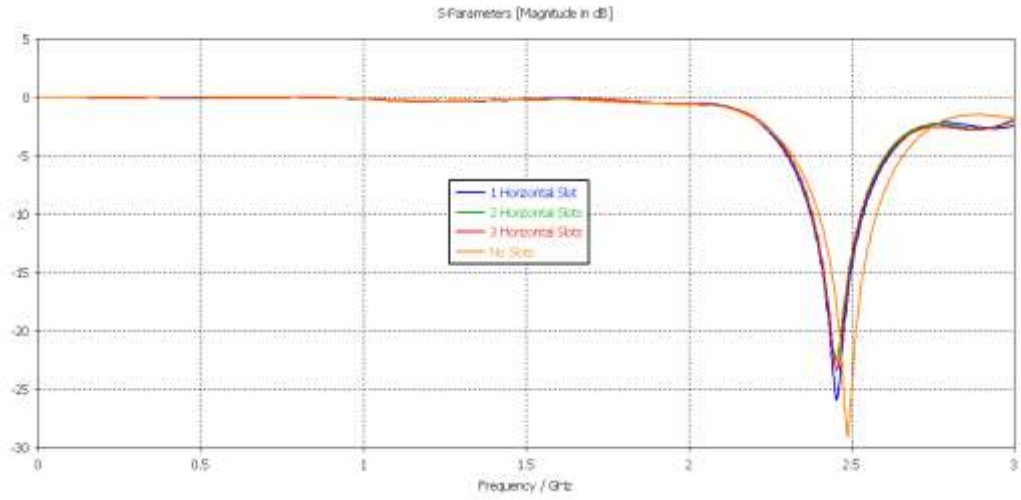

(b) Return loss of the high band port (S_{11})

Figure 3.36: Comparison between return losses for ground plane with the different numbers of horizontal slots as referred above and most favourable situation with no slots, being fed by the coaxial cable 2

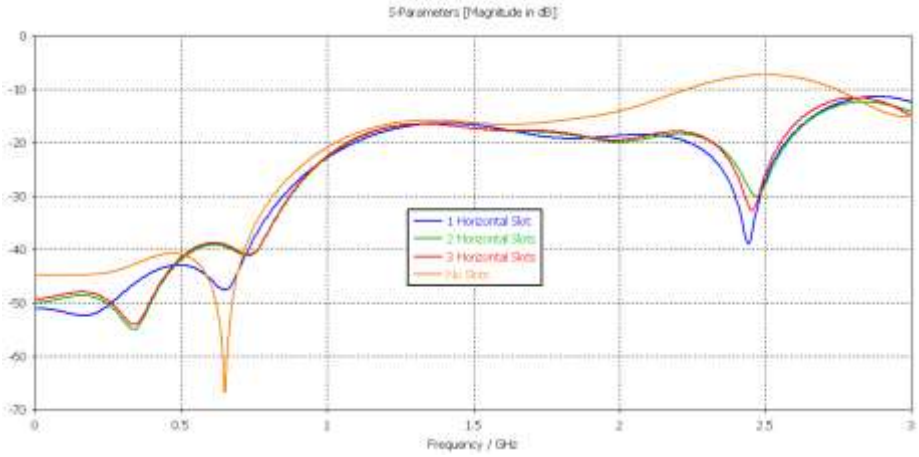

(a) Decoupling between the high band port and the low band port (S_{21})

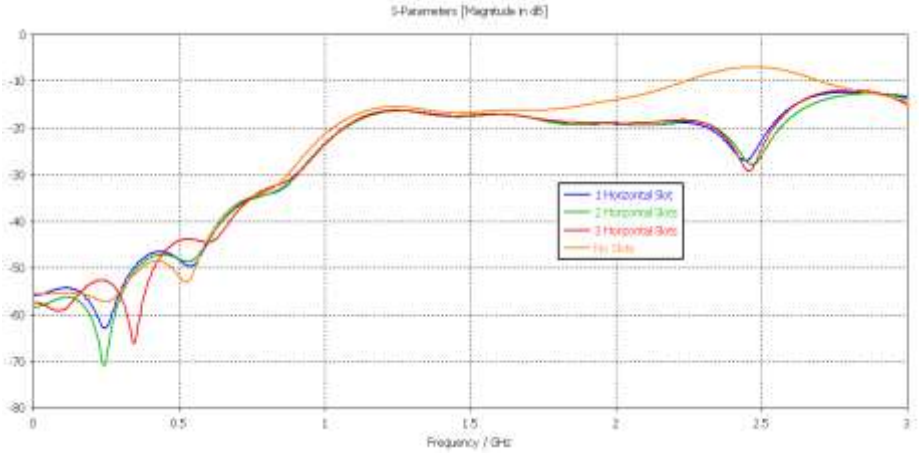

(b) Decoupling between the high band port and the low band port (S_{12})

Figure 3.37: Comparison of decoupling between ports for ground plane with the different numbers of horizontal slots as referred above and most favourable situation with no slots, being fed by the coaxial cable 2

To obtain the S-Parameters shown in Figure 3.38, the CST macro called *Optimiser* was used in order to tune the antenna parameters (h, W, L_HB, L_LB and gap), coaxial cables position and the slots length and position, by setting as target the before-mentioned magnitude (dB) of -10 dB for S-Parameters in the operating bands.

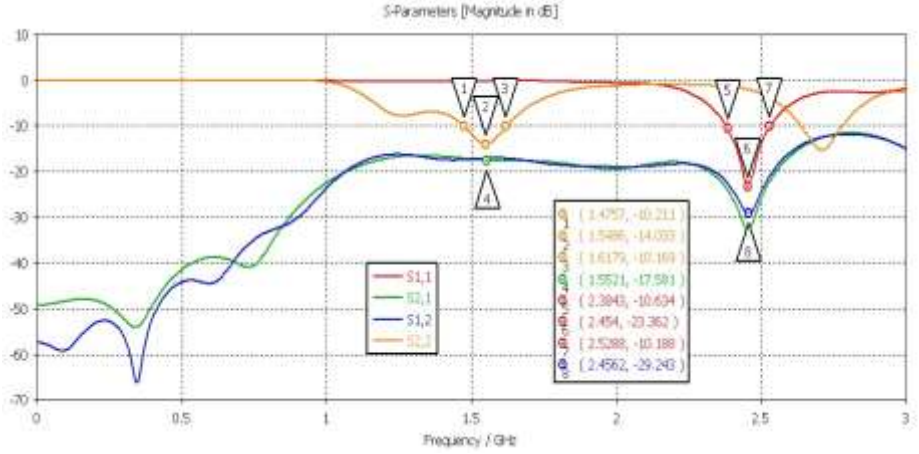

Figure 3.38: S-Parameters for the most favourable solution of defected ground plane with three slots

Surface Current Distribution

In a separate analysis, Figure 3.39 and Figure 3.40 show how the RF surface electrical currents flow through the defected ground plane and radiating parts of the antenna, at the two frequencies of interest (1.5 GHz and 2.45 GHz). Figure 3.39(a) and Figure 3.40(a) show the surface current density range, on a logarithmic scale.

(a) Surface current density range

(b) Surface current distribution on the ground plane (2.45 GHz)

(c) Surface distribution current on the ground plane (1.5 GHz)

Figure 3.39: Simulated surface current distribution on the ground plane for the antenna with three horizontal slots on the ground plane, being fed by the coaxial cable 2

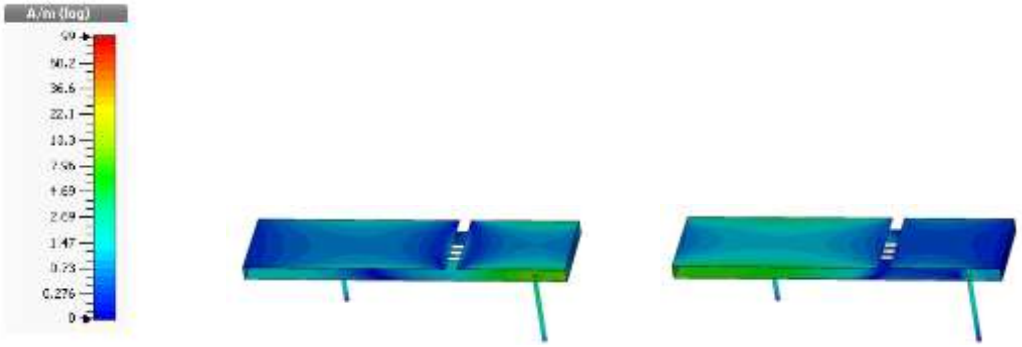

(b) Surface current density range

(d) Surface current distribution on the radiating patches (2.45 GHz)

(e) Surface current distribution on the radiating patches (1.5 GHz)

Figure 3.40: Simulated surface current distribution on the radiating patches for the antenna with three horizontal slots on the ground plane, being fed by the coaxial cable 2

From Figure 3.39(c), it can be observed how the system of three slots acts as a band-stop filter at 1.5 GHz, with a notorious contrast in terms of surface current density on the ground plane, in the proximity of slots. Figure 3.40(b) demonstrates how the isolation enhancement of the low band port translates itself into a better surface current density on the radiating part dimensioned for 2.45 GHz.

Radiation Patterns and Efficiency

The antenna far-field radiation characteristics are studied for the case of three slots. Figure 3.41 shows the standard set of coordinates used for the graphical representation of the antenna 2D radiation patterns (gain in decibels). In this case, θ correspond to the angle measured clockwise off the z-axis, and φ correspond to the angle measured counter clockwise off the x-axis.

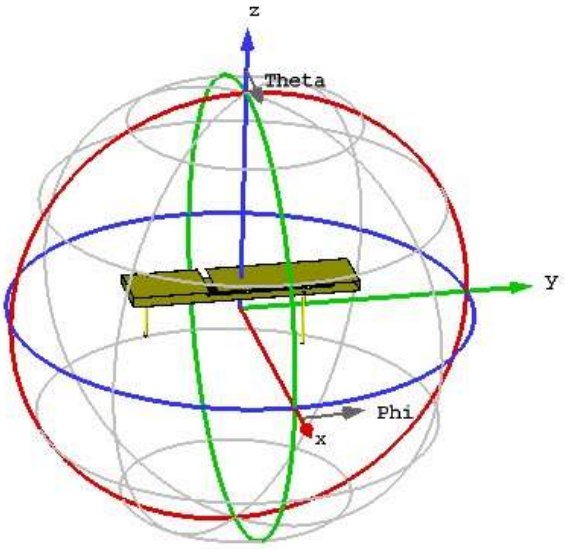

Figure 3.41: Set of coordinates to evaluate the radiation patterns in the flat antenna

The simulated radiation patterns in xz (φ=90°, varying θ) yz (φ=90°, varying θ), and xy (θ=90°, varying φ) planes were evaluated considering the two centre frequencies of interest (1.5 GHz and 2.45 GHz), as can be seen in Figure 3.42. The radiation patterns presented below were computed by using the CST Microwave Studio™. The 2D radiation patterns presented below are normalised to the highest value of the simulated results.

In xz-plane, in respect to both centre frequencies, the presented radiation patterns show that the antenna exhibits a quasi-omnidirectional behaviour. In yz-plane, the radiation patterns, at 1.5 GHz, are almost bidirectional with large back lobes. Considering the classical dipole radiation pattern, it can be noted that there is some resemblance to this antenna, in relation to xz (H-plane) and yz (E-plane) patterns. This similarity to dipole radiation patterns is more visible at the lowest frequency. Moreover, the xy-plane pattern looks quasi-omnidirectional, even considering some asymmetry caused by the geometry and feed positioning.

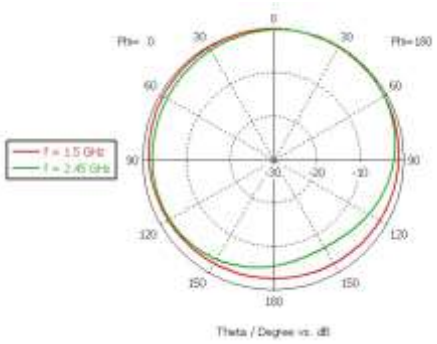

(a) Constant Phi = 0° (xz-plane)

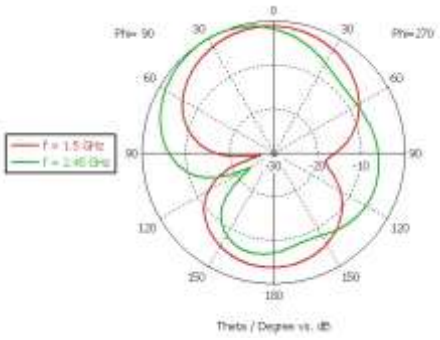

(b) Constant Phi = 90° (yz-plane)

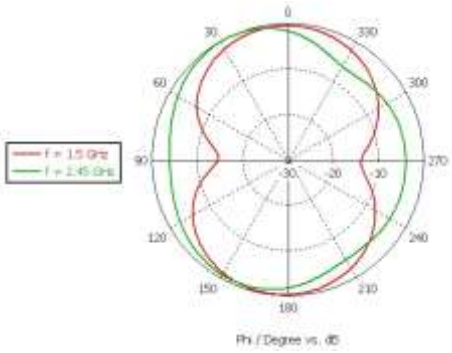

(c) Constant Theta = 90° (xy-plane)

Figure 3.42: Radiation patterns at 1.5 GHz and 2.45 GHz for flat antenna

In relation to the antenna with three horizontal slots, at 1.5 GHz, the estimated radiation efficiency is ~ 96% and, considering the impedance mismatch loss of the antenna when connected to the coaxial cable, the antenna estimated total efficiency is ~ 87%. At 2.45 GHz, the antenna radiation efficiency is ~ 84.4% and its total efficiency reduces to ~ 84.0%, showing almost no loss due to impedance mismatch.

3.4.3 Diagonal Slots

This subsection shows the simulation results, by using diagonal slots placed on the ground plane, centred in the proximity of the gap between the radiating elements. The physical length of the slots is once again dimensioned with a quarter-wavelength long, at approximately the centre frequency of 1584.5 MHz.

After doing some slight changes in respect to the dimensions, placement and number of slots, the effect of the diagonal quarter-wavelength slots is then observed. By varying the number of diagonal slots placed near the low band feeding port, Figure 3.43 shows the three different cases of interest. Figure 3.44 and Figure 3.45 show the most favourable simulation results against the most favourable case with no slots for the S-Parameters.

(a) Ground plane with one diagonal slot

(b) Ground plane with two diagonal slots

(c) Ground plane with three diagonal slots

Figure 3.43: Defected ground plane with diagonal slots

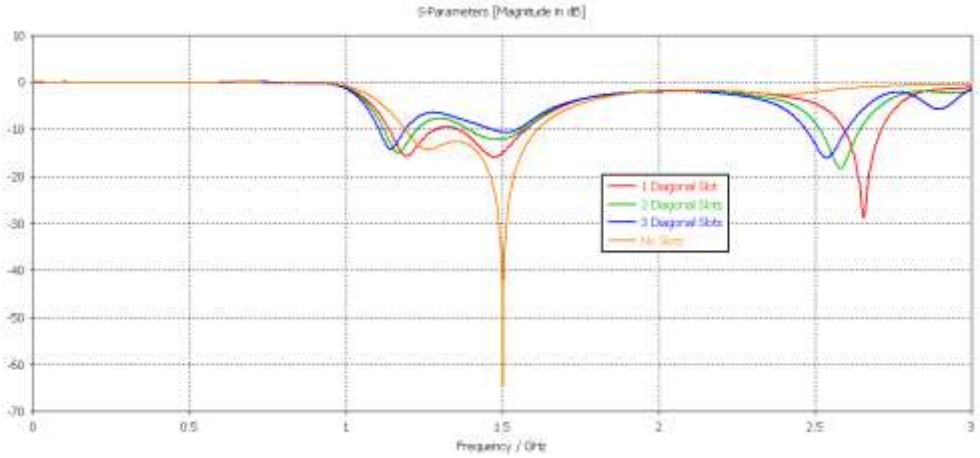

(a) Return loss of the low band port (S_{22})

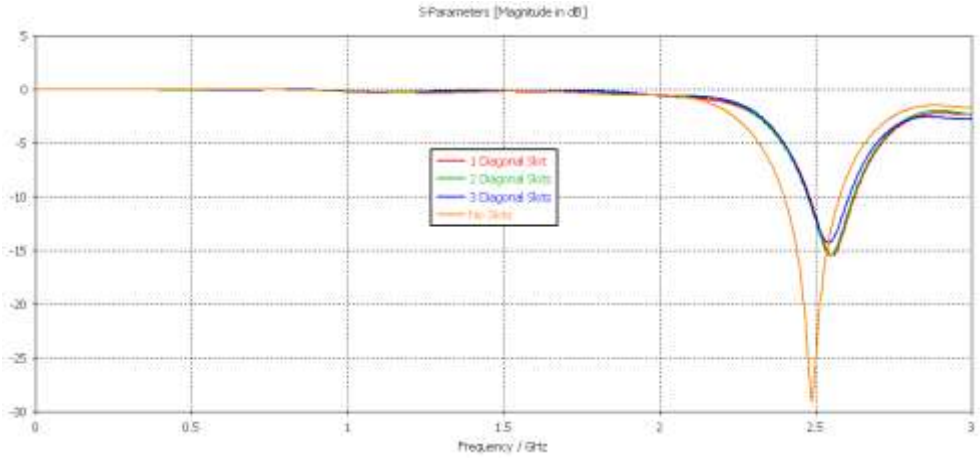

(b) Return loss of the high band port (S_{11})

Figure 3.44: Comparison between return losses for ground plane with different numbers of diagonal slots as referred above and the most favourable case with no slots, being fed by the coaxial cable 2

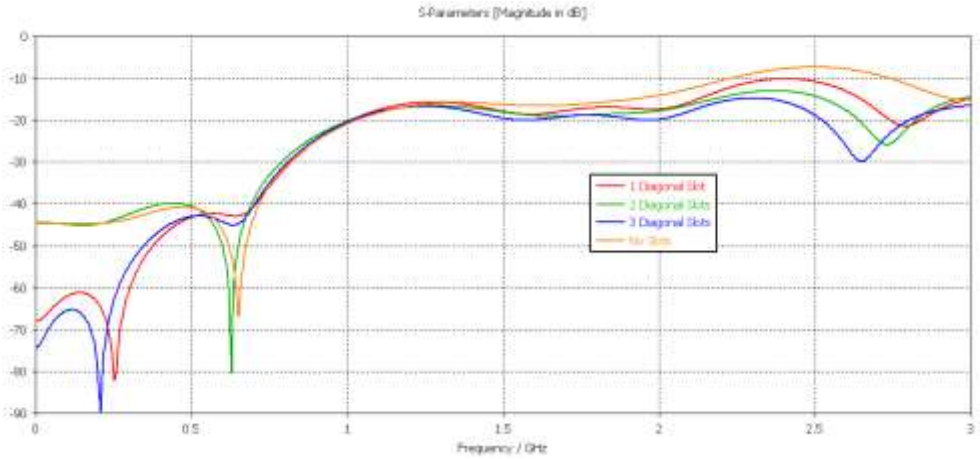

(a) Decoupling between the high band port and the low band port (S_{21})

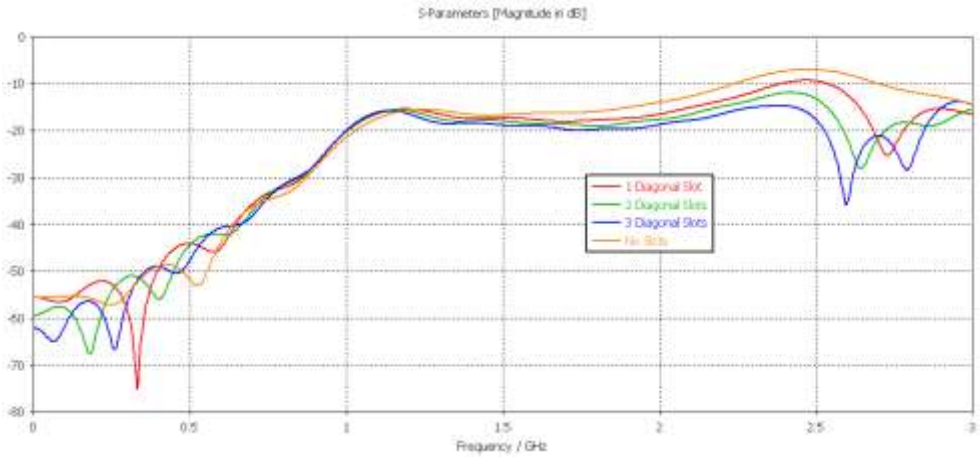

(b) Decoupling between the high band port and the low band port (S_{12})

Figure 3.45: Comparison of decoupling between ports for ground plane with different numbers of diagonal slots as referred above and the most favourable case with no slots, being fed by the coaxial cable 2

Radiation Patterns and Efficiency

In relation to the antenna with three diagonal slots, at 1.5 GHz, the radiation efficiency is ~ 97% and, considering the impedance mismatch loss of the antenna when connected to the coaxial cable, the antenna total efficiency is ~ 86%. At 2.45 GHz, the antenna radiation efficiency is ~ 88% and its total efficiency reduces to ~ 75%. As a conclusion, it is inferred that the solution with horizontal slots (Figure 3.38) shows better results than this solution with diagonal slots. For this reason, it was decided to not present figures for simulated radiation patterns and surface electrical currents flow through the defected ground plane and radiating parts of the antenna (as done in 3.4.2). In the next section, the experimental setup will consider the solution with three horizontal slots.

3.5 Flat Antenna Fabrication and Test

In this subsection, the antenna is measured in a flat condition, i.e., without any applied deformations. S-Parameters and the operation bands are presented. The radiation patterns were

not considered, because of the complexity of its measurement when considering small antennas. The results obtained in this subsection are crucial to the evolution of this work since they can be compared with the closer to target simulated results presented in section 3.4 (see Figure 3.38).

This experimental step was performed in the RF Laboratory using a Vector Network Analyser (VNA) E5071C from Agilent Technologies. Before starting the measurements, the VNA was calibrated over the frequency range 0 to 4 GHz.

The antenna feed point is directly connected to the VNA through a RF cable, which may cause some undesired effects, such as electromagnetic scattering and current distribution along the cable. These effects could significantly change the return loss results of the antenna. The final prototype was connected with the aid of a 50 Ω SubMiniature version A (SMA) connector, which was soldered on the antenna.

3.5.1 Fabrication Method

The first step of the fabrication method consisted on exporting the antenna layout from CST Microwave Studio™ to ABViewer software, and on designing the production film mask with an appropriate scale factor (2:1) in order to reduce certain construction imperfections when down scaled. The CST and ABViewer layouts can be seen, respectively, in Figures 3.46(a) and 3.46(b). And besides, Figure 3.46(c) and Figure 3.46(d) show different views of the antenna prototype.

In an intermediate step, a grease and oxidation free *Kapton*® film surface was assured. The third step of the fabrication method consisted on using the photolithography technique (previously described in section 2.2), in which an etching chemical process is carried out to shape the *Kapton*® copper to the intended geometry, from the use of a photo-resistive solution, sensitive to Ultraviolet (UV) rays (caustic soda and water, normally) to cleaning of the photo-resistive coating by means of a suitable solvent (acetone or isopropyl alcohol, for example). In that regard were used the following equipment in the printing circuit laboratory of Instituto de Telecomunicacões (IT): *Repromaster 2200* as camera; *Agfa Rapiline 43* as film processor; *Laif Galvanotechnik* as UV machine; and finally, *Rota-Spray 'Plus'* as etching machine. Additionally, a very low permittivity foam was used to give mechanical robustness without affecting the electrical properties of the antenna.

In respect to the antenna prototype, the metal parts consisted of a metallised layer of *Kapton*®, instead of only copper. There is a difference between the copper and *Kapton*®, with respect to mechanical properties, there is not a significant difference in terms of their electrical properties. Such properties are those that directly correlate with S-Parameters as well as radiation patterns and efficiency. That was, in fact, the main reason why pure copper was always used through all the simulations.

Kapton® polyimide is a flexible base laminate. This polymer-based material has been commonly used in printed circuits, when the flexibility is one of the project key requirements. It is largely used because of its good combination of physical, chemical and electrical properties (see [73]). Taking into the account the antenna is composed of two parallel metal layers connected by two other perpendicular ones, the antenna prototype was built using copper foil with a thickness of 0.05 mm.

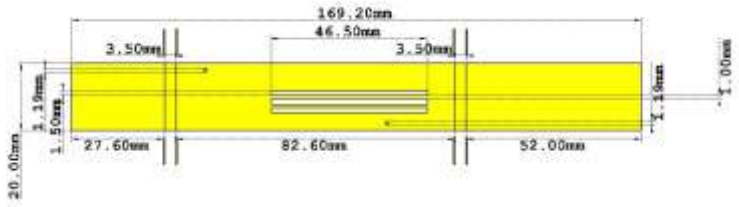

(a) Top view of the unfolded antenna with the respective dimensions (CST layout)

(b) Production mask for the photolithography process (ABViewer layout)

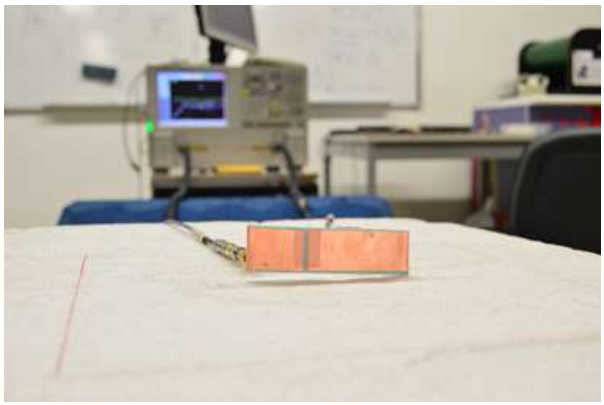

(c) Top metal layer of the antenna prototype

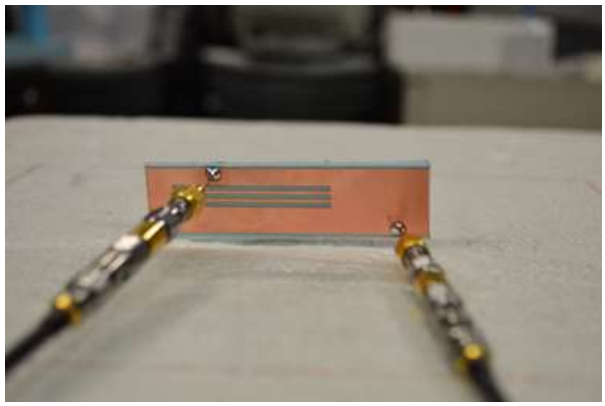

(d) Ground plane metal layer of the antenna prototype

Figure 3.46: Final prototype of the flat antenna and measurement scenario

3.5.2 Experimental S-Parameters Results

As can be seen in the experimental results presented in Figure 3.47 and considering the operating bands of interest in section 1.2, the antenna prototype shows a - 10 dB impedance bandwidth that does not properly cover all the frequencies of interest. In relation to the lower frequencies, based on upper L1 bands, the -10 dB impedance bandwidth should cover the frequency range of [1559,1610] MHz, instead of [1275,1400] MHz (see S_{22}).In relation to the higher frequencies, based on Wi-Fi and BT bands, the -10 dB impedance bandwidth should cover the frequency range of [2400,2495] MHz, instead of [2300,2450] MHz (see S_{11}). Finally, S_{21} and S_{12} should have the resonance peak at 2447.5 MHz, instead of roughly 2900 MHz.

To sum up, there is a frequency downshift in the bands of interest, which is much more pronounced in the lowest band (200~300 MHz, approximately), while in the highest band there are variations of approximately 50~100 MHz. Contrarily to this frequency downshifting behaviour, the resonance peak of decoupling has a frequency upshift of approximately 400~500 MHz. In addition, it should be noted that in many reported works, it is very common a frequency downshift in

experimental results. Besides, it can be seen with the naked eye some imperfections in the antenna prototype, especially in respect to the radiating elements/patches and the distance between them. Moreover, although the electronic equipment used was carefully calibrated, possible calibration or interference errors may also have arisen.

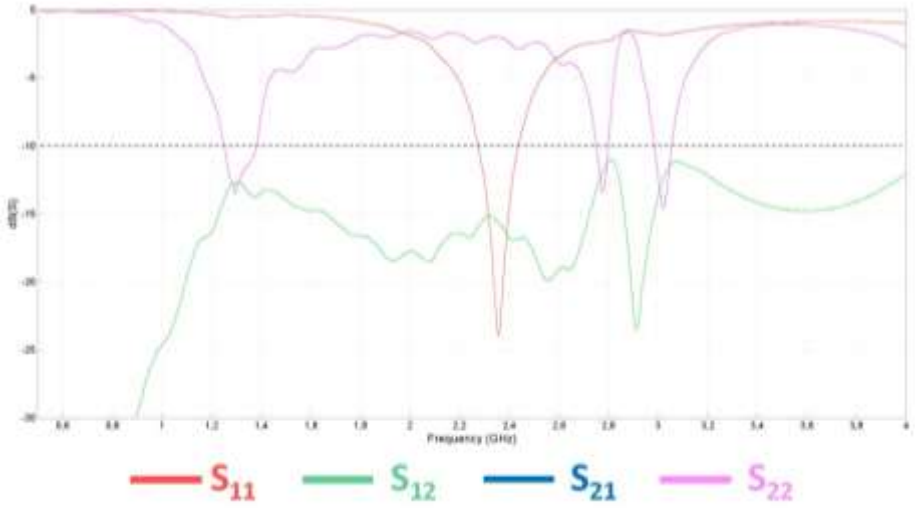

Figure 3.47: Experimental S-Parameters results for the flat antenna ($S_{12} = S_{21}$)

In order to improve these results, a Genetic Algorithm (GA), based on the Darwinian concepts of natural selection and evolution, could be implemented to this CST model. These algorithms are powerful optimisation techniques, being useful in a wide area of electromagnetics, that has been used to enhance the performance of the antennas by optimising a variety of their parameters such as bandwidth, gain and size (among many others, an example is shown in [74]).

3.6 Discussion and Conclusions

The design and development of a compact dual-band antenna prototype with two metal layers were carried out in this chapter. The study of free-space performance of the proposed antenna consisted of a series of simulations of return loss curves, radiation patterns and efficiency. Experimental results were realised, concerning the return loss.

Before starting a parametric study of the antenna dimensions and feed (sections 3.2 and 3.3, respectively), certain initial conditions were presented. These included a description of the antenna structure and geometry, with its duly justified initial values (3.1.1); the chosen materials for the antenna patches/radiating elements, substrate and ground plane (3.1.2); and the initial approach for the feed line and feed point (3.1.3). In the whole simulation process, it is worth noting that the pure copper was the material used for the 3D CST model of the antenna patches and ground plane, whereas for the substrate, it was used an air substrate. An RG405/U-086 semi-rigid coaxial cable was chosen as feed line.

The parametric study of the antenna dimensions included the following parameters: height h, width W, high band radiating element length L_HB, low band radiating element length L_LB and gap (subsections 3.2.1-3.2.5). The parametric study of antenna high band and low band feed lines included three stages: feed lines placed at the same side (3.3.1), on opposite sides (3.3.2) and

other positions (3.3.3). Moreover, the effect of the coaxial cable is analysed, including a comparison with the use of discrete ports (3.3.4).

In order to suppress undesired mutual coupling problems, a study of the effect of defected ground structures (finite cuts) was carried out. Horizontal and diagonal slots placed on the ground plane were the chosen strategies (3.4.2 and 3.4.3). Here, the RG405/U-086 semi-rigid coaxial cable was replaced by the EZ 47-TP/M17 one. Then, after finding out that the defected ground plane with three slots has proven to be the optimal solution (see Figure 3.38), it became feasible to build and test, in free-space, an antenna prototype with *Kapton*® film, low permittivity foam (for mechanical support), and fed by the EZ 47-TP/M17 coaxial cable, together with a Sub-Miniature Version A (SMA) connector.

The simulations results have shown a - 10 dB impedance bandwidth that covers the goal Wi-Fi and

BT bands, centred at 2.45 GHz, and in the upper-bands of radio-navigation services of interest (GPS L1, Galileo E1 and GLONASS G1).

Because of the experiment process, it was found that the two operation bands were slightly downshifted, in such a way that the measured S-Parameters did not validate the $S_{ij} \leq 10$ dB criterion in the whole range of frequencies of interest. This downshift was much more evident in the upper-bands of radio-navigation services with deviations of 200~300 MHz (S_{22}), while in Wi-Fi and BT bands there were variations of 50~100 MHz (S_{11}). Contrarily to this frequency downshifting behaviour, the resonance peaks of decoupling (S_{12} and S_{21}) had a frequency upshift of 400~500 MHz This noticeable performance loss is perhaps due to possible errors in the fabrication process.

Chapter 4

Antenna Integration in an Ankle Bracelet

In section 4.1 is shown the reference bracelet model that is used for bending and casing of the antenna optimised in the previous chapter (see most favourable results in Figure 3.38). Here, it is stated the inevitable repercussions which comprises the antenna design using the CST software. The simulation results related to the effects in this context are also reported here.

Section 4.2.1 shows the description of the proposed biological model, used as a reference, in order to evaluate the effect of the human body in the overall performance of the antenna. Inspired by the real purpose of the reference bracelet, it was created a 3D model for the following parts of human body: ankle and foot.

4.1 Effect of Bending and Casing

4.1.1 Reference Ankle Bracelet

One of the most pertinent ways the bracelet device's materials could influence in antenna performance is by means of their dielectric properties. A 3D model must be built, with a suitable choice of materials, in order to emulate a real case. To that end, it is used a GPS ankle bracelet device based on a commercial company. Again, this choice was mainly done due to the author's interest in bracelet devices for personnel tracking, security purposes and medical/health care purposes. Figure 4.1 shows the 3D CST model of the reference ankle bracelet, in different views.

(a) Side view of the 3D CST model of the bracelet

(b) Front view of the 3D CST model of the bracelet

(c) 3D CST model of the bracelet in perspective

Figure 4.1: Different views of the used reference bracelet for the antenna casing

Despite seeming to have a cylindrical geometry, this ankle bracelet features an elliptical geometry. In fact, it is "elliptical ring-shaped", in which its width is along the y-axis, its height is along the z-axis, and their semi-major and semi-minor axis are along the y-axis and x-axis, respectively. The values of their parameters can be seen in Table 4.1.

Table 4.1: Values for the parameters of the reference ankle bracelet

Parameter	Value [mm]
Outer Ring Semi-Major Axis	50
Outer Ring Semi-Minor Axis	45
Inner Ring Semi-Major Axis	45
Inner Ring Semi-Minor Axis	40
Width	6
Height	35
Rings Thickness	1

Furthermore, the 3D CST model of the reference ankle bracelet is composed by a common thermoplastic polymer with an electrical permittivity of 2.8 (called ABS).

4.1.2 Geometry, Substrate Material and Feed Line

Flexible antennas have been especially suitable for wearable applications. In addition to their flexibility, antennas should be small, robust and low-profile, in order to achieve an optimised integration into wearable devices.

Throughout the simulations in a bending scenario, an ellipsoidal structure had to be attached on the antenna back-side ground plane, in accordance with the shape of the reference ankle bracelet (see Figure 4.1). To achieve this, it was necessary to add an intermediate layer between the ground plane and the radiating elements. With this step, it became possible to use the CST tool, known as *Layer Stackup Bending*. However, since each layer must be composed by the same material to use this tool, the shorting walls needed to be removed, before applying such *Layer Stackup Bending* over the cylindrical surface. Then, the shorting walls were attached to the side surfaces of the already bent intermediate layer.

The robustness of the antenna in study under a bending scenario would be guaranteed with the same low permittivity foam used in the experimental stage (see subsection 3.5.1), although it would have to be resized to accommodate the geometry change. However, this foam was not included in the simulations, as it is not expected to affect the electrical properties of the antenna. In relation to the feed line used through the simulations, it was necessary to replace the EZ47-TP/M17 coaxial cable (see subsection 3.4.2) by discrete ports. Apart from being easier to integrate into the 3D CST model of the ankle bracelet, it does not cause significant impact on antenna performance.

4.1.3 S-Parameters

The return loss and - 10 dB operating bands of interest must be analysed under a bending scenario, since these parameters are likely to be changed. In Figure 4.2, it is possible to see the difference between the optimal solution for the flat antenna in free-space (green line) and bending scenario (red line), in respect to these parameters. Note that the bending was done along the z-axis (see Figure 4.6).

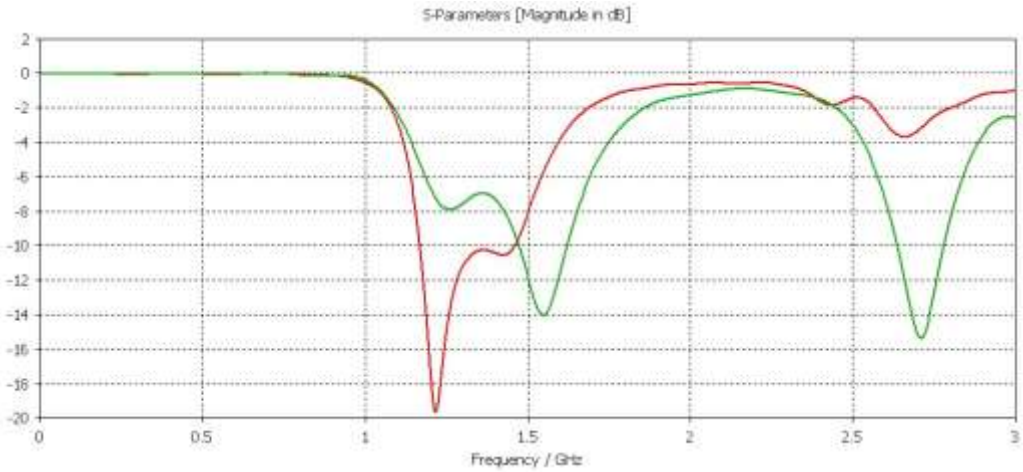

(a) Return loss of the low band port (S_{22})

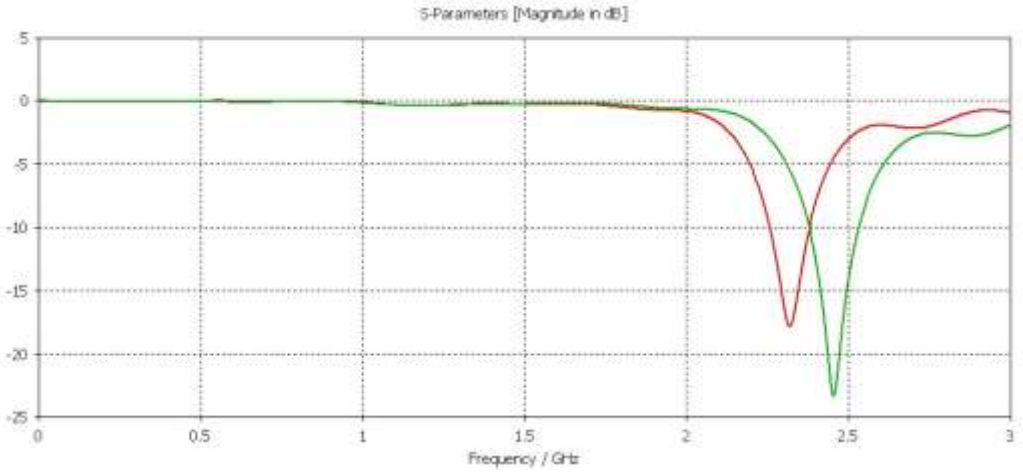

(b) Return loss of the high band port (S_{11})

Figure 4.2: Comparison of return losses for the optimal free-space solution and bending scenario

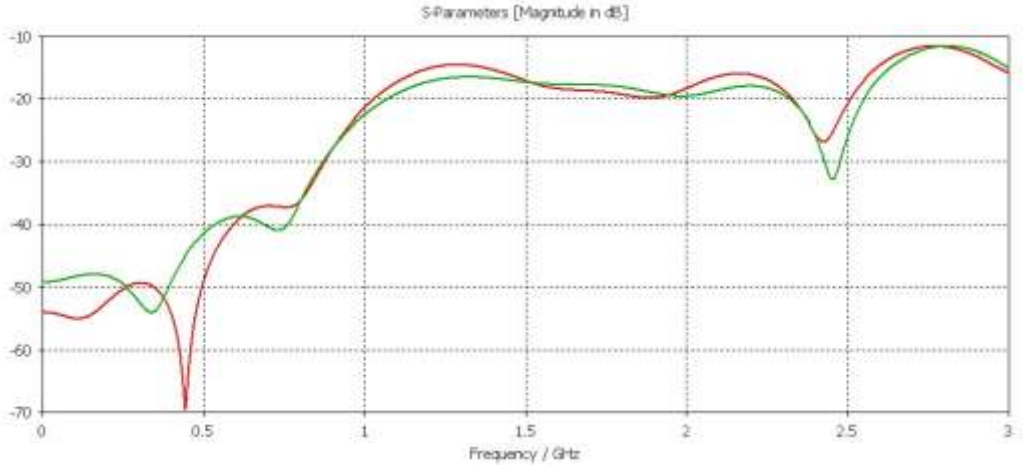

(a) Decoupling between the high band port and the low band port (S_{21})

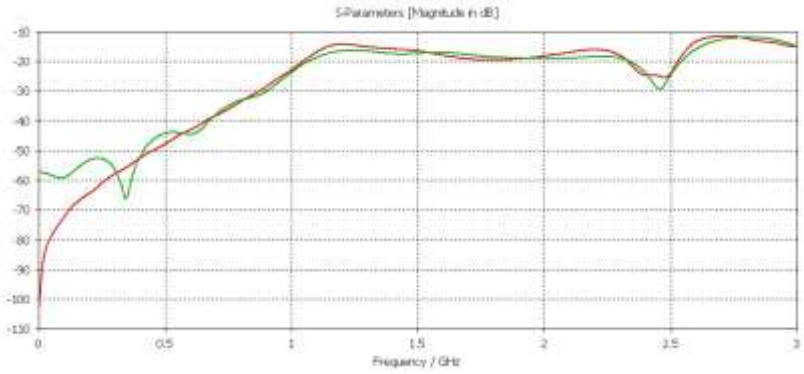

(b) Decoupling between the low band port and the high band port (S_{12})

Figure 4.3: Comparison of decoupling between ports for optimal free-space solution and bending scenario.

It can be concluded that the resizing of the antenna dimensions in accordance with the curved structure of the ankle bracelet caused an operating frequency downshift. It can be explained by the fact that the resizing has translated into an increase of the radiating elements length (+ 0.57 mm and + 1.93 mm in the low and high band elements, respectively).

Apart from the evaluation of return loss and -10 dB operating bands of interest under a bending scenario, it is also important to evaluate the casing scenario, by considering the presence of the whole reference ankle bracelet. At this time, in Figure 4.4 and Figure 4.5, the free-space (green line), bending (red line) and casing (blue line) scenarios can be compared for the same parameters.

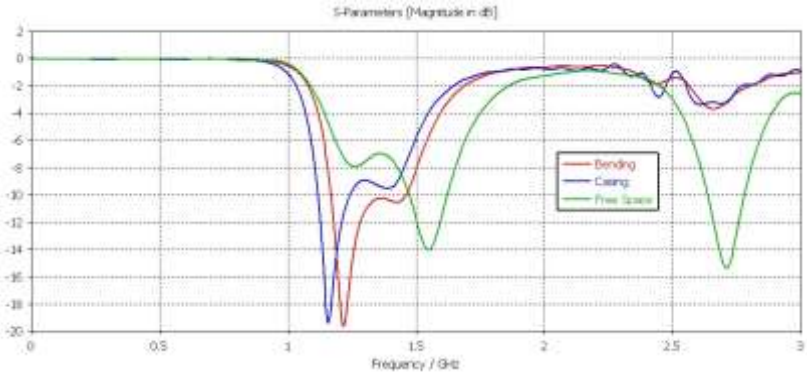

(a) Return loss of the low band port (S_{22})

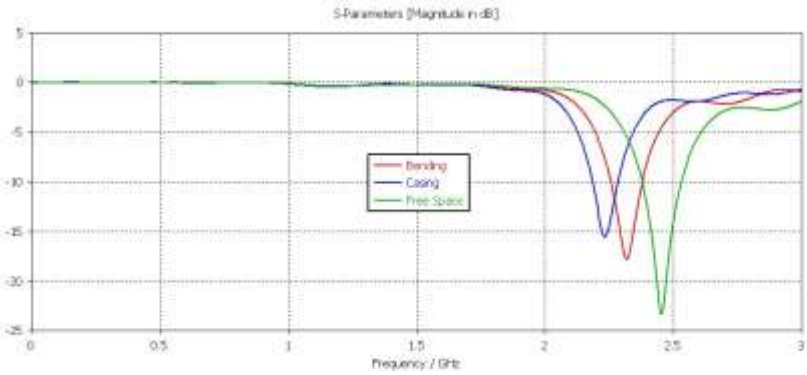

(b) Return loss of the high band port (S_{11})

Figure 4.4: Comparison of return losses for the optimal free-space solution and bending and casing scenarios

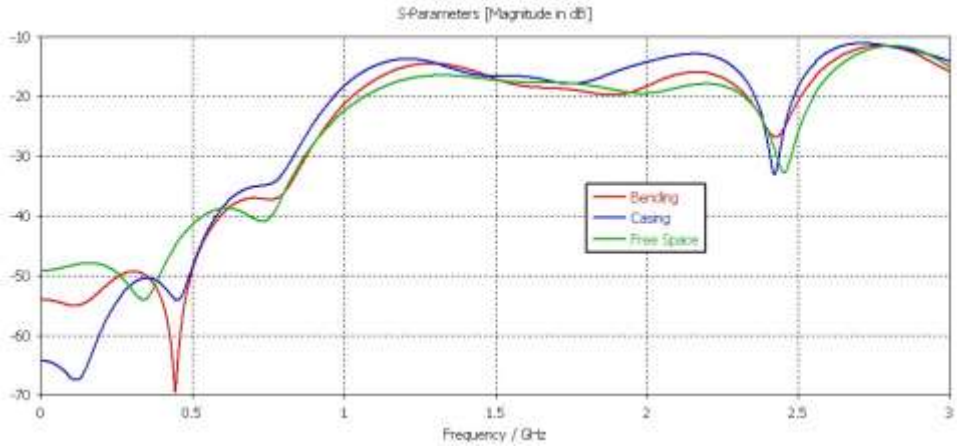

(a) Decoupling between the high band port and the low band port (S_{21})

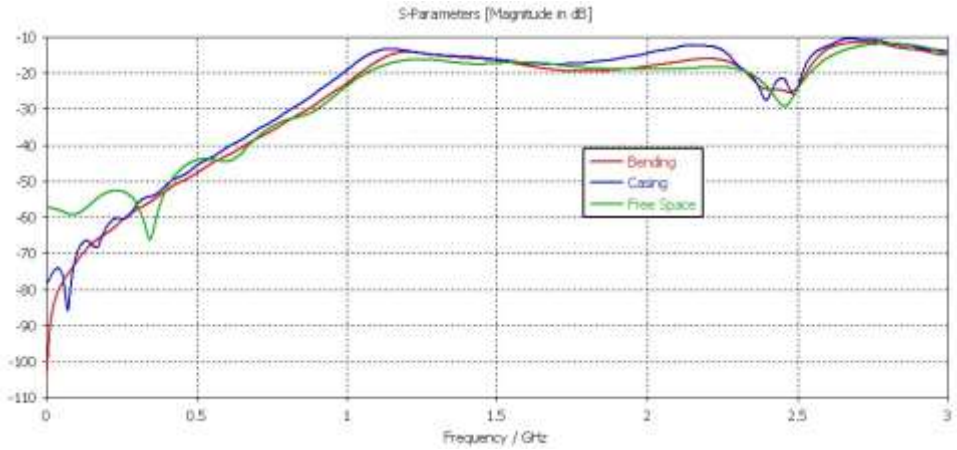

(b) Decoupling between the high band port and the low band port (S_{12})

Figure 4.5: Comparison of decoupling between ports for the optimal free-space solution, bending and casing scenarios

In this way, Figure 4.4 and Figure 4.5 lead to conclude that the casing of the reference antenna caused a small frequency downshift, when compared with the free-space and bending scenarios. In fact, structures covering antennas, usually called radomes (from radar dome), affect the radiation as well as the antennas resonance when they are placed in the proximity to or touching the antennas. Enclosing an antenna with plastic material downshifts their operating frequencies. Plastic has a higher dielectric constant than air. Therefore, the relative proximity of the plastic makes the antenna see a higher effective dielectric constant, leading to an increase of the electrical length of the antenna, as well as a reduction of the operating frequencies.

4.1.4 Radiation Patterns and Efficiency

The antenna far-field radiation characteristics are investigated. Figure 4.6 shows the standard set of coordinates used for the graphical representation of the antenna 2D radiation patterns (gain in decibels).

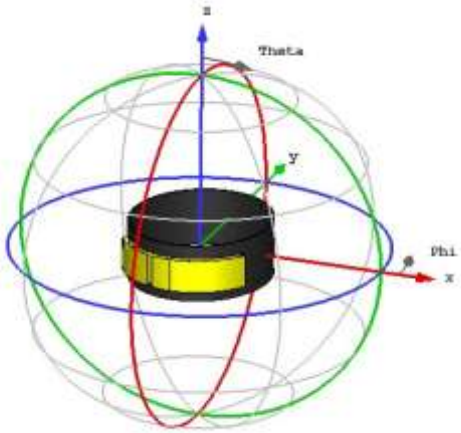

Figure 4.6: Set of coordinates to evaluate the radiation patterns in the bending and casing scenarios

The simulated radiation patterns in xz (φ=0°, varying θ), yz (φ=90°, varying θ), and xy (θ=90°, varying φ) planes were evaluated considering the downshifted centre frequencies of interest, because of bending operation done in CST Microwave Studio™ (1.22 GHz and 2.32 GHz), as can be seen in Figure 4.7. In addition, Figure 4.8 presents the radiation patterns at the two centre frequencies of interest (1.5 GHz and 2.45 GHz). Again, the radiation patterns presented below have been computed using the CST Microwave Studio™. It is important to note that the 2D radiation patterns presented below are normalised to the maximum value of the simulated results.

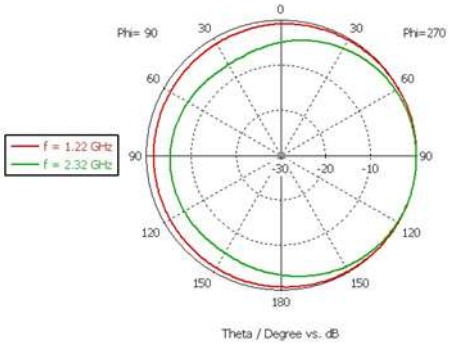

(a) Constant Phi = 90° (yz-plane)

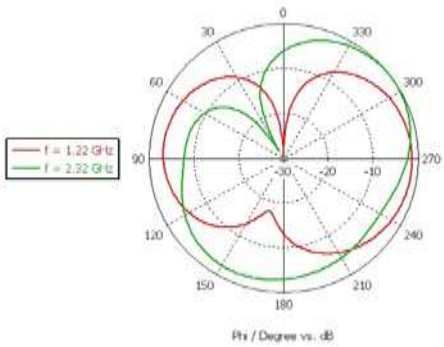

(b) Constant Theta = 90° (xy-plane)

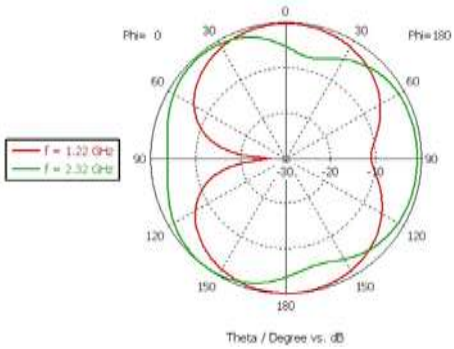

(c) Constant Phi = 0° (xz-plane)

Figure 4.7: Radiation patterns at the centre frequencies, 1.22 GHz and 2.32 GHz, for the bent antenna

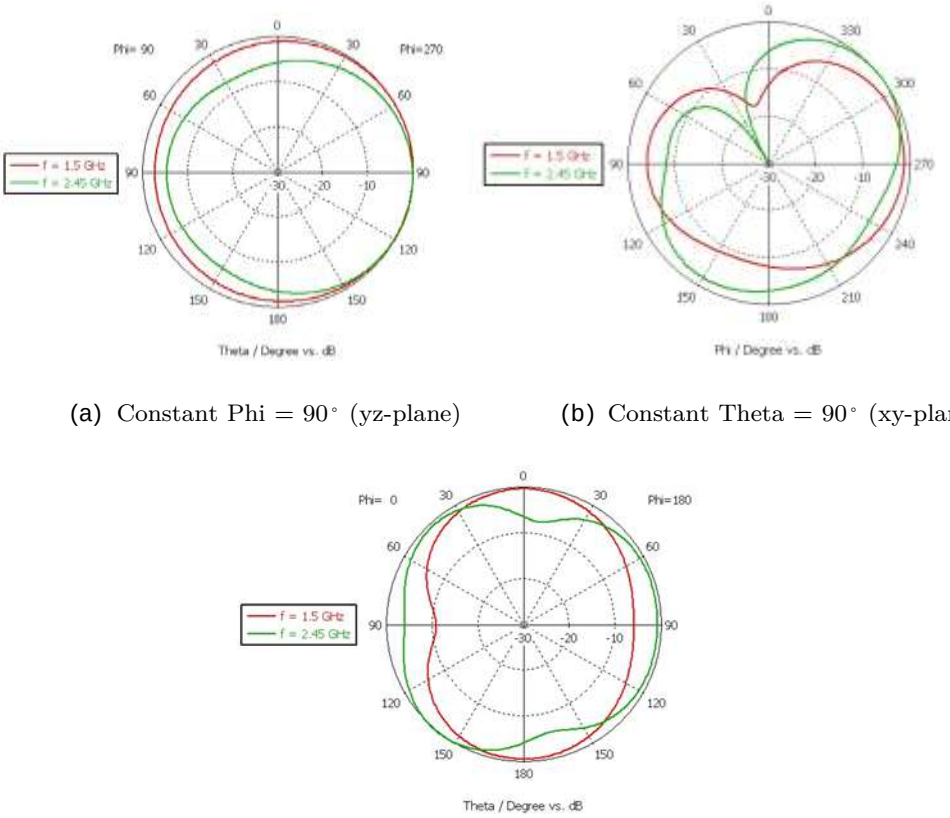

(a) Constant Phi = 90° (yz-plane)

(b) Constant Theta = 90° (xy-plane)

(c) Constant Phi = 90° (yz-plane)

Figure 4.8: Radiation patterns at the goal centre frequencies, 1.5 GHz and 2.45 GHz, for the bent antenna

From Figure 4.7, regardless of the bending process for both the downshifted operating frequencies, (1.22 GHz and 2.32 GHz), the shape of radiation patterns remains almost the same. At these two frequencies, bending deformations have no significant influence in the antenna radiation patterns, when compared with the radiation patterns of the flat antenna in free-space (see Figure 3.42). Using again the classical dipole radiation pattern as reference point, this antenna looks like a dipole antenna, with its length along the x-axis. The xy-plane pattern (E-plane) looks like a dipole pattern, and the yz-plane pattern (H-plane) looks quasi-omnidirectional, even considering some asymmetry caused by the geometry and feed positioning. This similarity is still more visible at the lowest frequencies. At the goal operating frequencies (1.5 GHz and 2.45 GHz), the resonance is lost, as seen before, which in turn leads the antenna to lose the dipole behaviour (see Figure 4.8). This loss is more visible in the xy-plane pattern (E-plane). In relation to the bent antenna, at 1.22 GHz, the estimated radiation efficiency is ~ 100% and the estimated antenna total efficiency is ~ 96%. At 2.32 GHz, the antenna radiation efficiency is ~ 84% and its total efficiency reduces to ~ 82%. In comparison with simulated results for the flat antenna (at the end of subsection 3.4.2), there is a gain increase caused by the ellipsoidal structure, noticeable in the highest operating frequency.

The simulated radiation patterns in the same planes were evaluated considering the downshifted centre frequencies of interest due to the bending and casing both together (1.16 GHz and 2.24 GHz), as can be seen in Figure 4.9, as well as the two centre frequencies of interest (1.5 GHz and 2.45 GHz), as can be seen in Figure 4.10.

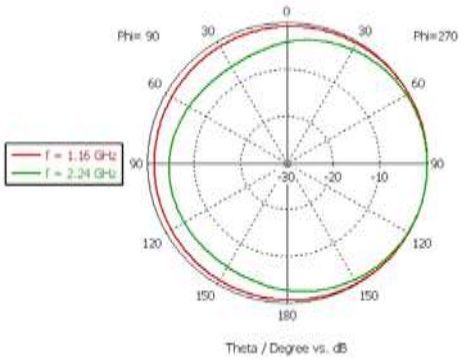

(a) Constant Phi = 90° (yz-plane)

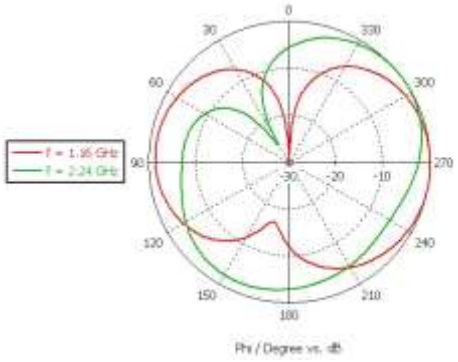

(b) Constant Theta = 90° (xy-plane)

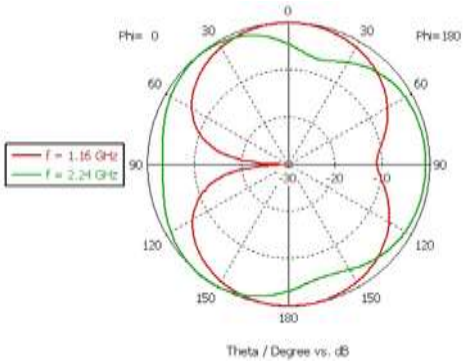

(c) Constant Phi = 90° (xz-plane)

Figure 4.9: Radiation patterns at the centre frequencies, 1.16 GHz and 2.24 GHz, for the bent and cased antenna

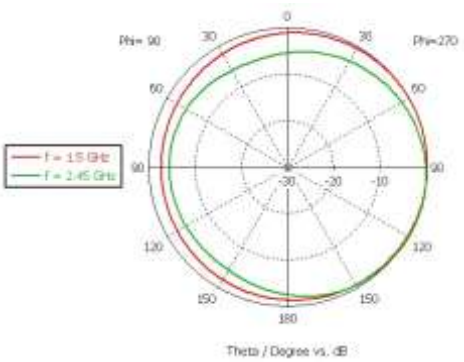

(a) Constant Phi = 90° (yz-plane)

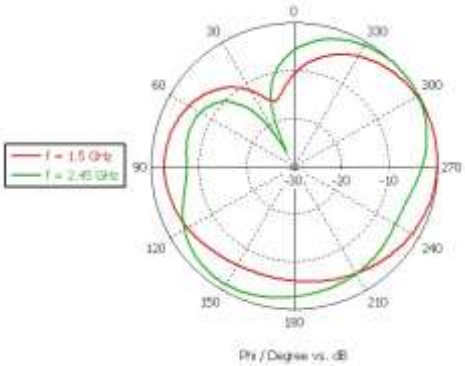

(b) Constant Theta = 90° (xy-plane)

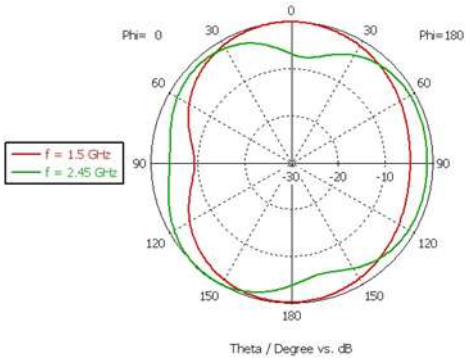

(c) Constant Phi = 90° (xz-plane)

Figure 4.10: Radiation patterns at the goal centre frequencies, 1.5 GHz and 2.45 GHz, for the bent and cased antenna

Again, when comparing these radiation patterns with those of the flat antenna in free-space (see Figure 3.42), it can be concluded from Figure 4.9 that this antenna can still be seen as a dipole antenna, despite of the bending and casing processes, for both the downshifted operating frequencies. The xy-plane pattern (E-plane) looks a dipole pattern, and the yz-plane pattern (H-plane) looks quasi-omnidirectional. This similarity is more visible at the lowest frequencies. From Figure 4.10, it can be seen that the similarity to dipole is lost, for the goal operating frequencies, 1.5 GHz and 2.45 GHz.

In relation to the bent and cased antenna, at 1.16 GHz, the radiation efficiency is ~ 100% and the antenna estimated total efficiency is ~ 94%. At 2.24 GHz, the antenna estimated radiation efficiency is ~ 87% and its total efficiency reduces to ~ 81%. In comparison with simulated results for the only bent antenna, the whole casing does not lead to significant differences.

4.2 Effect of Human Body

4.2.1 Biological Model

As seen before in section 2.4, human body proximity causes the electromagnetic absorption in tissues that may modify antenna parameters such as its impedance bandwidth, radiation pattern, polarisation and efficiency. This section depicts the performance of the chosen antenna near a biological model of the human ankle and foot.

Unlike the voxel models, which are complex and demands longer computer times, simplified models are sufficiently suitable to predict how the antenna performs near the human body. In order to decrease the computational effort associated with a full human model, a four-tissue layered human model with a simplified geometry shape was considered appropriate, and a single-layered model was taken for the ankle and foot (see Figure 4.11). The considered ankle model consists of a 120 mm long elliptical model, and four tissue layers that represent bone, muscle, fat, and skin. Based on previous simulations, it was concluded that a more detailed biological description of the foot was not very influential, so it was decided to use an even more simplified model by considering the foot as a single-layered brick. The foot model consists of a brick with 250 x 76 x 40 mm^3, which represents bone. In this way, this model has well-defined edges, which makes it a better solution

in terms of computational resources allocated for the simulations. Table 4.2 presents the thicknesses of each body tissue layer that compose the ankle model.

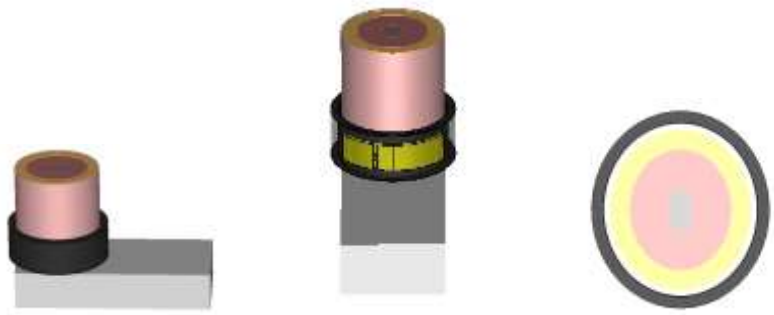

(a) Side view of the 3D CST model of ankle and foot with the bracelet device

(b) Front view of the 3D CST model of ankle and foot with the bracelet device

(c) Top view of the 3D CST model from an ankle cut with the bracelet device

Figure 4.11: Different views of the used biological model for the study of the antenna near human body

Table 4.2: Values for tissue layers of the human ankle model

Tissue	Thickness [mm]
Skin	2
Fat	10
Muscle	20
Bone	11 (Semi-Major Axis)

Since the human body is a non-homogeneous and multi-layer medium, it is very important to study the properties of each tissue comprised in the reference model. Accurate modelling of any real body part requires the dispersion characterisation of each body tissue, in respect to operating frequency range of the antenna under study. The bone, muscle, fat, and skin materials properties were taken from CST Microwave Studio^{TM} *Material Library*. In order to evaluate the SAR, Table 4.3 shows the definition of values for body tissues density.

Table 4.3: Density of human body tissues

Tissue	Density [kg.m^{-3}]
Skin	1100
Fat	910
Muscle	1041
Bone	1850

4.2.2 S-Parameters

In order to investigate the return loss and -10 dB operating bands of interest of the antenna near the human body, simulations were carried out using the proposed biological model. From Figure 4.12 and Figure 4.13, in respect to S-Parameters, it can be confronted the four study cases: flat antenna in free-space (green line), bending (red line), casing (orange line) and under the influence of a biological model (blue line).

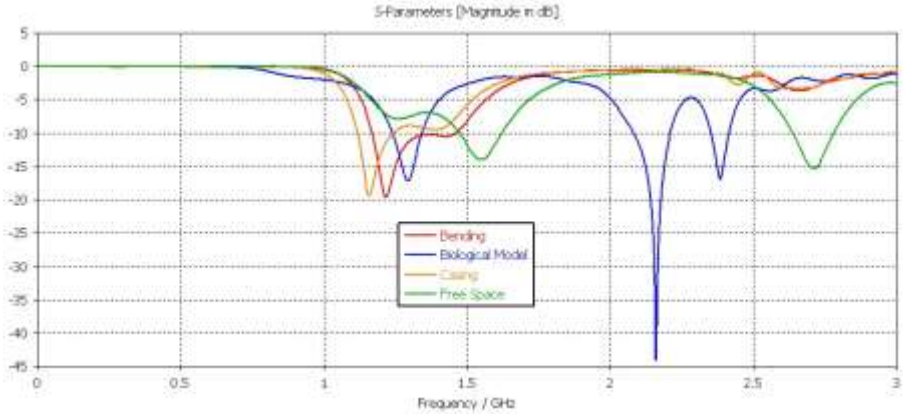

(a) Return loss of the low band port (S_{22})

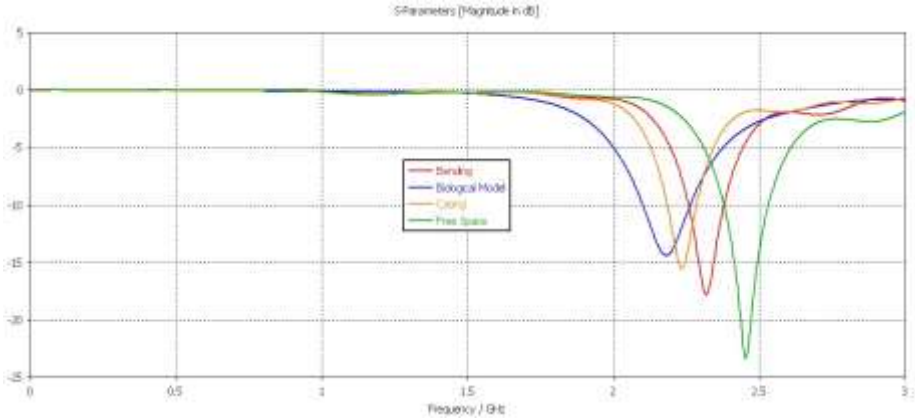

(b) Return loss of the high band port (S_{11})

Figure 4.12: Comparison of return losses for all the different scenarios

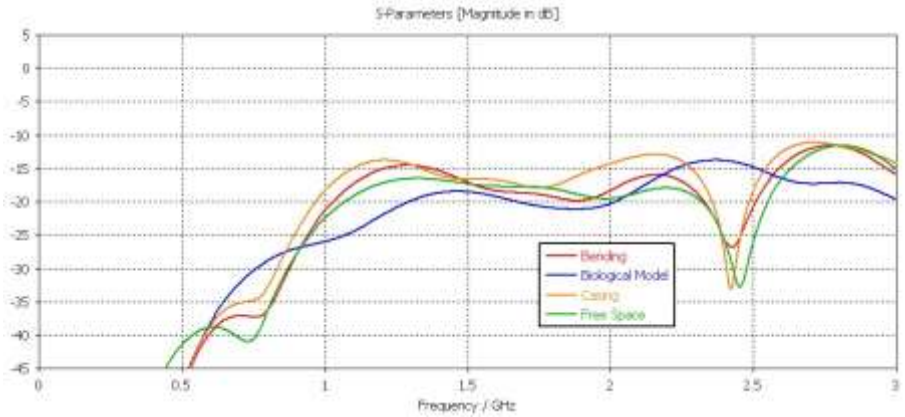

(a) Decoupling between the high band port and the low band port (S_{21})

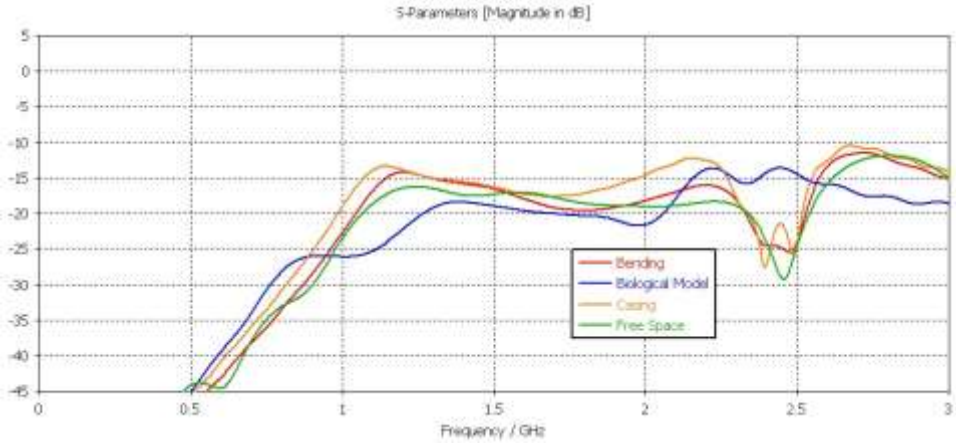

(b) Decoupling between the high band port and the low band port (S_{12})

Figure 4.13: Comparison of decoupling between ports for all the different scenarios

From the results, it can be observed a significant difference in return loss when the suggested antenna cased by the ankle bracelet is placed close to the human ankle and foot model. For 2 mm between the ankle bracelet and the biological model, the results show that the lowest operating frequency is shifted downwards from 1584.5 to 1291.9 MHz, in comparison with the free-space curve. The highest operating frequency is also shifted downwards from 2447.5 to 2187.8 MHz, in comparison with the free-space curve. Both modulus of S_{11} and S_{22} decreased, due to the expected losses caused by the human body. In relation to the mutual S-Parameters, both peak frequencies are lost but are still below -10 dB.

4.2.3 Radiation Patterns and Efficiency

The antenna far-field radiation characteristics near the proposed biological model are studied. Figure 4.14 shows the standard set of coordinates used for the graphical representation of the antenna 2D radiation patterns (gain in decibels). θ and φ correspond to the same angles as the ones represented in Figure 4.6.

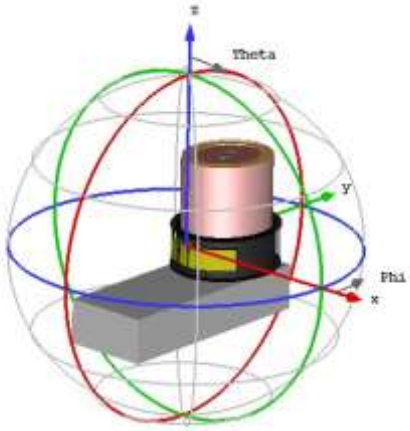

Figure 4.14: Set of coordinates used in order to evaluate the radiation patterns near the human body.

The simulated radiation patterns in xz (φ=0°, varying θ) yz (φ=90°, varying θ), and xy (θ=90°, varying φ) planes were evaluated considering the downshifted centre frequencies of interest due to the proximity of the biological model of the human body done in CST Microwave Studio™(1.29 GHz and 2.19 GHz), as can be seen in Figure 4.15. Moreover, Figure 4.16 shows the radiation patterns for the two centre frequencies, 1.5 GHz and 2.45 GHz.

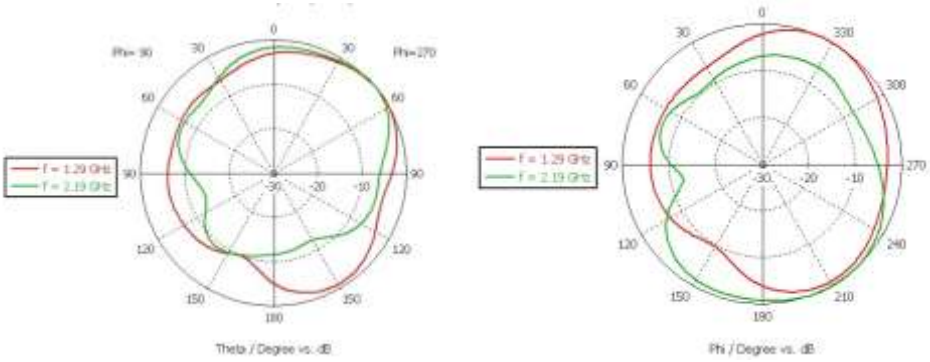

(a) Constant Phi = 90° (yz-plane)

(b) Constant Theta = 90° (xy-plane)

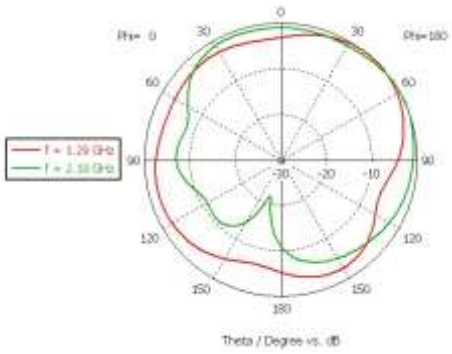

(c) Constant Phi = 0° (xz-plane)

Figure 4.15: Radiation patterns at the centre frequencies, 1.29 GHz and 2.19 GHz (biological model)

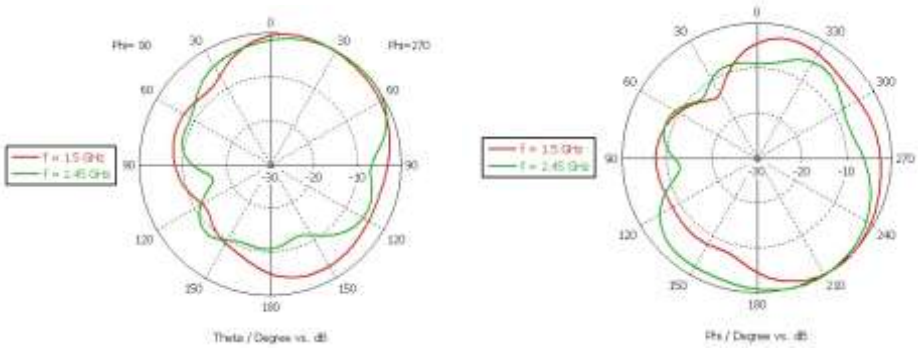

(a) Constant Phi = 90° (yz-plane)

(b) Constant Theta = 90° (xy-plane).

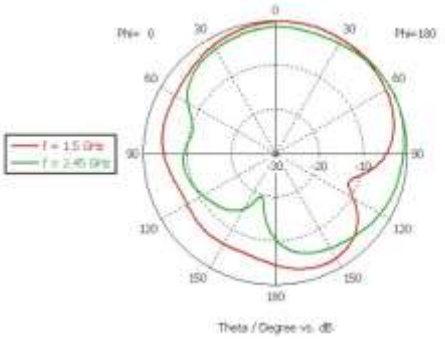

(c) Constant Phi = 0° (xz-plane)

Figure 4.16: Radiation patterns at the goal centre frequencies, 1.5 GHz and 2.45 GHz (biological model)

It is important to compare these radiation patterns with those of the flat antenna in free-space, and also with those of the antenna in bending and casing scenarios (see Figure 3.42, and Figure 4.7 to Figure 4.10). Figure 4.15 and Figure 4.16 show that the proximity of the biological model of the ankle modifies their shapes, reducing the antenna gain, in each plane. This happens for both the downshifted operating frequencies, 1.29 GHz and 2.19 GHz, and the goal operating frequencies, 1.5 GHz and 2.45 GHz.

In relation to the simulation results for radiation efficiency and total radiation efficiency, it can be concluded that their maximums occurred at the highest downshifted operating frequency ($f =$ $2.19 GHz$), with values of ~-8.1 dB (~ 15%) and -8.4 dB (~ 14%), respectively. The radiation efficiency and total radiation efficiency, at the lowest downshifted frequency ($f = 1.29 GHz$) reached values of ~-8.7 dB (~ 13.6%) and ~-8.8 dB (~ 13.2%), respectively. Here, it is possible to see a big decrease in the radiation efficiency, when compared with all the previous results (presented in subsections 3.4.2, 3.4.3 and 4.1.4). As expected, this decrease in the antenna total efficiency is mainly due to the absorption by the human ankle tissues.

4.2.4 Levels of SAR

In this subsection, the levels of SAR caused by the proposed biological model are analysed. Since the antenna under study was designed for wearable applications, it is crucial to evaluate the effects of EM fields near the human body (as already seen in section 2.4).

The amount of energy which is absorbed or dissipated by the human body tissues when exposed to an electromagnetic field is called SAR. It can be defined as the power absorbed per mass of tissue and its results are obtained from the equation presented in [75]. In order to calculate the values of SAR caused by the antenna, there are some aspects that should be taken into account, namely the conductivity, geometry and mass density of the body part exposed to certain electric field strength, depending on the relative position to the antenna.

According to ICNIRP in extremities such as hands, wrists, feet, and ankles, higher levels of SAR up to 4 W/kg for any 10 g of tissue are permitted [76]. The ankle region has a narrow cross-section and contains high conductivity muscle. Thus, the channelling of the current through this tissue produced high-localised values of SAR. Values of SAR depend on the conductivity of the human body tissues, which in turn depends on the operating frequency. Although the proposed antenna is not meant to be used in the transmission mode with significant power at the Radionavigation Service bands, a SAR evaluation has been performed. The analysis of the SAR effects was

performed in CST Microwave Studio™ with the ankle bracelet placed 2 mm far from the four-layered human ankle model. The elliptical model was chosen for its similarity to a real human ankle, without compromising its simulation time in comparison with other simpler human models.

Values of SAR depend on the conductivity of the human body tissues, which in turn depends on the operating frequency. However, considering SAR, the Radionavigation Service bands are generally not involved in signal transmission issues. In this respect, the highest operating frequency (that was shifted downwards from 2447.5 to 2187.8 MHz, due to human tissues, as seen before) was chosen as the only frequency of interest for this simulation stage.

For a default input power of 1 W, the 3D Maximum of SAR, considering 10g of tissue, has occurred at the highest downshifted operating frequency ($f = 2.19 GHz$) with a value of 2.814W/kg (as shown in Figure 4.17).

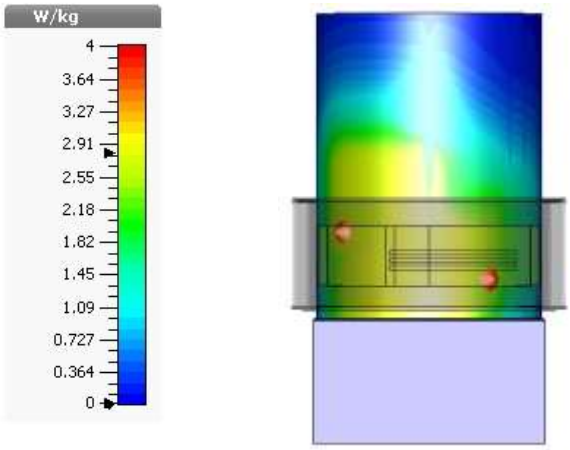

(a) Range of SAR (b) Distribution of SAR in biological model for the worst case

Figure 4.17: Levels of SAR.

4.3 Discussion and Conclusions

The antenna optimised and developed in Chapter 3 was submitted to a set of simulations in non-free-space conditions. The study of non-free-space performance of the proposed antenna consisted of a series of simulations of return loss curves, operation bands, radiation patterns and efficiency.

Before starting the series of simulations for bending and casing scenarios, it is presented the description of geometry, substrate and feed line changes (in subsection 4.1.2) and of the commercial ankle bracelet model (see Figure 4.1) and Table 4.1). With the aid of CST tool called *Layer Stack-up Bending*, the back-side of the antenna ground plane was bent over the inner part of a commercial ankle bracelet model without being cased (see Figure 4.6).

Conclusions are summarised next. Simulated results have shown acceptable radiation patterns for the different cuts of the antenna (as shown in Figure 4.7 and Figure 4.8) and good radiation efficiency, in this scenario. However, S-Parameters and bandwidths were significantly affected (see

Figure 4.2 and Figure 4.3). In addition, resizing the antenna in accordance with the curved structure of the ankle bracelet model caused an operating frequency downshift. Here, the lack of an explicit manner to transform the inevitable resized antenna dimensions into other dimensions capable of overcoming the operation bands downshifting has proven to be the main adversity in respect to bending and casing process.

The antenna performance was evaluated under casing scenario, by considering the presence of the whole reference ankle bracelet model. Simulated results have shown acceptable radiation patterns (as shown in Figure 4.9 and Figure 4.10) and radiation efficiency. However, S-Parameters and operating bands were again significantly affected (see Figure 4.4 and Figure 4.5), by causing a small frequency downshift, when compared with the free-space and bending scenarios. This evidence was explained in part by the fact that the ABS plastic of the ankle bracelet model has a higher dielectric constant than air. This resulting higher effective dielectric constant led to a higher electrical length of the antenna and an operating frequency downshifting.

The antenna attached into the ankle bracelet model was also simulated in the close proximity of human body (see Figure 4.11). It was found that the human body proximity strongly influences the antenna impedance matching and radiation patterns when compared with the free-space, bending and casing scenarios. As was expected, the antenna estimated total efficiency was also reduced due to the losses caused by the human ankle tissues. Here, the estimated radiation efficiency and total radiation efficiency were always below 20% with maximums of ~ 15% and ~ 14% at the highest downshifted operating frequency (f = 2.19 GHz). In relation to the maximum of SAR, by considering 10 g of tissue, it was observed that has occurred at the highest downshifted operating frequency (f = 2.19 GHz) with a value of 2.814 W/kg (as shown in Figure 4.17(a)). This value of SAR meets the maximum limit of 4 W/kg for the antenna placed close to the human ankle and foot model.

Chapter 5

Conclusions and Future Work

5.1 Conclusions

The main goal of this project was to study antennas to be used in the close vicinity of the human body for special applications, including security, health/medical care, and personnel tracking applications. To this end, a compact dual-band antenna prototype with two metal layers with acceptable performance was designed, built and studied. More precisely this project aims at the design of a flexible antenna to be integrated into a commercial ankle bracelet device.

The antenna developed in this project was intended to operate in the Wi-Fi and BT bands, centred at 2.45 GHz, and in the upper Navigation Services L1 bands (GPS L1, Galileo E1 and GLONASS G1). The whole design and fabrication of this dual-band antenna, as well as its radiation performance in free-space and some non-free-space conditions, were analysed throughout this dissertation. Decoupling techniques along with bending, casing and near-body scenarios were considered with regard to the analysis of the radiation performance.

The free-space performance of the proposed antenna was investigated through numerical simulations and measurements. The simulated results encompassed the following elements: return loss curves, operation bands, radiation patterns and efficiency.

The developed antenna was submitted to bending and casing simulations. In CST Microwave Studio™, the antenna back-side was attached inside an "elliptical ring-shaped" model. It was concluded from simulated results that there is an acceptable radiation performance under bending and casing scenarios. However, the antenna S-Parameters were affected with shifts in operating frequencies. It was concluded that resizing of the antenna dimensions in accordance with the curved structure of the ankle bracelet model causes a resonance downshift, when compared to the free-space scenario. Here, the lack of an explicit manner to transform the inevitable resized antenna dimensions, caused by the bending process, into other dimensions capable of overcoming the operation bands downshifting has revealed to be the main adversity in respect to bending and casing process.

The proposed antenna was simulated in the close proximity of a human body. In order to understand how the body tissues influences the antenna parameters, simulations were carried out using an approximated model of human ankle and foot. It was concluded that the human body proximity strongly influences the antenna impedance matching and radiation patterns when compared to the free-space scenario. As was expected, the antenna total efficiency is also reduced due to the absorption by the human ankle tissues. Here, the total radiation efficiency is always below 20% and the SAR values are slightly below 3 W/kg (below the SAR limit of 4 W/kg for the antenna placed close to the human ankle).

Considering the objectives presented in section 1.2, the antenna should have good performance, under free-space (Chapter 3) and non-free-space conditions (Chapter 4), in terms of operating frequencies, bandwidth and radiation efficiency. The miniaturisation of the antenna structure to

fit into a commercial ankle bracelet model was accomplished. Even though some undesired frequency shifts in the bands of interest were observed, the fabrication and testing of the antenna prototype in a free-space scenario led to a reasonable agreement with the simulation results. Even though the simulation results of the antenna in non-free-space conditions (bending, casing and human body proximity) were promising for a proof-of-concept.

5.2 Future Work

This dissertation has presented a compact and flexible dual-band antenna with two metal layers suitable for security, health/medical care, and personnel tracking applications, in the vicinity of the human body. The radiation performance, design optimisation, fabrication method, flexibility and robustness of the antenna in study were the major concerns in this project. However, further research could be done in the field of wearable technology.

In respect to the antenna design, although it was carefully analysed throughout this work, design changes could be considered in order to increase the overall bandwidth. Following the same approach as that of the dissertation, in which there are as many operating bands as radiating elements, additional radiating elements could be integrated. Note that these radiating elements might even be placed on different metal layers, increasing this way the range of possibilities. This trade-off between the number of operating bands, and the complexity of the antenna structure and associated coupling problems could represent an even more interesting challenge. Concerning the materials, a dielectric superstrate layer of higher permittivity between patch antennas and respective ground planes could be used to increase the antenna radiation efficiency, directivity and compactness, being the radiation more oriented towards the outside of the ankle bracelet and human body. According to [77], another way of enhancing the total radiation efficiency, compactness of the antenna and levels of SAR is to design Meander Line Antenna (MLA)s instead of rectangular patches.

Moreover, other fabrication methods should be adopted for future work. As mentioned in 2.2, 3D/Additive Manufacturing (AM) printing is a relatively new and high technological method, which allows creating complex structures by printing layer after layer from a digital model.

Regarding mitigation of coupling effects, apart from the use of slots on the ground plane, other possible coupling suppression techniques should be investigated. In this context, many simulations have been done with double-square Split Ring Resonator (SRR)s and Complementary Split Ring Resonator (CSRR)s placed on the ground plane, in order to filter the surface currents at 2.45 GHz. The dimensioning of these structures was carried out, considering each integrated part of its structure [70] [71]. Even though some results were achieved through a parametric study and trial and error, as there is not a very implicit or explicit way to proceed from the step, in which the Split Ring Resonator (SRR)s and Complementary Split Ring Resonator (CSRR)s were analysed without the antenna, to the step with the influence of the antenna. During this transition, the antenna geometry led to not very conclusive results. Future work could also explore in this direction.

Concerning the overall optimisation procedure of the antenna, methods based on GAs, referred at the end of Chapter 3, has been applied to dual-band antennas because of several current paths present on the patch [74]. For this reason, this technique might be suitable for the antenna under study, but requires validation.

Moreover, a more realistic approach could be considered, by building and testing an antenna prototype integrated into electronic modules, such as an electronic chip. Here, the study of the EMC performance could be considered under the constraints of typical miniature electronic devices. The electromagnetic coexistence of systems and their mutual interaction could be a matter of further research. Furthermore, placing the antenna inside a real ankle bracelet, in the proximity of the human body, could give added value to this work. In respect to feeding lines, these tests would lead to an inevitable change of coaxial cables and connectors, such as *U.FL* cables and connectors, due to the constraint of having flexible coaxial cables instead of semi-rigid ones. A comparison between the experimental results obtained with a phantom model and a real model of a human ankle and foot could even be considered, in order to get a more successful proof-of-concept. Finally, the proposed antenna could also be tested under other interesting scenarios: other deformation types, such as crumpling and/or twisting; by considering the movement of the human body; and under exposure to extreme environmental conditions.

Bibliography

[1] C.-X. Wang, F. Haider, X. Gao, X.-H. You, Y. Yang, D. Yuan, H. M. Aggoune, H. Haas, S. Fletcher and E. Hepsaydir, “Cellular architecture and key technologies for 5G wireless communication networks”, *IEEE Communications Magazine,* vol. 52, pp. 122-130, 2014.

[2] A. Gatherer, IEEE Communications Society, 12 January 2017. [Online, accessed on 17 June 2019], https://www.comsoc.org/publications/ctn/ten-communications-technology-trends-2017.

[3] M. Gee, A. Ho, J. Raab, [Online, accessed on 17 June 2019], https://time.com/see-the-wearable-tech-of-the-future.

[4] M. R. Llenas, "Study of Antenna Concept for Wearable Devices"*, KTH Royal Institute of Technology*, *MSc Thesis*, 2015.

[5] “GPS Antennas”, [Online, accessed on 17 June 2019], http://www.antenna-theory.com/design/gps.php.

[6] “Wi-Fi Antennas”, [Online, accessed on 17 June 2019], http://www.antenna-theory.com/design/wifi.php.

[7] Y. Li, Z. Zhang, Z. Feng and H. R. Khaleel, “Fabrication and Measurement Techniques of Wearable and Flexible Antennas”, *WIT Transactions on State-of-the-art in Science and Engineering,* vol. 82, p. 7, 2014.

[8] S. J. Ha and C. W. Jung, “Reconfigurable beam steering using a microstrip patch antenna with a U-slot for wearable fabric applications”, *IEEE Antennas and Wireless Propagation Letters,* vol. 10, pp. 1228-1231, 2011.

[9] H. Wang, Z. Zhang, Y. Li and Z. Feng, “A dual-resonant shorted patch antenna for wearable application in 430 MHz band”, *IEEE Transactions on Antennas and Propagation,* vol. 61, pp. 6195-6200, 2013.

[10] P. Macleod and others, "A review of flexible circuit technology and its applications", *PRIME Faraday Partnership*, 2002.

[11] L. Yang, A. Rida, R. Vyas and M. M. Tentzeris, “RFID tag and RF structures on a paper substrate using inkjet-printing technology”, *IEEE Transactions on Microwave Theory and Techniques*, vol. 55, pp. 2894-2901, 2007.

[12] A. Scidà, S. Haque, E. Treossi, A. Robinson, S. Smerzi, S. Ravesi, S. Borini and V. Palermo, “Application of graphene-based flexible antennas in consumer electronic devices”, *Materials Today,* vol. 21, pp. 223-230, 2018.

[13] A. Sarycheva, A. Polemi, Y. Liu, K. Dandekar, B. Anasori and Y. Gogotsi, "2D titanium carbide (MXene) for wireless communication", *Science Advances,* vol. 4, p. eaau0920, 2018.

[14] H. R. Khaleel, H. M. Al-Rizzo, D. G. Rucker and S. Mohan, "A compact polyimide-based UWB antenna for flexible electronics", *IEEE Antennas and Wireless Propagation Letters*, vol. 11, pp. 564-567, 2012.

[15] J. Virtanen, T. Bjorninen, L. Ukkonen and L. Sydanheimo, "Passive UHF inkjet-printed narrow-line RFID tags", *IEEE Antennas and Wireless Propagation Letters*, vol. 9, pp. 440-443, 2010.

[16] M. Koohestani, J.-F. Zürcher, A. A. Moreira and A. K. Skrivervik, "A novel, low-profile, vertically-polarized UWB antenna for WBAN", *IEEE Transactions on Antennas and Propagation*, vol. 62, pp. 1888-1894, 2014.

[17] G. A. Casula, G. Montisci and G. Mazzarella, "A wideband PET inkjet-printed antenna for UHF RFID", *IEEE Antennas and Wireless Propagation Letters*, vol. 12, pp. 1400-1403, 2013.

[18] S. Nikolaou, G. E. Ponchak, J. Papapolymerou and M. M. Tentzeris, "Conformal double exponentially tapered slot antenna (DETSA) on LCP for UWB applications", *IEEE Transactions on Antennas and Propagation*, vol. 54, pp. 1663-1669, 2006.

[19] G. DeJean, R. Bairavasubramanian, D. Thompson, G. E. Ponchak, M. M. Tentzeris and J. Papapolymerou, "Liquid crystal polymer (LCP): A new organic material for the development of multilayer dual-frequency/dual-polarization flexible antenna arrays", *IEEE Antennas and Wireless Propagation Letters,* vol. 4, pp. 22-26, 2005.

[20] D. C. Thompson, O. Tantot, H. Jallageas, G. E. Ponchak, M. M. Tentzeris and J. Papapolymerou, "Characterization of liquid crystal polymer (LCP) material and transmission lines on LCP substrates from 30 to 110 GHz", *IEEE Transactions on Microwave Theory and Techniques,* vol. 52, pp. 1343-1352, 2004.

[21] H. R. Khaleel, H. M. Al-Rizzo and A. I. Abbosh, "Design, fabrication, and testing of flexible antennas", in *Advancement in Microstrip Antennas With Recent Applications*, IntechOpen, 2013.

[22] T. W. Koo, D. Kim, J. I. Ryu, H.-M. Seo, J. G. Yook and J. C. Kim, "Design of a label-typed UHF RFID tag antenna for metallic objects", *IEEE Antennas and Wireless Propagation Letters*, vol. 10, pp. 1010-1014, 2011.

[23] H. F. Abutarboush, M. F. Farooqui and A. Shamim, "Inkjet-printed wideband antenna on resin-coated paper substrate for curved wireless devices", *IEEE Antennas and Wireless Propagation Letters,* vol. 15, pp. 20-23, 2015.

[24] V. Lakafosis, A. Rida, R. Vyas, L. Yang, S. Nikolaou and M. M. Tentzeris, "Progress towards the first wireless sensor networks consisting of inkjet-printed, paper-based RFID-enabled sensor tags", *Proceedings of the IEEE*, vol. 98, pp. 1601-1609, 2010.

[25] B. S. Cook and A. Shamim, "Utilizing wideband AMC structures for high-gain inkjet-printed antennas on lossy paper substrate", *IEEE Antennas and Wireless Propagation Letters,* vol. 12, pp. 76-79, 2013.

[26] S. Koulouridis, G. Kiziltas, Y. Zhou, D. J. Hansford and J. L. Volakis, "Polymer--ceramic composites for microwave applications: fabrication and performance assessment", *IEEE Transactions on Microwave Theory and Techniques,* vol. 54, pp. 4202-4208, 2006.

[27] S. Hage-Ali, N. Tiercelin, P. Coquet, R. Sauleau, H. Fujita, V. Preobrazhensky and P. Pernod, "A millimeter-wave microstrip antenna array on ultra-flexible micromachined polydimethylsiloxane (PDMS) polymer", *IEEE Antennas and Wireless Propagation Letters,* vol. 8, pp. 1306-1309, 2009.

[28] C. P. Lin, C. H. Chang, Y. T. Cheng and C. F. Jou, "Development of a flexible SU-8/PDMS-based antenna", *IEEE Antennas and Wireless Propagation Letters*, vol. 10, pp. 1108-1111, 2011.

[29] C. Hertleer, H. Rogier, L. Vallozzi, L. Van Langenhove and others, "A textile antenna for off-body communication integrated into protective clothing for firefighters", *IEEE Transactions on Antennas and Propagation,* vol. 57, p. 919, 2009.

[30] T. Kaufmann and C. Fumeaux, "Wearable textile half-mode substrate-integrated cavity antenna using embroidered vias", *IEEE Antennas and Wireless Propagation Letters,* vol. 12, pp. 805-808, 2013.

[31] S. Y. Y. Leung and D. C. C. Lam, "Performance of printed polymer-based RFID antenna on curvilinear surface", *IEEE Transactions on Electronics Packaging Manufacturing*, vol. 30, pp. 200-205, 2007.

[32] S. Merilampi, L. Ukkonen, L. Sydänheimo, P. Ruuskanen and M. Kivikoski, "Analysis of silver ink bow-tie RFID tag antennas printed on paper substrates", *International Journal of Antennas and Propagation*, vol. 2007, 2007.

[33] A. Blayo and B. Pineaux, "Printing processes and their potential for RFID printing", in *Proceedings of the 2005 Joint Conference on Smart Objects and Ambient Intelligence: innovative context-aware services: usages and technologies*, 2005.

[34] A. Karwa, "Printing Studies with Conductive Inks and Exploration of New Conducting Polymer Compositions Materials Science and Engineering", *Rochester Institute of Technology, Rochester, New York, Thesis*, 2006.

[35] M. I. Maksud, M. S. Yusof and M. M. A. Jamil, "Study on finite element analysis of fine solid lines by flexographic printing in printed antennas for RFID transponder", *International Journal of Integrated Engineering*, vol. 4, 2012.

[36] G. Shaker, S. Safavi-Naeini, N. Sangary and M. M. Tentzeris, "Inkjet printing of ultrawideband (UWB) antennas on paper-based substrates", *IEEE Antennas and Wireless Propagation Letters*, vol. 10, pp. 111-114, 2011.

[37] H. S. Lee, J. G. Kim, S. Hong and J. B. Yoon, "Micromachined CPW-fed suspended patch antenna for 77 GHz automotive radar applications", in *The European Conference on Wireless Technology,* 2005.

[38] S. Kim, Y. J. Ren, H. Lee, A. Rida, S. Nikolaou and M. M. Tentzeris, "Monopole antenna with inkjet-printed EBG array on paper substrate for wearable applications", *IEEE Antennas and Wireless Propagation Letters*, vol. 11, pp. 663-666, 2012.

[39] J. Heirons, S. Jun, A. Shastri, B. Sanz-Izquierdo, D. Bird, L. Winchester, L. Evans and A. McClelland, "Inkjet printed GPS antenna on a 3D printed substrate using low-cost machines", in *Proceedings of 2016 Loughborough Antennas & Propagation Conference (LAPC)*, 2016.

[40] S. Jun and B. Sanz-Izquierdo, "A CPW-fed antenna on 3D printed EBG substrate", in *Proceedings of 2015 Loughborough Antennas & Propagation Conference (LAPC)*, 2015.

[41] E. Macdonald, R. Salas, D. Espalin, M. Perez, E. Aguilera, D. Muse and R. B. Wicker, "3D printing for the rapid prototyping of structural electronics", *IEEE Access,* vol. 2, pp. 234-242, 2014.

[42] M. Liang, C. Shemelya, E. MacDonald, R. Wicker and H. Xin, "3-D printed microwave patch antenna via fused deposition method and ultrasonic wire mesh embedding technique", *IEEE Antennas and Wireless Propagation Letters,* vol. 14, pp. 1346-1349, 2015.

[43] B. Sanz-Izquierdo and E. A. Parker, "Frequency selective surfaces formed by partially metalising 3D printed shapes", in *Proceedings of 9th European Conference on Antennas and Propagation (EuCAP)*, 2015.

[44] S. Jun, B. Sanz-Izquierdo and E. A. Parker, "3D printing technique for the development of non-planar electromagnetic bandgap structures for antenna applications", *Electronics Letters,* vol. 52, pp. 175-176, 2015.

[45] B. Sanz-Izquierdo and E. A. Parker, "3-D printing of elements in frequency selective arrays", *IEEE Transactions on Antennas and Propagation,* vol. 62, pp. 6060-6066, 2014.

[46] S. Jun, B. Sanz-Izquierdo and M. Summerfield, "UWB antenna on 3D printed flexible substrate and foot phantom", in *Proceedings of 2015 Loughborough Antennas & Propagation Conference (LAPC)*, 2015.

[47] B. Sanz-Izquierdo and S. Jun, "WLAN antenna on 3D printed bracelet and wrist phantom", in *Proocedings of Loughborough Antennas and Propagation Conference (LAPC)*, 2014.

[48] Y. Huang, X. Gong, S. Hajela and W. J. Chappell, "Layer-by-layer stereolithography of three-dimensional antennas", in *Proceedings of IEEE Antennas and Propagation Society International Symposium*, 2005.

[49] D. M. Pozar, "Microwave Engineering", Wiley, 2004.

[50] J. Tak and J. Choi, "A low-profile dipole array antenna with monopole-like radiation for on-body communications", *Journal of Electromagnetic Engineering and Science,* vol. 15, pp. 245-249, 2015.

[51] S. Y. Jun, A. Elibiary, B. Sanz-Izquierdo, L. Winchester, D. Bird and A. McCleland, "3-D Printing of Conformal Antennas for Diversity Wrist Worn Applications", *IEEE Transactions on Components, Packaging and Manufacturing Technology,* vol. 8, pp. 2227-2235, 2018.

[52] N. Cho, T. Roh, J. Bae and H.-J. Yoo, “A planar MICS band antenna combined with a body channel communication electrode for body sensor network”, *IEEE Transactions on Microwave Theory and Techniques*, vol. 57, pp. 2515-2522, 2009.

[53] M. K. Magill, G. A. Conway and W. G. Scanlon, “Tissue-independent implantable antenna for in-body communications at 2.36--2.5 GHz”, *IEEE Transactions on Antennas and Propagation,* vol. 65, pp. 4406-4417, 2017.

[54] D. K. Das, “Study of Dual Band Wearable Antennas Using Commonly Worn Fabric Materials”, *North South University*, Bangladesh , *PhD dissertation,* 2017.

[55] Y. Hao, A. Alomainy, P. S. Hall, Y. I. Nechayev, C. G. Parini and C. C. Constantinou, “Antennas and propagation for body centric wireless communications”, in *Proceedings of Wireless Communications and Applied Computational Electromagnetics,* 2005.

[56] C. A. Fernandes, "Near-Body Radiowave Propagation", University of Lisbon, Radiowave Propagation Course, 2017.

[57] A. W. Astrin, H. B. Li and R. Kohno, “Standardization for body area networks”, *IEICE Transactions on Communications,* vol. 92, pp. 366-372, 2009.

[58] D. P. Tobón, T. H. Falk and M. Maier, “Context awareness in WBANs: a survey on medical and non-medical applications”, *IEEE Wireless Communications,* vol. 20, pp. 30-37, 2013.

[59] A. Alam, R. Jermyn, M. Joseph, S. Patel, U. Jorde and O. Saeed, “Improved quality of life scores and exercise capacity with remote pulmonary artery pressure monitoring in patients with chronic heart failure”, *Journal of the American College of Cardiology,* vol. 67, p. 1299, 2016.

[60] A. K. Sisodia, S. Arya and D. Punetha, “Providing a better life for amyotrophic lateral sclerosis patient or spinal cord injured patient by artificial neural network or braingate”, *International Journal on Recent and Innovation Trends in Computing and Communication,* vol. 4, pp. 508-513, 2016.

[61] M. V. Ramesh, D. Raj, V. S. Kalavampra and N. Dilraj, “Design of wireless real time artificial sphincter control system for urinary incontinence”, in *Proceedings of International Symposium on Technology Management and Emerging Technologies*, 2014.

[62] D. Curone, G. Dudnik, G. Loriga, J. Luprano, G. Magenes, R. Paradiso, A. Tognetti and A. Bonfiglio, “Smart garments for safety improvement of emergency/disaster operators”, in *Proceedings of 29th Annual International Conference of the IEEE Engineering in Medicine and Biology Society*, 2007.

[63] J. Trajkovikj and A. K. Skrivervik, “Diminishing SAR for Wearable UHF Antennas”, *IEEE Antennas and Wireless Propagation Letters,* vol. 14, pp. 1530-1533, 2015.

[64] M. Lapinski, M. Feldmeier and J. A. Paradiso, “Wearable wireless sensing for sports and ubiquitous interactivity”, in *Proceedings of Sensors 2011 IEEE*.

[65] D. Gaetano, P. McEvoy, M. J. Ammann, J. E. Browne, L. Keating and F. Horgan, “Footwear antennas for body area telemetry”, *IEEE Transactions on Antennas and Propagation,* vol. 61, pp. 4908-4916, 2013.

[66] D. Gaetano, P. McEvoy, M. J. Ammann, C. Brannigan, L. Keating and F. Horgan, "Footwear and wrist communication links using 2.4 GHz and UWB antennas", *Electronics*, vol. 3, pp. 339-350, 2014.

[67] "086 semi-rigid coax cable with copper outer conductor", 2013. [Online, accessed 17 June 2019], https://www.pasternack.com/images/ProductPDF/RG405-U-STRAIGHT.pdf.

[68] D. Jasteh, P. Gardner and P. S. Hall, "Isolation enhancement in a dual port antenna", in *Proceedings of Antennas and Propagation Conference (LAPC), Loughborough*, 2013.

[69] K. C. Kerby, "Ground plane slot structures for isolation of cosited microstrip antennas", *University of Illinois at Urbana-Champaign*, *PhD dissertation*, 2009.

[70] W. Ali, E. Hamad, M. Bassiuny and M. Hamdallah, "Complementary split ring resonator based triple band microstrip antenna for WLAN/WiMAX applications", *Radioengineering*, vol. 26, pp. 78-84, 2017.

[71] F. Raval, S. Purohit and Y. P. Kosta, "Dual-band wearable antenna using split ring resonator", *Waves in Random and Complex Media,* vol. 26, pp. 235-242, 2016.

[72] "EZ-47-TP/M17", [Online, accessed on 17 June 2019], https://www.ezform.com/product/ez-47-tpm17-2.

[73] H. R. Khaleel, "Design and fabrication of compact inkjet printed antennas for integration within flexible and wearable electronics", *IEEE Transactions on Components, Packaging and Manufacturing Technology,* vol. 4, pp. 1722-1728, 2014.

[74] M. Lamsalli, A. El Hamichi, M. Boussouis, N. Amar Touhami and T. Elhamadi, "Genetic algorithm optimization for microstrip patch antenna miniaturization", *Progress In Electromagnetics Research,* vol. 60, pp. 113-120, 2016.

[75] K. Shiba, M. Nukaya, T. Tsuji and K. Koshiji, "Analysis of current density and specific absorption rate in biological tissue surrounding transcutaneous transformer for an artificial heart", *IEEE Transactions on Biomedical Engineering,* vol. 55, pp. 205-213, 2007.

[76] G. Kang and O. P. Gandhi, "Effect of dielectric properties on the peak 1-and 10-g SAR for 802.11 a/b/g frequencies 2.45 and 5.15 to 5.85 GHz", *IEEE Transactions on Electromagnetic Compatibility*, vol. 46, pp. 268-274, 2004.

[77] S. Bhattacharjee, M. Mitra and S. R. Bhadra Chaudhuri, "An effective SAR reduction technique of a compact meander line antenna for wearable applications", *Progress In Electromagnetics Research*, vol. 55, pp. 143-152, 2017.

[78] Z. J. S. Subirana , JM. J. Jornoza, and M. Hernandez-Pajares, "GNSS Bands", 2011. [Online, accessed on 17 June 2019], https://gssc.esa.int/navipedia/index.php/GNSS_signal.

[79] S. I. G. Bluetooth, "Groups: Specification of the Bluetooth system", *Ver1.0 Draft Foundation,* 1999.

[80] I. Poole, "Wi-Fi/WLAN Channels, Frequencies", 2016. [Online, accessed on 17 June 2019], https://www.electronics-notes.com/articles/connectivity/wifi-ieee-802-11/channels-frequencies-bands-bandwidth.php

Appendix A

Frequency Bands

This thesis focuses on a wearable antenna to work on the following wireless services: GPS [78], BT [79] and 2.4 GHz Wi-Fi [80] conveniently described in the very beginning of thesis (in chapter Introduction). However, these frequency slots along the whole spectrum are sufficiently sparse, justifying that these frequency bands be shown in detail in Figure A.1, Figure A.2 and Figure A.3.

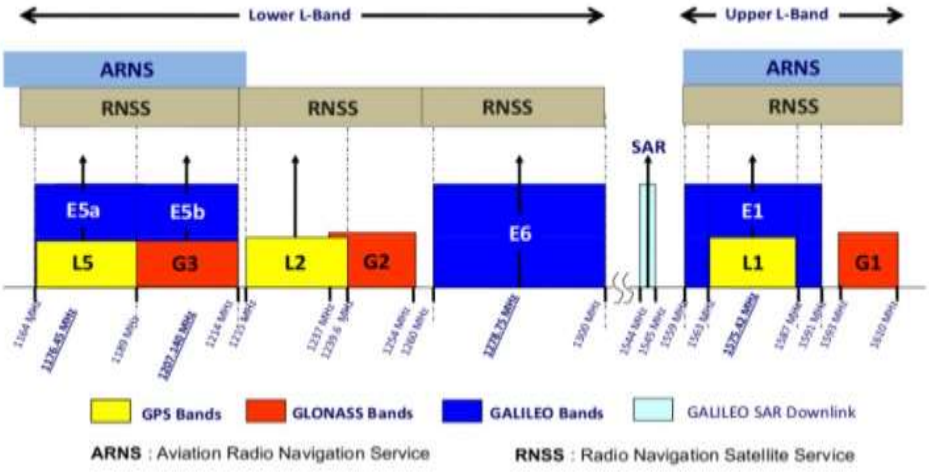

Figure A.1: GPS, GLONASS and Galileo navigational frequency bands

Geography	Regulatory Range	RF Channels
USA, Europe and most other countries[1)]	2.400-2.4835 GHz	f=2402+k MHz, k=0,...,78
Spain[2)]	2.445-2.475 GHz	f=2449+k MHz, k=0,...,22
France[3)]	2.4465-2.4835 GHz	f=2454+k MHz, k=0,...,22

(a) BT operating bands

Geography	Lower Guard Band	Upper Guard Band
USA	2 MHz	3.5 MHz
Europe (except Spain and France)	2 MHz	3.5 MHz
Spain	4 MHz	26 MHz
France	7.5 MHz	7.5 MHz
Japan	2 MHz	2 MHz

(b) BT guard bands

Figure A.2: BT operating and guard frequency bands

CHANNEL NUMBER	LOWER FREQUENCY MHZ	CENTER FREQUENCY MHZ	UPPER FREQUENCY MHZ
1	2401	2412	2423
2	2406	2417	2428
3	2411	2422	2433
4	2416	2427	2438
5	2421	2432	2443
6	2426	2437	2448
7	2431	2442	2453
8	2436	2447	2458
9	2441	2452	2463
10	2446	2457	2468
11	2451	2462	2473
12	2456	2467	2478
13	2461	2472	2483
14	2473	2484	2495

Figure A.3: 2.4 GHz frequency channels

Appendix B

Standard Microwave Antennas

Table B.1: Categories of microwave antennas with their respective examples, and main properties and uses

Antenna Category	Examples	Main Properties and Uses
Wire	• Dipoles; • Monopoles; • Yagi-Uda.	• Low gains; • Mostly used at High Frequency (HF) to Ultra-High Frequency (UHF); • Light weight; • Low cost; • Simple design.
Aperture	• Open-ended waveguides; • Rectangular/Circular horns; • Reflectors; • Lenses.	• Moderate to high gains; • Commonly used at microwave and mm-Wave frequencies.
Printed	• Printed dipoles; • Printed monopoles; • Printed slots; • Microstrip patch antennas.	• Made with photolithographic methods; • Both radiating elements and feed line fabricated on dielectric substrates; • Easily inserted into wearable devices; • Commonly used at microwave and mm-Wave frequencies.
Array	• Consistent arrangement of antenna elements and respective feeding network, such as: • Yagi-Uda arrays; • Reflector arrays; • Printed arrays; • Phased arrays.	• Radiation patterns can be controlled by varying excitation properties (gain, beam pointing angle, side lobe levels, etc.); • Used in MIMO systems.